Three-dimensional analysis for traffic-induced vibration of highway bridges and its applications

Kim, Chul Woo

(Degree)
博士（工学）

(Date of Degree)
2003-09-19

(Date of Publication)
2014-06-27

(Resource Type)
doctoral thesis

(Report Number)
乙2708

(URL)
https://hdl.handle.net/20.500.14094/D2002708

Doctoral Dissertation

Three-Dimensional Analysis for Traffic-Induced Vibration of Highway Bridges and Its Applications

September, 2003

The Graduate School of Science and Technology
Kobe University, Japan

Chul Woo KIM

金 哲 佑
キム チョール

Doctoral Dissertation

Three-Dimensional Analysis for Traffic-Induced Vibration of Highway Bridges and Its Applications

(道路橋交通振動の三次元解析とその適用)

September, 2003

The Graduate School of Science and Technology
Kobe University, Japan

Chul Woo KIM

CONTENTS

Acknowledgments

A journey is easier when you travel together. Interdependence is certainly more valuable than independence. This thesis is the result of six years of work whereby I have been accompanied and supported by many people. It is a pleasant aspect that I have now the opportunity to express my gratitude for all of them.

I wish to express sincere appreciation to my advisor, Professor Mitsuo Kawatani of Kobe University for his support, encouragement, for proofreading of hundreds of thesis drafts, and helping me throughout my research project. This study was conducted under his guidance during the past six years. I owe him lots of gratitude for having me shown this way of research. He could not even realize how much I have learned from him.

In addition, special thanks are due to the members of my committee: Professor Yasutoshi Kitamura, Professor Shiro Takada and Professor Hiroshi Kanki of Kobe University. Their advice and patience are very appreciated.

My sincere thanks are due to Professor Nobuo Nishimura of Osaka University who firstly invites me to the bridge dynamics and introduces Professor Kawatani to me. I would like to thank Professor Hitoshi Furuta of Kansai University for his encouragement in many conferences.

A special thanks also goes to Mr. Naoki Kawada of Asia Civil Engineering Co. Ltd., who enriched my knowledge with his experience in the field of bridge design. I would also like to thank to the members of the LAB. Dr. Nomura, Mr. Yoshida, Mr. He, Mr. Kamizono, Mr. Tsuji, Mr. Takahashi, Mr. Tona, Mr. Sobukawa, Mr. Sakada and secretary Mrs. Furui and Mr. Lee and Mr. Kanbara of Osaka University for their supports and their comradeship.

Lastly, I am extremely grateful to my parents and my brother for their understand and support. I would like to express my gratitude for the constant support, understanding and love that I received from my wife Yunjeong and my two daughters Soree and Shina.

I dedicate this thesis to my loved family: Yunjeong, Soree and Shina.

Kobe, Japan, September 2003
Chul-Woo Kim

Summary

The major goal of this dissertation is devoted to investigate two main subjects, development of the general three-dimensional traffic-induced vibration analysis and its application to dynamics of steel girder bridges. To meet the needs, a numerical model for the traffic-induced vibration of bridges is presented.

The probabilistic assessment of code specified impact factors for decks of highway bridges are carried out based on the Monte-Carlo simulation (MCS) method, because the rational criterion of performance level of RC decks, which are more easily damaged than other structural members in steel highway bridges due to directly subjected to wheel loads of vehicles, provides useful assessment tool for decision making related to the inspection, repair, upgrading and replacement of existing steel plate girder bridges based on life-cycle cost.

A pioneering research on dynamic responses of web plates of the two-girder steel bridge with elastomeric bearings is carried out in this study to examine the effect of deck's deformation on those of web plates, since the investigation on dynamic responses of the web plate can give useful information in solving fatigue and infrasound problems of bridges. The end-cross beam reinforcement taken as a countermeasure reducing traffic-induced vibration is applied to two-girder bridges, and a removing bumps at expansion joints, so called a overlay bump, is considered as another method to reduce the traffic-induced vibration.

The effectiveness of the three-dimensional finite element analysis is verified by comparing with the field-test data.

The investigation on the dynamic response of the two-girder bridge by means of the full 3-D model shows that the dynamic response of girders are amplified by a biased running of a vehicle or series of vehicles because of its simplified lateral bracing system. It indicates that the lower torsional rigidity of two-girder bridges than conventional multi-girder bridges can give rise to additional vibration effects on girders due to biased running of vehicles. This study also demonstrates that, for two-girder bridges with wide girder spacing, the deformation of decks can give influence to the out-of-plane response of web plates.

It is observed that the end-cross beam reinforcement can give vibration reduction effects on the deck slab near expansion joints as well as the end-cross beam. For the twin-girder bridge system with wide cantilever deck slabs, the reinforcing to the bracket can be recommended. The end-cross beam reinforcement and removal of bumps in combination of the vibration control can give an effective reduction against environmental vibrations.

Nomenclatures

a_j	:	*j-th* generalized coordinate of a bridge
a_k	:	Gaussian random variable with zero mean
$\boldsymbol{a}$	:	Generalized displacement vector of a bridge
$\dot{\boldsymbol{a}}$	:	Generalized velocity vector of a bridge
$\ddot{\boldsymbol{a}}$	:	Generalized acceleration vector of a bridge
$\boldsymbol{C}_b$	:	Damping matrix of a bridge
$\boldsymbol{C}_s$	:	Damping matrix of the vehicle-bridge interaction system
$\overline{\boldsymbol{C}}_b$	:	Normalized damping matrix of a bridge
C_{vmku}	:	Damping coefficient of vehicles
dB	:	Deci-Bel
$\boldsymbol{D}$	:	Displacement vector of a bridge
$\dot{\boldsymbol{D}}$	:	Velocity vector of a bridge
DIF	:	Dynamic Increment Factor
DLC	:	Dynamic Load Coefficient
f	:	Frequency (Hz)
$\boldsymbol{F}_s$	:	Force vector of the vehicle-bridge interaction system
g	:	Gravity acceleration ($9.81 \mathrm{m/s^2}$)
h_{bi}	:	Damping constant according to *i-th* mode
J_{xvk}	:	Mass moment of inertia of vehicles on x-axis
J_{yvk}	:	Mass moment of inertia vehicles on y-axis
k_x, k_y, k_z	:	Spring constant of elstomeric bearings at each axis
$k_{\theta x}$, $k_{\theta y}$, $k_{\theta z}$	:	Rotational spring constant of elstomeric bearings at each axis
$\boldsymbol{K}_b$	:	Stiffness matrix of a bridge
$\boldsymbol{K}_s$	:	Stiffness matrix of the vehicle-bridge interaction system
$\overline{\boldsymbol{K}}_b$	:	Normalized stiffness matrix of a bridge
K_{vmku}	:	Spring constant of vehicles
L_{cr}	:	Critical headway of vehicles
m_i, m_j	:	External moment at nodes i and j, respectively
m_{vlm}	:	Mass of vehicles
$\boldsymbol{M}_b$	:	Mass matrix of a bridge
$\boldsymbol{M}_s$	:	Mass matrix of the vehicle-bridge interaction system
$\overline{\boldsymbol{M}}_b$	:	Normalized mass matrix of a bridge

MCS	:	Monte-Carlo Simulation
OAL	:	Over all acceleration level (dB)
p_f	:	External force act on a rigid node of a structure system
$P_{mu}(t)$	:	Dynamic wheel load at time t
PSD	:	Power Spectral Density
q_f	:	Unknown force at a hinge
q_i	:	*i-th* generalized coordinate of the vehicle-bridge interaction system
$\dot{q}_i$	:	*i-th* generalized velocity of the vehicle-bridge interaction system
R_{vmku}	:	Displacement at each part of the vehicle system
RMS	:	Root Mean Square
$S(\Omega)$	:	PSD function for a roadway surface roughness
T	:	Kinematic energy of the vehicle-bridge interaction system
U_d	:	Dissipation energy of the vehicle-bridge interaction system
v	:	Vehicle speed
V	:	Potential energy of the vehicle-bridge interaction system
VAL	:	Vibration Acceleration Level (dB)
VL	:	Vibration Level (dB)
VRL	:	Vibration Reduction Level (dB)
w_i	:	Vertical displacement at a node i
$w(t, x_{vmu})$	:	Displacement of bridge at x_{vmu} of time t
WL_{st}	:	Static wheel load
W_{vmu}	:	Static axle-load
$\boldsymbol{W}$	:	Displacement vector of the vehicle-bridge interaction system
$\dot{\boldsymbol{W}}$	:	Velocity vector of the vehicle-bridge interaction system
$\ddot{\boldsymbol{W}}$	:	Acceleration vector of the vehicle-bridge interaction system
Z_{vl1}	:	Displacement of a vehicle (Bouncing)
Z_{vs2}	:	Displacement at an axle (Axle-hop)
Z_{ovmu}	:	Relative displacement between bridge deformation and roughness
Z_{rvmu}	:	Roadway roughness
$\boldsymbol{Z}$	:	Displacement vector of the vehicle system
α	:	Roughness coefficient
β	:	Shape parameter for the PSD function of roadway profiles
β_T	:	Target reliability index
ε	:	Tolerance in Newmark's β method
ϕ_j	:	Modal vector
Φ	:	Modal matrix

λ	:	Wave number (m/c)
λ_{xv}, λ_{xvm}, λ_{yvm}	:	Geometry of the vehicle system
μ_{DLC}	:	Mean of the DLC value
μ_{DIF}	:	Mean of the DIF value
π	:	Circular constant
θ_i	:	Angular displacement at a node i
θ_{xv11}	:	Angular displacement of the vehicle system (Rolling)
θ_{xv12}, θ_{xv22}	:	Axle tramp at front and rear axles, respectively
θ_{yv11}	:	Angular displacement of the vehicle system (Pitching)
θ_{yv22}	:	Axle wind-up (Rear axle)
$\rho_{DLC,DIF}$	:	Correlation coefficient of DLC and DIF values
σ_{dy}	:	RMS values of the dynamic component of wheel loads
ω	:	Circular frequency (rad/s)
Ω	:	Spatial frequency (c/m)
Ψ	:	Distribution vector

Chapter 1

Introduction

1.1 General

In the last two decades, there has been a significant increase in numbers of new bridge construction due to rapid urban development and economical growth in many areas of the world. Consequently, the challenges to state-of-practice of bridge engineering are becoming broader range in recent years. While bridge engineers still stride to build safe and economical bridges to meet the transportation needs of the public by using innovative computer modeling and analytical techniques, many countries are now faced with the problem of developing innovative solutions to enhance the performance level of existing bridges.

Modern bridge design requires not only strength but also cost-efficiency as well as aesthetic features. These technical situations have bridge engineers bring about a concept of innovative design strategy. The concept includes both innovations of structural systems and materials. The adoption of new materials and improved design methods has resulted in lighter and more flexible bridges. However, heavy vehicles have become larger and have increased in number. Highway bridges therefore are increasingly susceptible to vibration.

Among the innovative design strategy to make steel bridges more economical, one of the most popular design concepts in short and medium span bridges has been the steel two-girder bridge that adopts the simplified structural system because of advantages it offers with regard to fabrication, erection and maintenance, etc. Questions that remain unanswered for the two-girder bridge are whether the undesirable vibration exists, and, if it exists, what kind of countermeasures can be applied to reduce the vibration.

The adoption of the wide girder spacing and simplified structural system of the two-girder bridge compared with the conventional multi-girder bridge can give rise to change of dynamic characteristics. As a result, the bridge becomes to be easily vibrated by external dynamic loads like wind and vehicle loads, etc. Consequently, the flexible innovative bridges can make better score if the undesirable vibration induced by structural characteristics of the bridge can be efficiently reduced.

Bridge responses induced by moving vehicles is an important aspect in design and structural evaluation of bridges, since highway bridges serve as a vital role in transportation systems. In a typical journey, a heavy vehicle crosses dozens of bridges. During crossing each bridge, it applies static loads and dynamic wheel loads that cause the bridge to vibrate. The repeated application of the dynamic wheel loads can lead to deterioration and a resulting reduction in service life of the bridge.

Generally, bridge engineers use the impact factor defined as the maximum of dynamic response on the maximum static response to a design or evaluation of bridge capacity. However, it is not enough to consider the time varying effect of vehicle loads as an impact factor because, behind this factor, there are a lot of phenomena that influence the bridge response. The important factors are: the characteristics of vehicles, the velocity of the vehicles, the characteristics of the bridge, the roadway roughness profile of the bridge surface, and multiple vehicles and their transverse positions. Bumps near an expansion joint usually cause excessive impulsive dynamic wheel loads with high-frequency characteristics. These impulsive high-frequency vibrations will attack the member near bumps, since the impulsive energy of a vehicle may be dissipated within a short period because of large damping of the vehicle. The impulsive load affects the impact factor of deck slabs near the expansion joint, and can also be one of sources to cause noises and vibrations.

In recent years, wide spreading urbanization of major cities and their skirts needs construction of highway viaducts that link commercial zones at an urban area and industrial zones at the skirts of the urban area. This leads to buildings being constructed closer to highway bridges, and an increased exposure of the buildings to traffic-induced vibration of bridges. Thus, especially for viaducts, the undesirable vibrations of bridges, so called environmental vibrations, occurred at the members near the expansion joint will influence to nearby grounds and buildings through supports and piers. Those undesirable vibrations on human reception have been one of major technical problems because of its high possession rates of viaducts in land scarce major cities.

Highway bridges typically have natural frequencies in the same range as those of heavy vehicles. Excitation of one system by the other is significant. The low damping of bridges does not significantly reduce the vibration caused by bridge-vehicle interactions. Notwithstanding the importance of traffic-induced bridge dynamics, major bridge failures are not normally caused by dynamic wheel loads of vehicles. Usually, the wheel loads cause more subtle problems and contribute to fatigue, surface wear, and cracking of concrete decks that leads to corrosion. Thus, dynamic loads continually degrade bridges and develop vibration problem including noise, and increase the necessity of regular maintenance and/or countermeasures against vibrations.

The recent design concept towards the performance based design like limit state design (LSD) including life-cycle management needs a rational criterion of performance level of reinforced concrete (RC) decks. The rational criterion of performance level of RC decks provides useful assessment tool for decision making related to the inspection, repair, upgrading and replacement of existing steel plate girder bridges based on life-cycle cost, since RC decks, being directly subjected to wheel loads of vehicles, are more easily damaged than other structural members in steel highway bridges. Moreover, the adoption of wide girder

spacing in steel two-girder bridges needs deck slabs with higher performance than those of conventional multi-girder bridges.

Since the dynamic response of bridges due to heavy vehicle loads is not adequately understood, it is not known what portion of the bridge damage is caused by the heavy vehicle load. Nevertheless, even if only a small percentage of the damage arises from bridge vibrations, then this accounts for significant expenditure.

A better understanding of the dynamics of the bridge-vehicle interaction system is necessary in order to build user-friendly and environment-friendly bridges to resist vibrations, to design better vehicles to reduce bridge damage, and/or to regulate vehicle loads and suspensions. Moreover, proper estimation of dynamic wheel loads of moving vehicles is also important in maintenance and management of roadway pavement and decks.

1.2 Objectives

The dynamic response of bridge structures subjected to moving vehicle loads has been an interesting topic in the field of the bridge engineering. Those dynamic responses of bridges have been considered in design as a form of impact factor. Studies about impact factor of bridges have been mainly focused on girders. However, those impact factor-related studies for deck slabs have not been fully investigated, even though some experimental researches suggest the need of considering effects of the bump near the expansion joint.

Moreover, the advent of innovative bridge design concept focused on lighter and more flexible but safer bridges has resulted in easily vibrating bridges, although heavy vehicles have become larger and have increased in number in recent years. In the serviceability (or performance) point of view, the advanced bridge design should fulfill the needs of the times: user- and environment-friendly bridges (or low vibration and noise bridges). Moreover, viaducts with the flexible structural feature may easily produce annoying vibration for people living and working in neighboring buildings to a distance a little far from the bridge. Vibration is therefore one of the more important consequences to be considered, when planning new viaducts and upgrading older ones.

However, these technical problems in relation to the traffic-induced vibration of bridges have not been fully investigated for the lack of public interests and of computer capacity that can process a proposed analytical method.

There are two ways to investigate the complicate bridge-vehicle interaction problem: experimental and analytical approaches. For experimental method, it needs much time and facilities, and costs a great. On the other hand, the analytical approach will be an economical way to investigate the bridge-vehicle interaction problem if the validity of the analytical

method is verified.

One of the most common analytical approaches to examine the bridge-vehicle interaction problem has been two-dimensional model for the bridge and the vehicle. It also has been reported that such a two-dimensional system gives good approximation for investigating the dynamic responses of main girders of bridges due to moving vehicles on rough roadway. For three-dimensional bridge-vehicle interaction system, it is usually adopted to simulate the behavior of local members of a bridge like deck slabs, cross beams, web plates, etc. A few three-dimensional analytical models for the bridge-vehicle interaction system thus have been developed.

Although the source that produces stress in a bridge under moving vehicles is a result of the static load of vehicles and the dynamic wheel loads induced by the vehicle-pavement-bridge interaction, most of the former studies have focused on main girder responses. However the dynamic wheel load is discussed, there is little verification with field-test data irrespective of its importance in bridge dynamics.

Models are therefore needed that can be used to predict the vibration with sufficient reliability, and at an affordable cost for the different planning stages.

To meet the technical needs, one of the major goals of this study is the development of analytical model to comprehensively simulate the dynamic wheel load of vehicles as well as bridge responses including the response of local members. Therefore, Lagrange equation of motion from Hamilton's principle is adopted to develop governing dynamic differential equations for bridge-vehicle interaction system that is treated in the time domain. A numerical model for the traffic-induced vibration of bridges is presented by using finite element method and modal analysis. Decks, web plates, upper and lower flanges of the bridge are idealized as flat shell elements with 5-DOF. Beam elements with 6-DOF are adopted in the FE modeling to idealize the stiffener, the girder, etc. of the bridge. To express the actual behavior of elastomeric bearings in the bridge, the double node with springs is used. In modeling PC decks, the prestressing force is considered in the numerical modeling. Newmark-β method is applied to solve the derived system governing equations of motion as a numerical integration method.

Confirming the reliability of the developed simulation method or algorithm is another important objective of this study, because numerical models can at present mainly serve as development tools to widen the understanding and to guide the development of empirical models. Simulated dynamic wheel loads and bridge responses are therefore compared with experimental results, to verify the validity of the analytical model.

To investigate the relationship between vehicle dynamics and bridge dynamics, the frequency relation between the dynamic wheel load and the bridge response is investigated, and also the correlation between the dynamic factor of the dynamic wheel load and dynamic

increment factor of the bridge responses is examined.

The RC deck is the member that is more easily damaged than other structural members in steel highway bridges due to directly subjected to wheel loads of vehicles. Therefore, the probabilistic assessment of the code specified impact factor for decks of highway bridges are carried out based on the Monte-Carlo simulation (MCS) method, because the rational criterion of performance level of RC decks provides useful assessment tool for decision making related to the inspection, repair, upgrading and replacement of existing steel plate girder bridges based on life-cycle cost.

A pioneering research on the dynamic response of web plates of the two-girder steel bridge is carried out to investigate the effect of deck's deformation on those of web plates, since the investigation on dynamic responses of the web plate can give useful information in solving fatigue and infrasound problems of the two-girder bridge.

To prevent the undesirable vibration at the end-cross beam of multi-girder bridges as well as enhancing the resistance of the expansion joint and the deck slabs near an expansion joint, countermeasures called as an end-cross beam replacement and an end-cross beam reinforcement have been devised and applied. However, advanced researches focused on the two-girder bridges with reinforcing up to cantilevered parts and reinforcing effects on high frequency related to vibration perception of human have not been advanced. Therefore, analytical investigations about reduction effects of high-frequency traffic-induced vibration of a twin-girder bridge by reinforcing end-cross beam are carried out. Another countermeasure against the vibration on highway bridges is the method to reduce the impulsive effect induced by the vehicle running over the bumps at expansion joints. The methods called deck extension and no joint are thus developed. Therefore the vibration reduction effect after removing the bump is investigated.

1.3 State-of-the arts

At the middle of the nineteenth century there was no agreement among engineers over the effect of a moving load on a beam. While some assumed that a load moving with high speed acts like a suddenly applied load and may produce deflections larger than those corresponding to static action, other argued that at very high speeds there was insufficient time for the load to drop through the distance of the expected dynamical deflection.

The very first milestone on vehicle-bridge interaction is started in 1847. Within the framework of a commission investigated by the English queen in 1847, Willis [1] carried out an entire series of laboratory tests as well as some field tests. Based on these tests he formulated a differential equation for the trajectory of a mass of constant magnitude

traversing a massless beam as a function of the speed of the mass. Not being able to solve the equation, Stokes [2] who worked with Willis at Cambridge found the solution in 1849, which discussed the reasons for the collapse of the Chester Railway Bridge. In 1889, Waddell [3] earned the honor of being the first time to treat highway bridges in the same manner as railway bridges distinguished between railways employing steam and electrical locomotives and are based on a great number of experiments.

Over the next century, investigations into bridge dynamics were mainly concerned with developing analytical solutions for simple cases of moving forces, moving masses and moving vehicle model. The moving-force model, in which a vehicle is modeled as a force, is the simplest model whereby researchers can capture the essential dynamic characteristics of a bridge under the action of a moving vehicle, but the interaction between the vehicle and bridge is ignored. Where the inertia of the vehicle cannot be regarded as small, a moving-mass model, in which a vehicle is modeled as a mass, is often adopted instead. However the moving-mass model suffers from its inability to consider the bouncing effect of the moving mass, which is significant in the presence of road surface irregularities or for vehicles running at high speeds. Digital computers introduced a new level of detail in bridge vibration research because the complexities of bridge and vehicle system could be modeled.

In the early 1920's, experimental investigations devoted exclusively to the behavior of highway bridges were carried out for the first time. Fuller described these efforts in 1928 and 1931 [4].

In the early 1950's, Van Eenam [5] performed exhaustive tests on a steel truss bridge. The test involved a total of eight vehicles and 30 measurement points. The results of his tests led him to the conclusion that the speed effect cannot play a significant role in comparison with other influences. In 1957, Biggs et al [6] reported studies of vehicle-bridge dynamics of simply supported bridges traversed by a vehicle with two undamped single mass oscillators. Investigations arising out of the AASHO road test extended these analyses to bridges with more complicated vehicle models [7, 8].

Veletsos and Huang [9] considered a two-dimensional multi-axle tractor-trailor model and lumped mass model of the bridge, and solved the bridge equation of motion by numerical integration. The vehicle model developed by Veletsos and Huang was generally employed to obtain the dynamic response of bridges by many authors.

Effects of bridge vibration due to moving vehicle on human perception were investigated by Kobori and Kajikawa [10] based on the non-stationary random process proposed by Iyengar et al [11]. Komatsu and Kawatani [12] applied vehicle-bridge interaction to a cable stayed bridge, and a series of moving vehicles is considered and the analytical results are verified by comparing with dynamic field test results.

Using the model developed by Veletsos and Huang [9], Gupta and Traill-Nash [13, 14]

investigated the effects of braking and initial bounce of the vehicle for a single span bridge. They idealized the bridge as an orthotropic plate and a beam with lumped masses.

Hayashikawa and Watanabe [15] applied the continuum method of dynamic analysis for a multi-span continuous beam under a concentrated moving load. Honda et al [16] studied the characteristics of roadway surface roughness of bridges to give the basic data of power spectral density (PSD) using dynamic response analysis of bridges under moving vehicles.

Mulcahy [17] utilized an orthotropic plate model of a single span bridge to obtain the dynamic response of bridge of a three-axle tractor-trailor vehicle, and considered the effects of braking and eccentric placement of the vehicle as well as bridge surface roughness.

Recently, Hwang and Nowak [18] developed a procedure for calculation of the dynamic load and it is subsequently used in the development of a reliability based design code. Green and Cebon [19] applied frequency domain calculation procedure using the fast Fourier transform to compute the dynamic response of a bridge to a arbitrary wheel loads. Yang et al [20] discussed the effects of the speed parameters, the vehicle/bridge frequency ratio, and damping of the bridge and roadway roughness on the impact factors. The influencing parameters on the dynamic behavior of a bridge idealized as a three-dimensional model are studied by Kou and Dewolf [21] using the finite element method.

The study by Kawatani and Kim [22] is one of pioneering works on dynamic response analysis of deck slabs of a steel pate girder bridge. The analytical strain responses are verified by comparing with in-field test results, and demonstrated good agreements. Based on the analytical method, the probabilistic assessment on deck slab's impact factor based on simulation technique due to single moving heavy vehicle are also carried out by Kim and Kawatani [23], and proposed the needs of considering effects of bump at expansion joint to impact factor of deck slabs. The effects of vehicle speed on dynamic features of the wheel loads and bridge responses are studied by Kawatani and Kim [24], and the research also investigated those effects on frequency relations between dynamic wheel loads and bridge responses.

A number of studies on reinforcing end parts of steel bridges have been performed to prevent the undesirable vibrations and enhance the resistance of expansion joints and deck slabs near the expansion joints. Chubb and Kennedy [25] observed somewhat clear reduction of the dynamic responses after stiffening end-sway bracing of an existing steel bridge by field test. Yamada and Kawatani [26] investigated the effect of girder-end reinforcement on reducing traffic-induced vibration of a conventional multi-girder steel bridge by analysis, and mainly focused on the reduction effects on responses of main girders and end-sway bracings.

It has been reported that reinforced concrete (RC) end-cross beams can extend life cycle of decks and expansion joints of steel girder bridges by Nanjo et al [27]. Nanjo et al. also suggested the possibility of suppressing traffic-induced undesirable vibrations. Kim and

Kawatani [28] investigated the effectiveness of end-cross beam reinforcement on high-frequency vibration of a two-girder bridge.

It is noteworthy that a detailed historical review can be found in the report of Cantieni [4], even though the detailed review of the literature with respect to the vehicle-bridge interaction is omitted in this paper.

1.4 Brief review of this study

This research work is composed of seven chapters, and the contents of each chapter are organized as follows:

The first chapter contains the introduction and a brief historical review of dynamic phenomena of bridges due to moving vehicles so called traffic-induced vibration of bridges.

The numerical modeling of vehicle-bridge-roadway roughness interaction system is presented based on the Lagrange equation of motion from Hamilton's principle in Chapter 2. The developed governing dynamic differential equations for the bridge-vehicle interaction system are treated in the time domain. The validity of numerical dynamic wheel loads is verified in Chapter 3 by comparing with the in-field test results, and dynamic characteristics of the vehicles are investigated.

In Chapter 4, the relationship between the dynamic response of vehicles and bridges are investigated by means of the experimentally verified analytical method. A pioneering investigation on the probabilistic assessment of deck's impact factors is also carried out based on the Monte-Carlo simulation technique.

A full 3-D dynamic response analyses for a steel two-girder bridge with PC deck slab under vehicles running is carried out to investigate not only dynamic responses of a two-girder bridge but the effect of the elastic deformation at an elastomeric bearing on dynamic responses of local members like web plates and decks in Chapter 5. To verify the validity of the analytical responses, the analytical acceleration responses and power spectra of the bridge members are compared with field test results.

In Chapter 6, the end-cross beam reinforcement taken as a countermeasure reducing traffic-induced vibration is applied to two-girder bridges, and vibration reduction effect is investigated. In addition, removing bumps at expansion joints is considered as another method to reduce the traffic-induced vibration.

Main conclusions obtained through the study are summarized in Chapter 7 with some technical proposals.

References

[1] Willis, R.: An essay on the effects produced by causing weights to travel over elastic bars, Extracted from the report of the commissioners, published as an Addendum in: Barlow, P., A treatise on the strength of timber, Cast and Malleable Iron, John Weale, London, 1851.

[2] Stokes, G. G.: Discussion of a differential equation relating to the breaking of railway bridges, Trans. of the Cambridge Philosophical Society, 8, Part V, No.LII, pp.707, 1849.

[3] Waddell, J. A. L.: New impact formulas needed in designing bridges of various type, Engineering News-Record 81, No.21, 1918.

[4] Cantieni, R.: Dynamic behavior of highway bridges under the passage of heavy vehicles, EMPA Report No. 220, 1992.

[5] Van Eenam, N.: Live load stress measurements on Fort London bridge, Final report, HRB Proc. 31, 1952.

[6] Biggs, J. M., Suer, H. S. and Louw, J. M.: The vibration of simple span highway bridges, ASCE transactions, 124, 291-318, 1959.

[7] The AASHO Road test, Bridge Research, HRB Special report 61D, National Academy of Sciences-National Research Council, Publication 953, 1962.

[8] Fenves, S. J., Veletsos, A. S. and Siess, C. P.: Dynamic studies of the AASHO road test bridges, The AASHO Road test, Bridge Research, HRB Special report 73, National Academy of Sciences-National Research Council, Publication 1012, 83-101, 1962.

[9] Veletsos, A. S. and Huang, T.: Analysis of dynamic response of highway bridges, J. of Engineering Mechanics Div., ASCE, **96**(EM5), 593-620, 1970.

[10] Kobori, T. and Kajikawa, Y.: Human response to bridge vibration under a single moving vehicle, Proc. of JSCE, No.248, 11-23, 1976. *(in Japanese)*

[11] Iyengar, R. N. and Iyengar K. T. S. R.: Probabilistic response analysis to earthquakes, Proc. of ASCE, No.EM3 (paper7321), June 1970.

[12] Komatsu, and Kawatani, M.: Study on dynamic response and impact of cable stayed girder bridges under moving vehicles, Proc. of JSCE, No.275, 13-28, 1978. (in Japanese)

[13] Gupta, R. K. and Traill-Nash, R. W.: Vehicle braking on highway bridges, J. of Engineering Mechanics Div., ASCE, **106**(EM4), 641-658, 1980.

[14] Gupta, R. K.: Dynamic load on highway bridges, J. of Engineering Mechanics Div., ASCE, **106**(EM2), 377-394, 1980.

[15] Hayashikawa, T and Watanabe, N.: Dynamic behavior of continuous beams with moving loads, J. of Engineering Mechanics Div., ASCE, **107**(EM1), 229-246, 1981.

[16] Honda, H., Kajikawa, Y. and Kobori, T.: Spectra of road surface roughness on bridges, J. of Structural Div., ASCE, **108**(ST9), 58-68, 1982.

[17] Mulcahy, N. L.: Bridge response with tractor-trailor vehicle loading, Earthquake

Engineering and Structural Dynamics, 11, 649-665, 1983.

[18] Hwang, E. S. and Nowak, A. S.: Simulation of dynamic for bridges, J. of Structural Engineering, ASCE, 117, 1423-1434, 1991.

[19] Green, M. F. and Cebon, D.: Dynamic response of highway bridges to heavy vehicle loads: Theory and experimental validation, J. of Sound and Vibration, **170**(1), 51-78, 1994.

[20] Yang, Y. B., Liao, S. S. and Lin, B. H.: Impact formulas for vehicles moving over simple and continuous beams, J. of Structural Engineering, ASCE, 121, 1644-1650, 1995.

[21] Kou J. W. and Dewolf, J. T.: Vibrational behavior of continuous span highway bridge-influence variables, J. of Structural Engineering, ASCE, **123**(23), 333-344, 1997.

[22] Kawatani, M. and Kim, C.W.: Effects of gap at expansion joint on traffic-induced vibration of highway bridge, Proc. of Developments in Short and Medium Span Bridge Engineering'98, CSCE, Calgary, Canada, CD-ROM, 1998.

[23] Kim, C. W. and Kawatani, M.: A probabilistic investigation on impact factor of deck slabs of highway bridges, Reliability and optimization of structural systems; Proc. of the 9th IFIP WG7.5 Working Conference on Reliability and Optimization of Structural Systems, Ann Arbor, Michigan, USA, 125-133, 2000.

[24] Kawatani, M. and Kim, C. W.: Computer simulation for dynamic wheel loads of heavy vehicles, Structural Engineering and Mechanics, **12**(4), 409-428, 2001.

[25] Chubb, M. S. and Kennedy Reid, I. L.: Crossbeam replacement, Bridge Modification, Thomas Telford, London, 241-254, 1995.

[26] Yamada, Y. and Kawatani, M.: Analytical study on reduction of traffic-induced vibration due to reinforcement procedure at girder end, J. of Structural Eng., JSCE, 43A, 737-746, 1997. *(in Japanese)*

[27] Nanjo, A., Mori, Y., Sasaki, K., Sonoda, K. and Kiso, S.: Experimental study on RC end cross beams for the seismic resistance of a steel plate girder bridge, J. of Construction Steel, JSSC, **8**, 179-186, 2000. *(in Japanese)*

[28] Kim, C. W. and Kawatani, M.: Reduction of traffic-induced high-frequency vibration of twin-girder bridge by end-cross beam reinforcement, Proc. of Structural Engineers World Congress 2002 (SEWC2002), T1-2-n-2, CD-ROM, Oct. 9-12, 2002, Yokohama, Japan, 2002.

Chapter 2

Analytical procedure of vehicle-bridge interaction system

2.1 Introduction

The vibration of girder bridges under moving vehicles has been widely studied by analytical and numerical methods during the last three decades [1-8]. As analytical methods are often limited to simple moving load problems, many researchers have resorted to various numerical methods, such as the finite element (FE) method. The mode superposition technique has also been widely employed in the analysis for vehicle-bridge interaction problems. The goal of this chapter is to develop a general procedure for determining the vehicle-bridge interaction system. Thus governing equations of the bridge-vehicle interaction system is derived using Lagrange's formulation, and a full three-dimensional numerical model for the traffic-induced vibration of bridges is presented by using FE method and modal analysis.

2.2 Idealization of vehicle

The two-axle cargo truck (one front axle and one rear axle) [9-10] is idealized as a vehicle of seven degree-of-freedom (7DOF) [see Fig. 2-1(a)]. The three-axle dump truck (one front axle and two rear axles) [11-12] is idealized as a vehicle model of eight degree-of-freedom (8DOF) [see Fig. 2-1(b)]. The vehicle body itself is considered to be rigid and supported by a set of linear springs and dashpots attached to each axle.

In Fig. 2-1, Z_{v11}, Z_{v12}, Z_{v22}, θ_{xv11}, θ_{xv12}, θ_{xv22}, θ_{yv11} and θ_{yv22} refer to bounce, parallel hop of front axle, parallel hop of rear axle, rolling, axle tramp of front axle, axle tramp of rear axle, pitching and axle windup motion of the rear axle of the vehicle model, respectively. m_{v11}, m_{v12} and m_{v22} indicate the concentrated mass of the vehicle body, front axle and rear axle, respectively. K_{vmku} and C_{vmku} are the spring constant and damping coefficient of a vehicle; the subscript k is the index for indicating vehicle body and axle ($k=1, 2$ indicating vehicle body and axle, respectively), m is the index for positions of axles or tires (if $k=1$ then $m=1, 2$ indicating front and rear axle, respectively; if $k=2$ then $m=1, 2, 3$ indicating the tire at the front-axle, front and rear tires of the rear axle, respectively) and u is the index for indicating left and right side of a vehicle ($u=1, 2$ indicating left and right side, respectively). The sign is taken as positive if the direction of a deformation is downward, the pitching is occurred from rear axle to front axle and the rolling is generated from the right side to the left side.

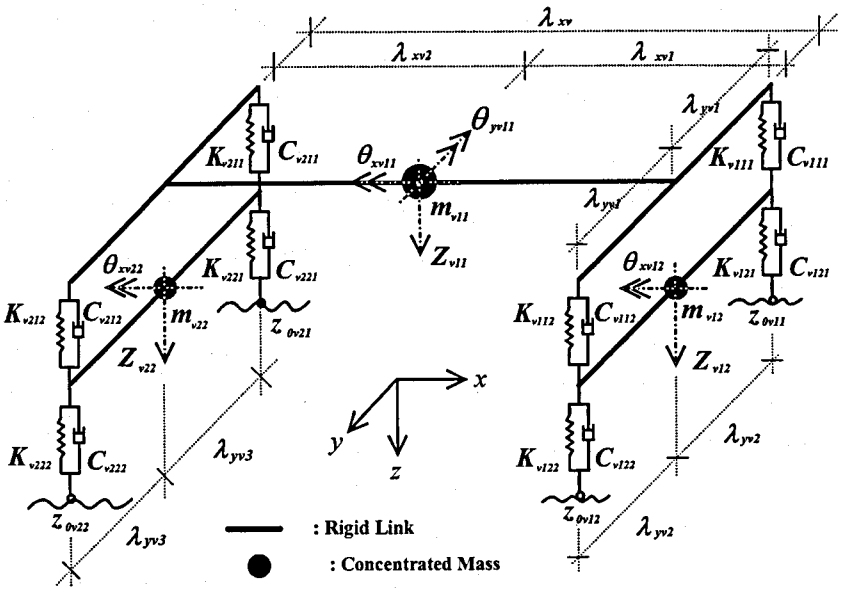

a) Two-axle vehicle with 7DOF

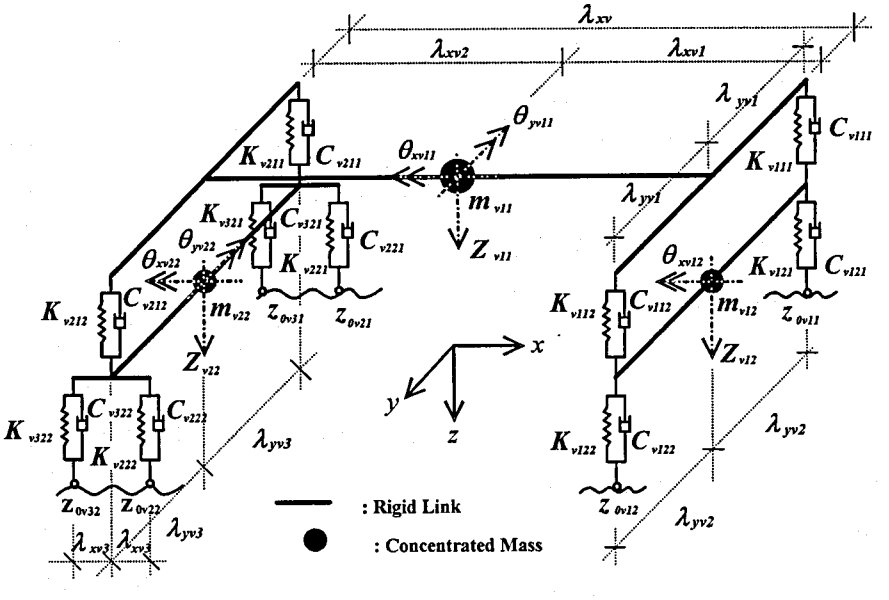

b) Three-axle vehicle with 8DOF

Fig. 2-1 Ideaized vehicle models

2.3 Idealization of bridge system

2.3.1 General

The finite element (FE) method and modal analysis are adopted as tools for idealizing bridges for dynamic response analysis.

To idealize members of the bridge super-structure, beam and flat shell element is used in bridge modeling [13-16]. Just as the two-dimensional rigid-jointed frame member is a combination of bar and beam elements, the flat shell element is a combination of in-plane and plate-bending elements [13-16].

It will be stated by many shell experts that when we compare the exact solution of a shell approximated by flat facets to the exact solution of a truly curved shell, considerable differences in the distribution of bending moments, etc., occur. It is arguable if this is true, but for simple elements the discretization error is approximately of the same order and excellent result can be obtained with flat shell element approximation [17-18].

It has been reported that, for many practical purposes, the flat element approximation gives very adequate answers and also permits an easy coupling with edge beam and rib members [18]. Indeed, in many practical problems the structure is in fact composed of flat surfaces, at least in part, and these can be simply reproduced. For these backgrounds, the flat shell element is adopted as an element to solve responses of web plates as well as decks of highway bridges in this study.

The concept of matrix condensation is a well-known procedure for reducing the number of unknown displacements in a static problem. For dynamic analysis, a similar type of condensation was introduced by Guyan [19], which brings in an additional approximation. To improve the calculation efficiency a process known as Guyan reduction is performed [19].

The QR method (or QR factorization) is adopted as a procedure for obtaining all the eigen-values of a symmetric matrix [20, 21].

The lumped mass system and Rayleigh damping [22] is adopted to form mass and damping matrices of the bridge model, respectively.

2.3.2 Double nodes

The effect of the hinges and supports like pin, roller, elastomeric bearings, etc. can be conveniently considered by means of double nodes defined as two nodes of independence that have the same coordinate [23].

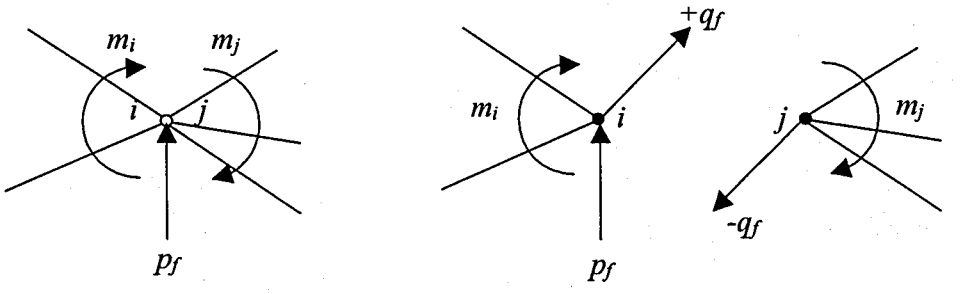

(a) Beam element with a hinge (b) Forces at the hinge

Fig. 2-2 Element end releases

(1) Pin support

When two nodes i and j are connected with a pin as shown in Fig. 2.2(a), the external forces act on the rigid node are p_f, m_i, and m_j. If the unknown force acting on nodes i and j of the structure divided into two groups is q_f as shown in Fig 2.2(b), then the system stiffness matrix can be written as Eq. (2.1). Adding the j^{th} row to the i^{th} row of the Eq. (2.1) and introducing the compatibility condition of $w_i=w_j$ at the nodes i and j introduce the deletion of the unknown force q_f, and the system stiffness matrix for structure with the pin support at a node becomes as Eq. (2.2).

$$\begin{matrix} \\ i^{th}\ Row \\ (i+1)^{th}\ Row \\ j^{th}\ Row \\ (j+1)^{th}\ Row \\ \\ \end{matrix}\begin{Bmatrix} \vdots \\ p_f+q_f \\ m_i \\ -q_f \\ m_j \\ \vdots \end{Bmatrix} = \begin{bmatrix} \vdots & \vdots & \vdots & \vdots & \vdots & \vdots \\ \cdots & K_{iw1} & K_{i\theta 1} & 0 & 0 & \cdots \\ \cdots & K_{iw2} & K_{i\theta 2} & 0 & 0 & \cdots \\ \cdots & 0 & 0 & K_{jw1} & K_{j\theta 1} & \cdots \\ \cdots & 0 & 0 & K_{jw2} & K_{j\theta 2} & \cdots \\ \vdots & \vdots & \vdots & \vdots & \vdots & \vdots \end{bmatrix} \begin{Bmatrix} \vdots \\ w_i \\ \theta_i \\ w_j \\ \theta_j \\ \vdots \end{Bmatrix} \tag{2.1}$$

$$\boldsymbol{K} = \begin{bmatrix} \vdots & \vdots & \vdots & \vdots & \vdots & \vdots \\ \cdots & K_{iw1}+K_{jw1} & K_{i\theta 1} & 0 & K_{j\theta 1} & \cdots \\ \cdots & K_{iw2} & K_{i\theta 2} & 0 & 0 & \cdots \\ \cdots & 0 & 0 & 1 & 0 & \cdots \\ \cdots & K_{jw2} & 0 & 0 & K_{j\theta 2} & \cdots \\ \vdots & \vdots & \vdots & \vdots & \vdots & \vdots \end{bmatrix} \tag{2.2}$$

(2) Elastic support

In the case that two nodes are connected with the elastomeric bearing, the element stiffness matrix of the spring equivalent to the rubber is expressed as Eq. (2.3) [24].

$$
\boldsymbol{K}_{sp.} = \begin{bmatrix}
k_x & & & & & & & & & & & \\
0 & k_y & & & & & & & & & & \\
0 & 0 & k_z & & & & & & & & & \\
0 & 0 & 0 & k_{\theta x} & & & & & & & & \\
0 & 0 & 0 & 0 & k_{\theta y} & & & & & & & \\
0 & 0 & 0 & 0 & 0 & k_{\theta z} & & & & & & \\
-k_x & 0 & 0 & 0 & 0 & 0 & k_x & & & & & \\
0 & -k_y & 0 & 0 & 0 & 0 & 0 & k_y & & & & \\
0 & 0 & -k_z & 0 & 0 & 0 & 0 & 0 & k_z & & & \\
0 & 0 & 0 & -k_{\theta x} & 0 & 0 & 0 & 0 & 0 & k_{\theta x} & & \\
0 & 0 & 0 & 0 & -k_{\theta y} & 0 & 0 & 0 & 0 & 0 & k_{\theta y} & \\
0 & 0 & 0 & 0 & 0 & -k_{\theta z} & 0 & 0 & 0 & 0 & 0 & k_{\theta z}
\end{bmatrix} \quad \text{sym.}
$$

(2.3)

where,

k_x, k_y, k_z : Spring constant of x, y and z directions, respectively (kN/m)

$k_{\theta x}, k_{\theta y}, k_{\theta z}$: Rotational spring of x, y and z directions, respectively ($kN \cdot m/rad$).

2.4 Assumptions

The assumptions considered in this study are:

1) The bridge follows Hooke's law, Navier's hypothesis, Saint-Venant's principle and small-deflection theory,
2) The ground acceleration and support settlement of the bridge are not considered.
3) The bridge is initially at rest before vehicle enters the span.
4) The vehicle speed and path is constant.
5) The vehicle body is treated as a rigid body: the elastic behavior of the body is not considered.
6) Suspension springs are assumed to be linearly elastic and the damping of the suspension system is considered to be viscous.
7) The damping of the elastomeric bearing itself is not considered.

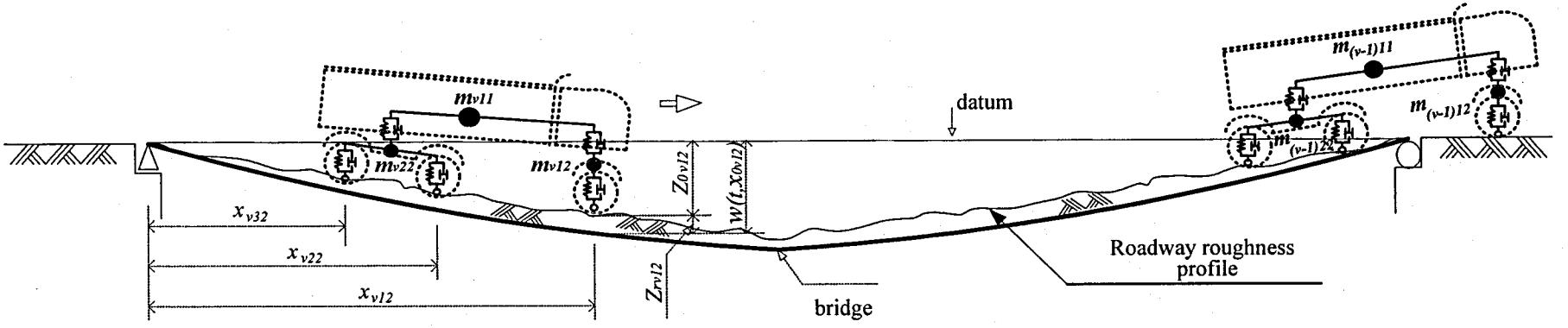

Fig. 2-3 General bridge-vehicle interaction system

2.5 Equation of motion for bridge-vehicle interaction system

Figure 2-3 is the idealized bridge-vehicle interaction system with pavement roughness in deformed state [25]. The variable z_{0vmu} denotes the vehicle displacement from the datum to the tire. The longitudinal position of the tire location x_{vmu} is relative to the bridge entry. The pavement roughness of the bridge at a tire is denoted by z_{rvmu}. The variable $w(t,x_{vmu})$ is the elastic deformation of the bridge at the location x_{vmu} of a time t. The subscript v indicates the v^{th} vehicle on the bridge. The subscripts m and u are the same indices explained in section 2.2

The method called Lagrange equation of motion has been known as one of the most popular methods to formulate a dynamic system since French mathematician Lagrange discovered a relationship that provides a method of great power and versatility for the formulation of the equations of motion for any dynamical system. Therefore, governing equations of the bridge-vehicle interaction system are derived from the energy method with Lagrange equation of motion as shown in Eq. (2.4) [26, 27].

$$\frac{d}{dt}\left(\frac{\partial T}{\partial \dot{q}_i}\right) - \frac{\partial T}{\partial q_i} + \frac{\partial V}{\partial q_i} = \frac{\partial U_d}{\partial \dot{q}_i} \tag{2.4}$$

where, T is kinematic energy of the system; V, potential energy of the system; U_d, dissipation energy of the system; q_i, the i^{th} generalized co-ordinate.

The kinematic energy, potential energy including strain energy and dissipation energy due to viscous damping of the bridge-vehicle interaction system are expressed in a set of generalized coordinates as follows [28]:

$$T = \frac{1}{2}\left[\dot{\boldsymbol{D}}^T \boldsymbol{M}_b \dot{\boldsymbol{D}} + \sum_{v=1}^{nveh}\left\{\sum_{k=1}^{2}\left(m_{v1k}\dot{Z}_{v1k}{}^2 + J_{xv1k}\dot{\theta}_{xv1k}{}^2 + J_{yvkk}\dot{\theta}_{yvkk}{}^2\right) + m_{v22}\dot{Z}_{v22}{}^2 + J_{xv22}\dot{\theta}_{xv22}{}^2\right\}\right] \tag{2.5}$$

$$V = \frac{1}{2}\left[\boldsymbol{D}^T \boldsymbol{K}_b \boldsymbol{D} + \sum_{v=1}^{nveh}\sum_{m=1}^{3}\sum_{u=1}^{2}\left\{K_{vm1u}R_{vm1u}{}^2 + K_{vm2u}\left(R_{vm2u} - Z_{0vmu}\right)^2 + 2\cdot W_{vmu}Z_{0vmu}\right\}\right] \tag{2.6}$$

$$U_d = \frac{1}{2}\left[\dot{\boldsymbol{D}}^T \boldsymbol{C}_b \dot{\boldsymbol{D}} + \sum_{v=1}^{nveh}\sum_{m=1}^{3}\sum_{u=1}^{2}\left\{C_{vm1u}\dot{R}_{vm1u}{}^2 + C_{vm2u}\left(\dot{R}_{vm2u} - \dot{Z}_{0vmu}\right)^2\right\}\right] \tag{2.7}$$

where,

nveh: Numbers of vehicle on the bridge

$$Z_{0vmu} = w(t, x_{vmu}) - Z_{rvmu} \tag{2.8}$$

$$R_{vmku} = \begin{cases} Z_{v11} - (-1)^m \lambda_{xvm}\theta_{yv11} - (-1)^u \lambda_{yv1}\theta_{xv11} - Z_{vm2} + (-1)^u \lambda_{yv(m+1)}\theta_{xvm2} \\ \qquad\qquad for \quad m=1,\ 2;\ k=1;\ u=1,\ 2 \\ Z_{v12} - (-1)^u \lambda_{yv2}\theta_{xv12} \\ \qquad\qquad for \quad m=1; \quad k=2;\ u=1,\ 2 \\ Z_{v22} + (-1)^m \lambda_{xv3}\theta_{yv2} - (-1)^u \lambda_{yv3}\theta_{xv22} \\ \qquad\qquad for \quad m=2,\ 3;\ k=2;\ u=1,\ 2 \\ 0 \qquad\qquad otherwise \end{cases} \tag{2.9}$$

$$W_{vmu} = \begin{cases} \frac{1}{2} g\left[(1 - \frac{\lambda_{xv1}}{\lambda_{xv}}) m_{v11} + m_{v12} \right] & m=1; \quad u=1,\ 2 \\ \frac{1}{4} g\left[(1 - \frac{\lambda_{xv2}}{\lambda_{xv}}) m_{v11} + m_{v22} \right] & m=2,\ 3;\ u=1,\ 2 \\ 0 & otherwise \end{cases} \tag{2.10}$$

The superscript dot in Eq. (2.4), Eq. (2.5) and Eq. (2.7) denotes differential with respect to time. J in Eq. (2.5) and g in Eq. (2.10) indicate mass moment of inertia of the vehicle and gravity, respectively. In Eqs. (2.5)-(2.7), $\boldsymbol{D}$ and $\dot{\boldsymbol{D}}$ indicate displacement and velocity vectors of the bridge, respectively; $\boldsymbol{M}_b$ and $\boldsymbol{K}_b$ respectively indicate reduced mass and stiffness matrices [19] of the bridge; $\boldsymbol{C}_b$, damping matrix of the bridge derived from assumption of linear relation between the mass and stiffness matrices, which can be expressed as Eq. (2.11) [22]:

$$\boldsymbol{C}_b = p\boldsymbol{M}_b + q\boldsymbol{K}_b \tag{2.11}$$

where,

$$p = \frac{2\omega_{b1}\omega_{b2}(h_{b1}\omega_{b2} - h_{b2}\omega_{b1})}{\omega_{b2}^2 - \omega_{b1}^2} \tag{2.12}$$

$$q = \frac{2(h_{b2}\omega_{b2} - h_{b1}\omega_{b1})}{\omega_{b2}^2 - \omega_{b1}^2} \tag{2.13}$$

In Eqs. (2.12) and (2.13), ω_{b1} and $\omega_{b2}$are the first and second natural circular frequencies of the bridge system, respectively; h_{b1} and h_{b2}, damping constants according to two modes of vibration with natural circular frequencies of ω_{b1} and ω_{b2}. In this study, h_{b2} is assumed to have same value with h_{b1} because of its difficulty to estimate the second damping constant h_{b2} [20].

The displacement vector of the bridge is written generally in terms of the normal coordinate as shown in Eq. (2.14).

$$\boldsymbol{D} = \sum_{j=1}^{n} \phi_j a_j = \boldsymbol{\Phi a} \tag{2.14}$$

where, $\boldsymbol{\Phi}$ and $\boldsymbol{a}$ are the modal matrix and the generalized displacement vector of the bridge, respectively.

The displacement of the bridge $w(t,x_{vmu})$ can be obtained by combination of the displacement and distribution vectors as shown in Eq. (2.15).

$$w(t, x_{vmu}) = \boldsymbol{\Psi}_{vmu}{}^{T} \boldsymbol{D} \tag{2.15}$$

where, Ψ_{vmu} is the distribution vector which delivers wheel loads of the v^{th} vehicle at a plate element to each node of the element, and represented as Eq.(2.16).

$$\boldsymbol{\Psi}_{vmu} = \left\lfloor 0;\cdots;0;\Psi_{k,vmu}(t);\Psi_{k+1,vmu}(t);\Psi_{k+2,vmu}(t);\Psi_{k+3,vmu}(t);\cdots;0 \right\rfloor \tag{2.16}$$

The final formulation of the governing differential equations for the bridge-vehicle interaction system is obtained from the relations in Eq. (2.4) to Eq. (2.16):

$$\overline{\boldsymbol{M}}_b\ddot{\boldsymbol{a}}+\overline{\boldsymbol{C}}_b\dot{\boldsymbol{a}}+\overline{\boldsymbol{K}}_b\boldsymbol{a}$$
$$+\boldsymbol{\Phi}^T\sum_{v=1}^{nveh}\sum_{m=1}^{3}\sum_{u=1}^{2}\boldsymbol{\Psi}_{vmu}\left\{\left(C_{vm2u}\cdot\boldsymbol{\Psi}_{vmu}{}^T\boldsymbol{\Phi}\dot{\boldsymbol{a}}+K_{vm2u}\boldsymbol{\Psi}_{vmu}{}^T\boldsymbol{\Phi}\boldsymbol{a}\right)-\left(C_{vm2u}\dot{R}_{vm2u}+K_{vm2u}R_{vm2u}\right)\right\} \tag{2.17}$$
$$=\boldsymbol{\Phi}^T\sum_{v=1}^{nveh}\sum_{m=1}^{3}\sum_{u=1}^{2}\boldsymbol{\Psi}_{vmu}\left(W_{vmu}+C_{vm2u}\cdot\dot{Z}_{rvmu}+K_{vm2u}\cdot Z_{rvmu}\right)$$

$$\sum_{v=1}^{nveh}\left\{m_{v11}\ddot{Z}_{v11}+\sum_{m=1}^{2}\sum_{u=1}^{2}\left(C_{vm1u}\dot{R}_{vm1u}+K_{vm1u}R_{vm1u}\right)\right\}=0 \tag{2.18}$$

$$-\sum_{v=1}^{nveh}\left[\sum_{u=1}^{2}\left\{\left(C_{v12u}\boldsymbol{\Psi}_{v1u}{}^T\boldsymbol{\Phi}\dot{\boldsymbol{a}}+K_{v12u}\boldsymbol{\Psi}_{v1u}{}^T\boldsymbol{\Phi}\boldsymbol{a}\right)+\sum_{k=1}^{2}(-1)^k\left(C_{v1ku}\dot{R}_{v1ku}+K_{v1ku}R_{v1ku}\right)\right\}\right.$$
$$\left.-m_{v12}\ddot{Z}_{v12}\right] \tag{2.19}$$
$$=-\sum_{v=!}^{nveh}\sum_{u=1}^{2}\left(C_{v12u}\dot{Z}_{rv1u}+K_{v12u}Z_{rv1u}\right)$$

$$-\sum_{v=1}^{nveh}\left[\sum_{m=2}^{3}\sum_{u=1}^{2}\left\{\left(C_{vm2u}\boldsymbol{\Psi}_{vmu}{}^T\boldsymbol{\Phi}\dot{\boldsymbol{a}}+K_{vm2u}\boldsymbol{\Psi}_{vmu}{}^T\boldsymbol{\Phi}\boldsymbol{a}\right)-\sum_{k=1}^{2}(-1)^k\left(C_{vmku}\dot{R}_{vmku}+K_{vmku}R_{vmku}\right)\right\}\right.$$
$$\left.-m_{v22}\ddot{Z}_{v22}\right] \tag{2.20}$$
$$=-\sum_{v=1}^{nveh}\sum_{m=2}^{3}\sum_{u=1}^{2}\left(C_{vm2u}\dot{Z}_{rvmu}+K_{vm2u}Z_{rvmu}\right)$$

$$\sum_{v=1}^{nveh}\left\{m_{v11}\lambda_{yv1}{}^2\ddot{\theta}_{xv11}-\sum_{m=1}^{2}\sum_{u=1}^{2}(-1)^u\lambda_{yv1}\left(C_{vm1u}\dot{R}_{vm1u}+K_{vm1u}R_{vm1u}\right)\right\}=0 \tag{2.21}$$

$$\sum_{v=1}^{nveh}\left[\sum_{u=1}^{2}\left\{(-1)^u\lambda_{yv2}\left(C_{v12u}\boldsymbol{\Psi}_{v1u}{}^T\boldsymbol{\Phi}\dot{\boldsymbol{a}}+K_{v12u}\boldsymbol{\Psi}_{v1u}{}^T\boldsymbol{\Phi}\boldsymbol{a}\right)\right.\right.$$
$$\left.\left.-\sum_{k=1}^{2}(-1)^k(-1)^u\lambda_{yv2}\left(C_{v1ku}\dot{R}_{v1ku}+K_{v1ku}R_{v1ku}\right)\right\}+m_{v12}\lambda_{yv2}{}^2\ddot{\theta}_{xv12}\right] \tag{2.22}$$
$$=\sum_{v=1}^{nveh}\sum_{u=1}^{2}(-1)^u\lambda_{yv2}\left(C_{v12u}\dot{Z}_{rv1u}+K_{v12u}Z_{rv1u}\right)$$

$$\sum_{v=1}^{nveh}\left[\sum_{m=2}^{3}\sum_{u=1}^{2}(-1)^{u}\left\{\lambda_{yv3}\left(C_{vm2u}\boldsymbol{\Psi}_{vmu}{}^{T}\boldsymbol{\Phi}\dot{\boldsymbol{a}}+K_{vm2u}\boldsymbol{\Psi}_{vmu}{}^{T}\boldsymbol{\Phi}\boldsymbol{a}\right)\right.\right.$$
$$\left.\left.-\sum_{k=1}^{2}(-1)^{k}\lambda_{yv3}\left(C_{vmku}\dot{R}_{vmku}+K_{vmku}R_{vmku}\right)\right\}+m_{v22}\lambda_{yv3}{}^{2}\ddot{\theta}_{xv22}\right] \tag{2.23}$$
$$=\sum_{v=1}^{nveh}\sum_{m=2}^{3}\sum_{u=1}^{2}(-1)^{u}\lambda_{yv3}\left(C_{vm2u}\dot{Z}_{rvmu}+K_{vm2u}Z_{rvmu}\right)$$

$$\sum_{v=1}^{nveh}\left\{m_{v11}\lambda_{xv1}\lambda_{xv2}\ddot{\theta}_{yv11}-\sum_{m=1}^{2}\sum_{u=1}^{2}(-1)^{m}\lambda_{xvm}\left(C_{vm1u}\dot{R}_{vm1u}+K_{vm1u}R_{vm1u}\right)\right\}=0 \tag{2.24}$$

$$-\sum_{v=1}^{nveh}\left[\sum_{m=2}^{3}\sum_{u=1}^{2}(-1)^{m}\lambda_{xv3}\left\{\left(C_{vm2u}\boldsymbol{\Psi}_{vmu}{}^{T}\boldsymbol{\Phi}\dot{\boldsymbol{a}}+K_{vm2u}\boldsymbol{\Psi}_{vmu}{}^{T}\boldsymbol{\Phi}\boldsymbol{a}\right)-\left(C_{vm2u}\dot{R}_{vm2u}+K_{vm2u}R_{vm2u}\right)\right\}\right.$$
$$\left.-m_{v22}\lambda_{xv3}{}^{2}\ddot{\theta}_{yv22}\right] \tag{2.25}$$
$$=-\sum_{v=1}^{nveh}\sum_{m=2}^{3}\sum_{u=1}^{2}(-1)^{m}\lambda_{xv3}\left(C_{vm2u}\dot{Z}_{rvmu}+K_{vm2u}Z_{rvmu}\right)$$

where, $\overline{\boldsymbol{M}}_b$, $\overline{\boldsymbol{C}}_b$ and $\overline{\boldsymbol{K}}_b$ in Eq. (2.17) refer to normalized mass, damping and stiffness matrices, respectively: $\overline{\boldsymbol{M}}_b=\boldsymbol{\Phi}^T\boldsymbol{M}_b\boldsymbol{\Phi}$; $\overline{\boldsymbol{C}}_b=\boldsymbol{\Phi}^T\boldsymbol{C}_b\boldsymbol{\Phi}$; $\overline{\boldsymbol{K}}_b=\boldsymbol{\Phi}^T\boldsymbol{K}_b\boldsymbol{\Phi}$.

The time varying wheel loads at each tire of the vehicle are estimated from the following relationship:

$$P_{vmu}(t)=W_{vmu}+C_{vm2u}\left[\dot{R}_{vm2u}-\left(\boldsymbol{\Psi}_{vmu}^{T}\boldsymbol{\Phi}\ \dot{\boldsymbol{a}}-\dot{Z}_{rvmu}\right)\right]$$
$$+K_{vm2u}\left[R_{vm2u}-\left(\boldsymbol{\Psi}_{vmu}^{T}\boldsymbol{\Phi}\ \boldsymbol{a}-Z_{rvmu}\right)\right];\quad \mathrm{m}=1,2,3 \tag{2.26}$$

The equations of the bridge-vehicle interaction are represented as following matrix formation by combining Eqs. (2.17)-(2.26):

$$\boldsymbol{M}_s\ddot{\boldsymbol{W}}+\boldsymbol{C}_s\dot{\boldsymbol{W}}+\boldsymbol{K}_s\boldsymbol{W}=\boldsymbol{F}_s \tag{2.27}$$

where, $\boldsymbol{M}_s$, $\boldsymbol{C}_s$ and $\boldsymbol{K}_s$ indicate the mass, damping and stiffness matrices of the bridge-vehicle

interaction system, respectively. The $\ddot{W}$, $\dot{W}$, W and F_s respectively refer to acceleration, velocity, displacement and force vectors of the system. Details about the system matrices are described in Appendix.

By eliminating elements of the column and row related to variable θ_{yv22} in the system matrices and replacing 1/4 of Eq. (2.10) to 1/2, the Eq. (2.27) can be applied to the bridge-vehicle interaction problem under two-axle vehicle (7DOF vehicle) running. The equation becomes applicable to the vehicle running on the rigid roadway by neglecting matrices and variables related to the bridge response.

2.6 Dynamic response analysis using Newmark's β method

The dynamic equation for the vehicle-bridge interaction derived in the section 2.5 is a non-stationary dynamic problem since the coefficient matrices of the equation vary according to the vehicle position. Therefore the matrices must be updated at every time step. But within every time step, the system maintains the linear properties. An unconditionally stable implicit numerical integration method can be used to solve the system equations (see Eq. (2.27) or Eq.(A-1)). In this study, the simultaneous differential equations of the bridge-vehicle interaction system are solved by the Newmark's β method as a numerical integration method [29].

In Fig. 2-4, the flow chart of the traffic-induced vibration analysis of bridges due to vehicle series as well as a single vehicle is appeared. The flow chart of the subroutine for dynamic response analysis by means of the iterative process (Newmark's β method) is shown in Figs. 2-5 and 2-6. The algorithm includes a process considering the randomness of influencing factors to dynamic responses combined with MCS technique.

The algorithm can consider the randomness of the vehicle speed, the roadway surface roughness, bump heights, the axle weight, spring constant according to the axle weight and the traveling position of vehicles.

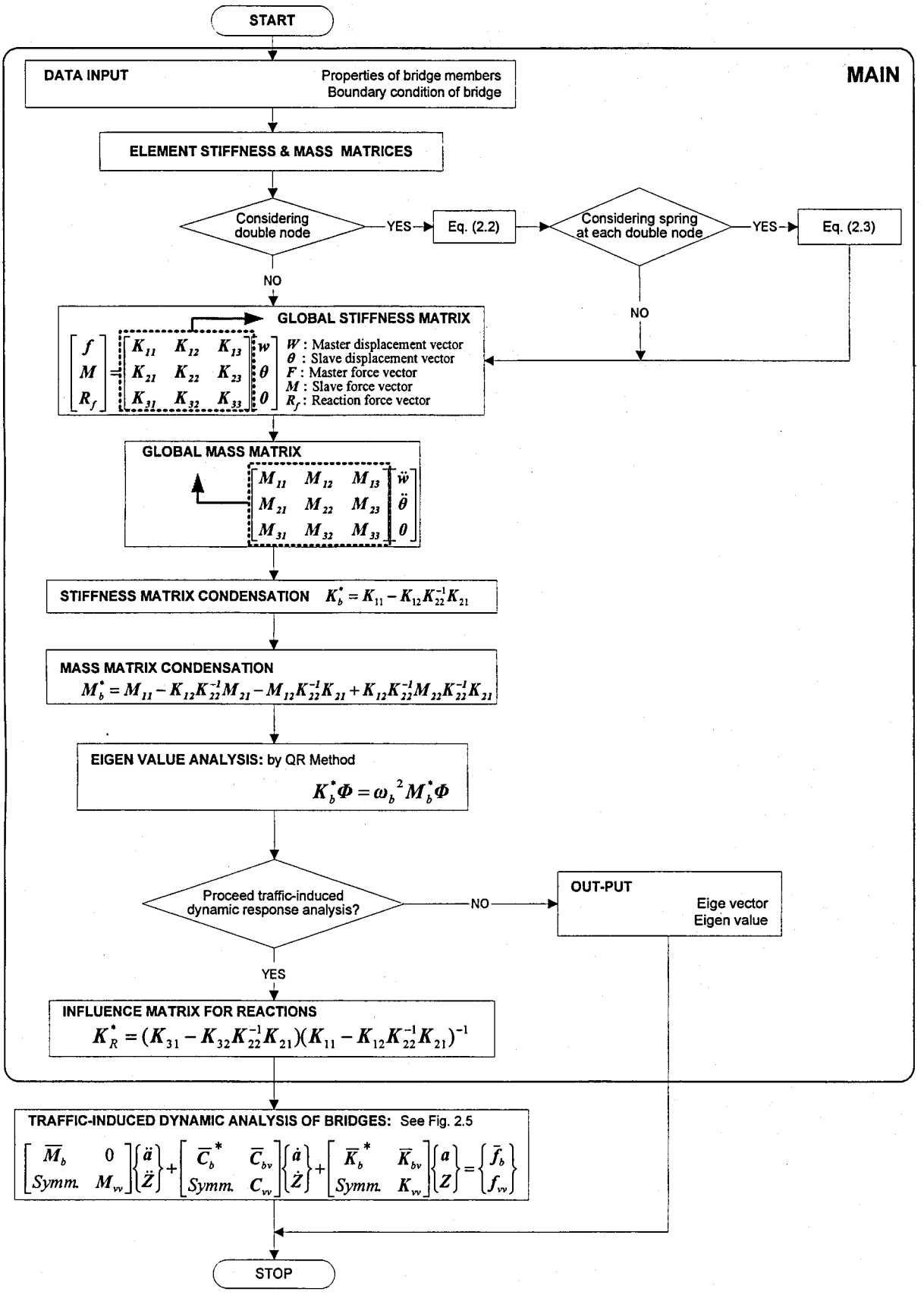

Fig. 2-4 Flow chart for traffic-induced dynamic analysis of bridges; Main algorithm

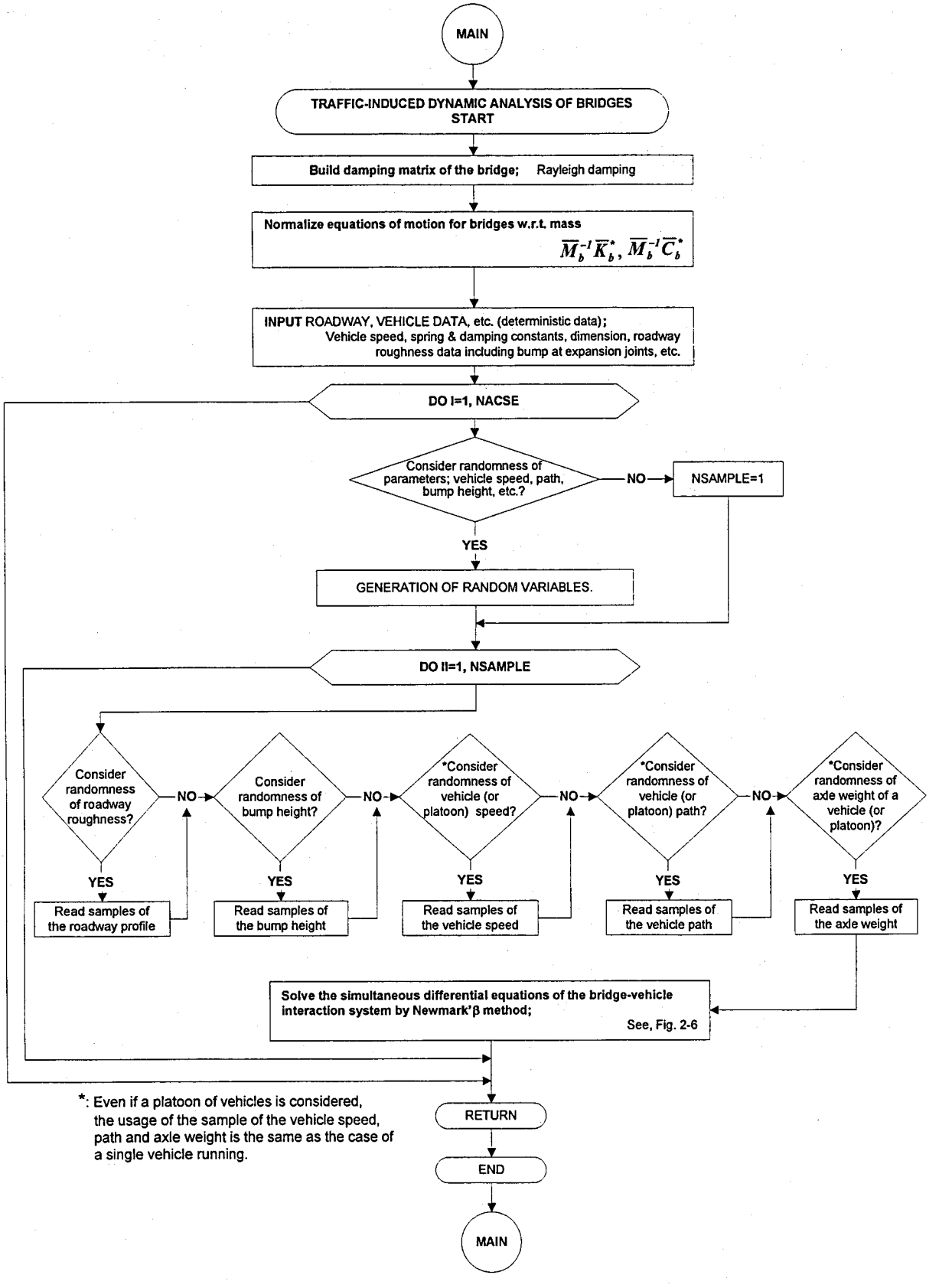

Fig. 2-5 Flow chart for dynamic response analysis of bridge due to a single vehicle as well as vehicle series

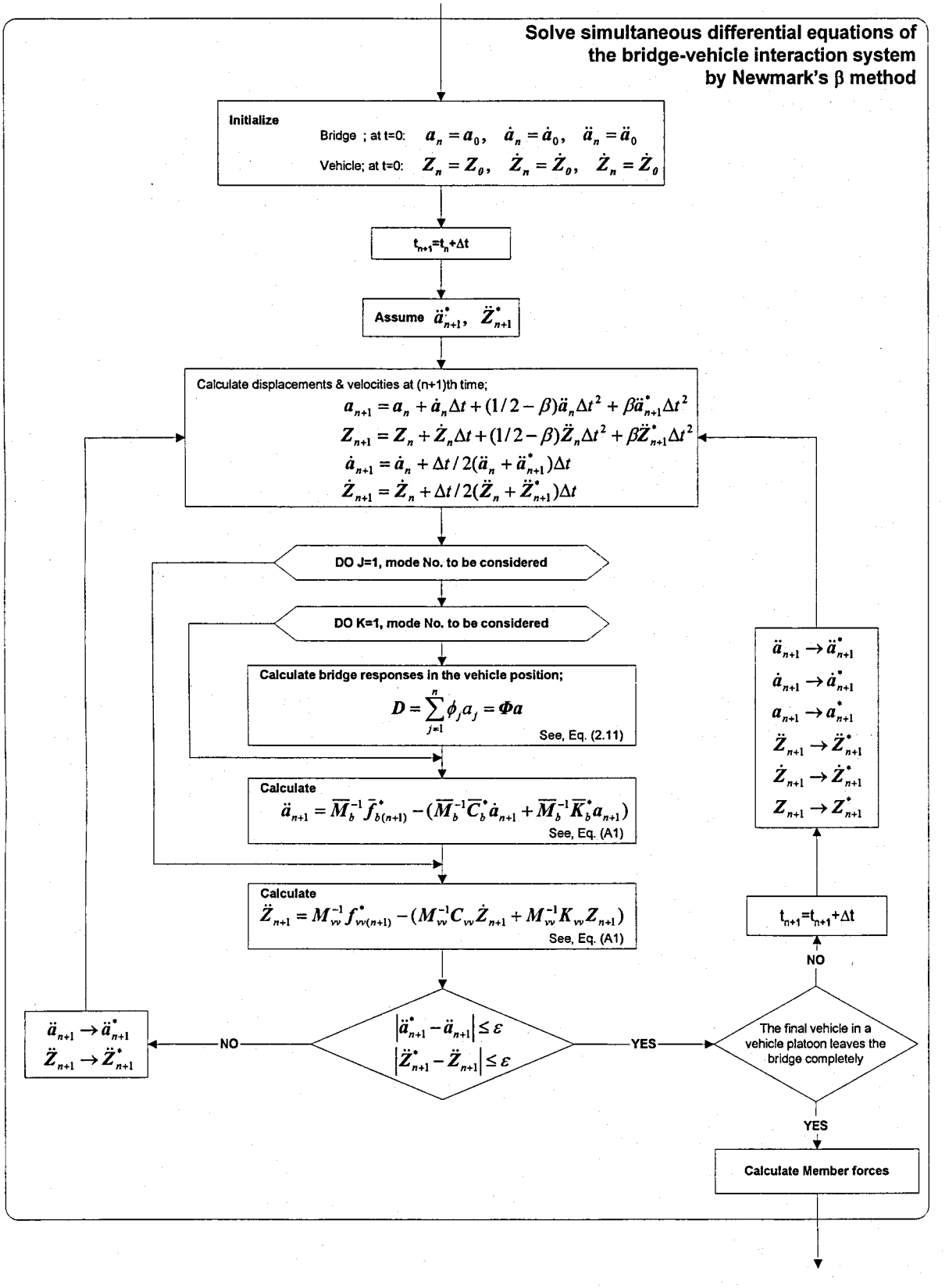

Fig. 2-6 Flow chart for numerical integration method (Newmark's β method) for traffic-induced vibration of bridges

References

[1] Frỳba, L.: Vibration of Solids and Structures under Moving Loads. London, Thomas Telford, 1999.

[2] Yang, Y. B. and Lin B. H.: Vehicle-bridge interaction analysis by dynamic condensation method, Journal of Structural Engineering, **121**(11), 1636-1643, 1995.

[3] Esmailzadeh, E. and Ghorashi, M.: Vibration analysis of a Timoshenko beam subjected to a travelling mass, Journal of Sound and Vibration, **199**(4), 615-628, 1997.

[4] Chatterjee, P. K., Datta, T. K. and Surana, C. S.: Vibration of continuous bridges under moving vehicles, Journal of Sound and Vibration, **169**(5), 619-632, 1994.

[5] Huang, D. Z. and Wang, T. L.: Vibration of highway steel bridges with longitudinal grades Computers and Structures, **69**(2), 235-245, 1998.

[6] Kou, J. W. and DeWolf, J. T.: Vibrational behavior of continuous span highway bridge-influencing variables, J. of Structural Eng., ASCE, **123**(3), 333-344, 1997.

[7] Green, M. F. and Cebon, D.: Dynamic interaction between heavy vehicles and highway bridges, Computers and Structures, **62**(2), 253-264, 1997.

[8] Pesterev, A. V. and Bergman, L. A.: Response of elastic continuum carrying moving linear oscillator, J. of Eng. Mechs., ASCE, **123**(8), 878-884, 1997.

[9] Hoogvelt, R. B. J. and Ruijs, P. A. J.: OECD-IR6 DIVINE Element 4. Computer simulation of heavy vehicle dynamic wheel loads, TNO Report 97.OR.016.1/H/PR, TNO, Delft, The Netherlands, 1997.

[10]Technical Report, DSTI/DOT/RTR/IR6(98)1FINAL, OECD, 1998.

[11]Kawatani, M. and Kim, C. W.: Effects of gap at expansion joint on traffic-induced vibration of highway bridge, Proc. of Developments in short and medium span bridge engineering'98 Calgary, Canada: CSCE, 1998, CD-ROM.

[12]Kim, C. W. and Kawatani, M.: A comparative study on dynamic wheel loads of multi-axle vehicle and bridge responses, Proc. of DETC'01 ASME 2001 Design Engineering Technical Conference and Computers and Information in Engineering Conference Pittsburgh, USA, ASME, 2001, CD-ROM.

[13]Bathe, K. J.: Finite element procedures in engineering analysis, Prentice-Hall, New York, 1982.

[14]Kim, C.W.: An experimental and analytical study for traffic-induced vibration on roadway bridges, Ph.D. Thesis, Chung-Ang University, Korea, 28-33, 1997.

[15]Washitsu, K., Miyamoto, H., Yamada, Y., Yamamoto, Y. and Kawai, T.: Handbook of the finite element method-II: Application, Baihukan, 1981. *(in Japanese)*

[16]Washitsu, K., Miyamoto, H., Yamada, Y., Yamamoto, Y. and Kawai, T.: Handbook of the finite element method-I: Fundamental, Baihukan, 1981. *(in Japanese)*

[17]Zienkiewicz, O.C. and Taylor, R.L.: The finite element method, Vol.2, Butterworth-Heinemann, Oxford, 2000.

[18]Ciarlet, P. G.: Conforming finite element method for shell problem. In J. Whiteman (ed.), The mathematics of finite elements and application, Vol.II, pp.105-123, Academic Press, London, 1977.

[19]Guyan, R. J.: Reduction of stiffness and mass matrices, AIAA J, **3**(2), 380, 1965.

[20]Weaver, W, Jr. and Johnston, P. R.: Structural dynamics by finite elements, Prentice-Hall, New Jersey, USA, 1987.

[21]Golub, G. and Van Loan, C.: *Matrix Computations*, Johns Hopkins University Press, Baltimore, MD, 2nd edition, 1989.

[22]Agabein, M. E.: The effect of various damping assumption on the dynamic response of structures, Bulletin of international institute of seismology and earthquake engineering, **8**, 217-236, 1971.
[23]Paz, M. and Leigh, W.: Integrated matrix analysis of structures-Theory and computation, Kluwer Academic Publishers, MA, USA , 2001.
[24]Kobori, T. and Kubo, M.: A practical dynamic analysis method of continuous girder bridge with spring connections on spring supports, Proceedings of JSCE, No.356/I-3, pp.395-403, 1985.4. *(in Japanese)*
[25]Mulcathy, N. L.: Bridge response with tractor-trailer vehicle loading, Earthquake Eng. and Structural Dynamics,**11**, 649-665, 1983.
[26]Hutton, S. G. and Cheung, Y. K.: Dynamic response of single span highway bridges, Earthquake Eng. and Structural Dynamics, **7**, 543-553, 1979.
[27]Hurty, W. C. and Rubinstein, M. F.: Dynamics of structures, p.90-103, Prentice-Hall, 1960.
[28]Kawatani, M. and Kim, C.W.: Computer simulation for dynamic wheel loads of heavy vehicles, Int. J. of Structural Engineering and Mechanics, **12**(4), 409-428, 2001.
[29]Newmark, N. M.: A method of computation for structural dynamics, J. of Eng. Mech. Div., ASCE, 96, 593-620, 1970.

Appendix

The Eq. (2.27) can be expressed as follows:

$$\begin{bmatrix} \overline{M}_b & 0 \\ Symm. & M_{vv} \end{bmatrix} \begin{Bmatrix} \ddot{a} \\ \ddot{Z} \end{Bmatrix} + \begin{bmatrix} \overline{C}_b^{\,*} & \overline{C}_{bv} \\ Symm. & C_{vv} \end{bmatrix} \begin{Bmatrix} \dot{a} \\ \dot{Z} \end{Bmatrix} + \begin{bmatrix} \overline{K}_b^{\,*} & \overline{K}_{bv} \\ Symm. & K_{vv} \end{bmatrix} \begin{Bmatrix} a \\ Z \end{Bmatrix} = \begin{Bmatrix} \bar{f}_b \\ f_{vv} \end{Bmatrix} \tag{A1}$$

where,

$$\overline{M}_b = \begin{bmatrix} M_{b1} & \cdots & 0 \\ \vdots & \ddots & \vdots \\ Symm. & \cdots & M_{bn} \end{bmatrix} \tag{A2}$$

$$M_{vv} = \begin{bmatrix} M_{v1} & & & \boldsymbol{0} \\ & \ddots & & \\ & & M_{vi} & \\ & & & \ddots \\ Symm. & & & M_{vnveh} \end{bmatrix} \tag{A2}$$

$$\boldsymbol{M}_{vi} = \begin{bmatrix} m_{i11} & & & & & & & \\ & m_{i12} & & & & & & \\ & & m_{i22} & & & 0 & & \\ & & & J_{xi11} & & & & \\ & & & & J_{xi12} & & & \\ & & Symm. & & & J_{yi22} & & \\ & & & & & & J_{yi11} & \\ & & & & & & & J_{xi22} \end{bmatrix} \tag{A4}$$

$$\overline{\boldsymbol{C}}_b^{\,*} = \begin{bmatrix} \overline{C}_{b1} + \Phi_1{}^T \sum_{v=1}^{nveh} \sum_{m=1}^{3} \sum_{u=1}^{2} \Psi_{vmu} C_{vm2u} \Psi_{vmu}{}^T \Phi_1 & & \boldsymbol{0} \\ & \ddots & \\ Symm. & & \overline{C}_{bn} + \Phi_n{}^T \sum_{v=1}^{nveh} \sum_{m=1}^{3} \sum_{u=1}^{2} \Psi_{vmu} C_{vm2u} \Psi_{vmu}{}^T \Phi_n \end{bmatrix} \tag{A5}$$

$$\overline{\boldsymbol{C}}_{bv} = \begin{bmatrix} \boldsymbol{C}_{b1} & \cdots & \boldsymbol{C}_{bi} & \cdots & \boldsymbol{C}_{bnveh} \end{bmatrix} \tag{A6}$$

$$\boldsymbol{C}_{bi} = \begin{bmatrix} 0 & C_{bi12} & C_{bi13} & 0 & C_{bi15} & C_{bi16} & 0 & C_{bi18} \\ \vdots & \vdots & \vdots & \vdots & \vdots & \vdots & \vdots & \vdots \\ 0 & C_{bin2} & C_{bin3} & 0 & C_{bin5} & C_{bin6} & 0 & C_{bin8} \end{bmatrix} \tag{A7}$$

where,

$$C_{bij2} = -\sum_{u=1}^{2} C_{i12u} \boldsymbol{\Psi}_{i1u}{}^T \boldsymbol{\Phi}_j \;, \quad C_{bij3} = -\sum_{m=2}^{3} \sum_{u=1}^{2} C_{im2u} \boldsymbol{\Psi}_{imu}{}^T \boldsymbol{\Phi}_j \;, \quad C_{bij5} = \sum_{u=1}^{2} (-1)^u \lambda_{yi2} C_{i12u} \boldsymbol{\Psi}_{i1u}{}^T \boldsymbol{\Phi}_j \;,$$

$$C_{bij6} = \sum_{m=2}^{3} \sum_{u=1}^{2} (-1)^u \lambda_{yi3} C_{im2u} \boldsymbol{\Psi}_{imu}{}^T \boldsymbol{\Phi}_j \;, \quad C_{bij8} = -\sum_{m=2}^{3} \sum_{u=1}^{2} (-1)^m \lambda_{xi3} C_{im2u} \boldsymbol{\Psi}_{imu}{}^T \boldsymbol{\Phi}_j \quad \text{and} \quad j=1\sim n^{th}$$

mode.

$$\boldsymbol{C}_{vv} = \begin{bmatrix} \boldsymbol{C}_{v1} & & & \boldsymbol{0} \\ & \ddots & & \\ & & \boldsymbol{C}_{vi} & \\ & & & \ddots \\ Symm. & & & \boldsymbol{C}_{vnveh} \end{bmatrix} \tag{A8}$$

$$\boldsymbol{C}_{vi} = \begin{bmatrix} C_i^{11} & C_i^{12} \\ C_i^{21} & C_i^{22} \end{bmatrix} \tag{A9}$$

where,

$$C_i^{11}\begin{bmatrix} \sum_{m=1}^{2}\sum_{u=1}^{2} C_{im1u} & -\sum_{u=1}^{2} C_{i11u} & -\sum_{u=1}^{2} C_{i21u} & -\sum_{m=1}^{2}\sum_{u=1}^{2}(-1)^u \lambda_{yi1} C_{im1u} \\ & \sum_{k=1}^{2}\sum_{u=1}^{2} C_{i1ku} & 0 & \sum_{u=1}^{2}(-1)^u \lambda_{yi1} C_{i11u} \\ & & \sum_{u=1}^{2}(C_{i21u} + \sum_{m=2}^{3} C_{im2u}) & \sum_{u=1}^{2}(-1)^u \lambda_{yi1} C_{i21u} \\ \textit{Symm.} & & & \sum_{m=1}^{2}\sum_{u=1}^{2} \lambda_{yi1}{}^2 C_{im1u} \end{bmatrix}$$

$$C_i^{12} = \begin{bmatrix} \sum_{u=1}^{2}(-1)^u \lambda_{yi2} C_{i11u} & \sum_{u=1}^{2}(-1)^u \lambda_{yi3} C_{i21u} & -\sum_{m=1}^{2}\sum_{u=1}^{2}(-1)^m \lambda_{xim} C_{im1u} & 0 \\ -\sum_{k=1}^{2}\sum_{u=1}^{2}(-1)^u \lambda_{yi2} C_{i1ku} & 0 & -\sum_{u=1}^{2} \lambda_{xi1} C_{i11u} & 0 \\ 0 & -\sum_{u=1}^{2}(-1)^u \lambda_{yi3}(C_{i21u} + \sum_{m=2}^{3} C_{im2u}) & \sum_{u=1}^{2} \lambda_{xi2} C_{i21u} & \sum_{m=2}^{3}\sum_{u=1}^{2}(-1)^m \lambda_{xi3} C_{im2u} \\ -\sum_{u=1}^{2} \lambda_{yi1}\lambda_{yi2} C_{i11u} & -\sum_{u=1}^{2} \lambda_{yi1}\lambda_{yi3} C_{i21u} & \sum_{m=1}^{2}\sum_{u=1}^{2}(-1)^m(-1)^u \lambda_{xim}\lambda_{yi1} C_{im1u} & 0 \end{bmatrix}$$

$$C_i^{22} = \begin{bmatrix} \sum_{k=1}^{2}\sum_{u=1}^{2} \lambda_{yi2}{}^2 C_{i1ku} & 0 & \sum_{u=1}^{2}(-1)^u \lambda_{xi1}\lambda_{yi2} C_{i11u} & 0 \\ & \sum_{u=1}^{2} \lambda_{yi3}{}^2(C_{i21u} + \sum_{m=2}^{3} C_{im2u}) & -\sum_{u=1}^{2}(-1)^u \lambda_{yi3}\lambda_{xi2} C_{i21u} & -\sum_{m=2}^{3}\sum_{u=1}^{2}(-1)^m(-1)^u \lambda_{xi3}\lambda_{yi3} C_{im2u} \\ & & \sum_{m=1}^{2}\sum_{u=1}^{2} \lambda_{xim}{}^2 C_{im1u} & 0 \\ \textit{Symm.} & & & \sum_{m=2}^{3}\sum_{u=1}^{2} \lambda_{xi3}{}^2 C_{im2u} \end{bmatrix}$$

$$C_i^{21} = C_i^{12}$$

A similar procedure can be employed to derive each element in $\overline{K}_b^*$, $\overline{K}_{bv}$ and K_{vv} matrices.

The displacement and force vectors shown in Eq. (A1) are defined as;

$$\{a;\ Z\} = \{a_1;\ \cdots;\ a_n;\ Z_1;\ \cdots;\ Z_i;\ \cdots;\ Z_{nveh};\} \tag{A10}$$

$$Z_i = \{Z_{i11};\ Z_{i12};\ Z_{i22};\ \theta_{xi11};\ \theta_{xi12};\ \theta_{xi22};\ \theta_{yi11};\ \theta_{yi22}\} \tag{A11}$$

$$\bar{f}_b = \Phi^T \left\{ \sum_{v=1}^{nveh} \sum_{m=1}^{3} \sum_{u=1}^{2} \Psi_{vmu} \left(W_{vmu} + K_{vm2u} Z_{rvmu} + C_{vm2u} \dot{Z}_{rvmu} \right) \right\} \tag{A12}$$

$$f_v = \{f_1;\ \cdots;\ f_i;\ \cdots;\ f_{nveh};\} \tag{A13}$$

$$\begin{aligned} f_i = \Bigg\{ & 0; -\sum_{u=1}^{2} (K_{i21u} Z_{ri1u} + C_{i21u} \dot{Z}_{ri1u}); -\sum_{m=2}^{3} \sum_{u=1}^{2} (K_{im2u} Z_{rimu} + C_{im2u} \dot{Z}_{rimu}); 0; \\ & \sum_{u=1}^{2} (-1)^u \lambda_{yi2} (K_{i12u} Z_{ri1u} + C_{i12u} \dot{Z}_{ri1u}); \sum_{m=2}^{3} \sum_{u=1}^{2} (-1)^u \lambda_{yi3} (K_{im2u} Z_{rimu} + C_{im2u} \dot{Z}_{rimu}); \\ & 0; -\sum_{m=2}^{3} \sum_{u=1}^{2} (-1)^m \lambda_{xi3} (K_{im2u} Z_{rimu} + C_{im2u} \dot{Z}_{rimu}) \Bigg\} \end{aligned} \tag{A14}$$

Chapter 3

Dynamic responses of vehicle

3.1 Introduction

Dynamic effects due to moving vehicles on bridges are of most concern at shorter spans. It has been reported that the traffic-induced vibration of bridges is greatly affected by the frequency characteristic of vehicle vibrations and surface roughness. Thus, the accurate identification of wheel loads on bridges is an important issue for the bridge design. Furthermore, the deterioration of pavement as well as decks is another output due to the time varying wheel load, and the proper estimation of the dynamic wheel load becomes important in maintenance and management of decks and roadway pavement. Many experimental studies on the dynamic wheel load have been carried out (e.g. [1, 2]). In spite of those efforts, most of the investigations are stagnated at qualitative estimations of the experimental data, because of the difficulty to understand the complicate mechanism of vehicles.

Table 3-1 Properties of two-axle vehicle

Geometry (m)	Tread	2.07
	Distance between front and rear axle	6.20
	Distance of tandem axle	0.00
	Distance between front axle and center of gravity	3.94
Mass (kg)	Sprung mass including payload	14,790
	Steer axle un-sprung mass	650
	Drive axle un-sprung mass	1,070
Spring constant of suspension (*kN/m*)	Front leaf spring	475
	Rear leaf spring	1,820
Spring constant of tire (*kN/m*)	Front tire	1,390
	Rear tire	1,170
Damping coefficient of suspension (*kN·s/m*)	Front left	7.810
	Front right	8.065
	Rear left	3.324
	Rear right	1.649
Damping coefficient of tire (*kN·s/m*)	Front tire	Not considered
	Rear tire	

This chapter contributes the verification of analytical responses of a vehicle model by using the equations of motion derived in Chapter 2. The vehicle to be verified by experimental data is the two-axle vehicle idealized as 7DOF (see, Fig. 2-1 (a)). Table 3-1 shows properties of the vehicle model [3, 4]. The roadway surface profile measured under the wheel tracks of each vehicle is used in analysis.

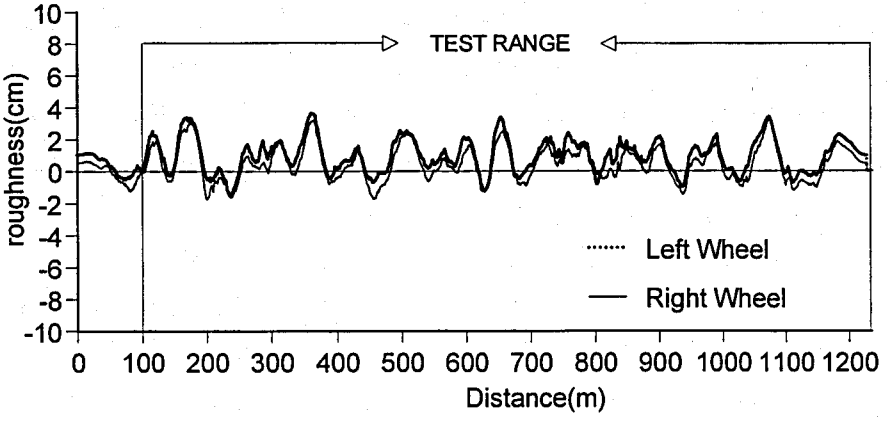

Fig. 3-1 Measured roadway surface profile under the wheel track of two-axle vehicle: P1-profile

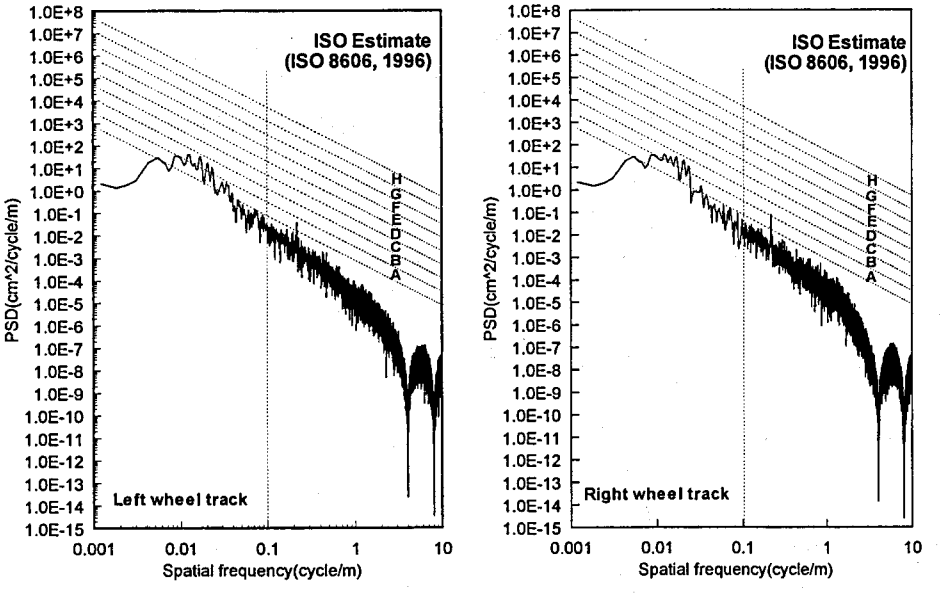

(a) Left wheel track (b) Right wheel track

Fig. 3-2 PSD curves of P1-profile shown in Fig. 3-1

The measured roadway profile under tracks of the two-axle vehicle (P1-profile) is shown in Fig. 3-1 [3, 4]. Figure 3-2 is the PSD curve of the measured roadway surface in Fig. 3-1with ISO estimate [5].

Within the eight classes of roads A to H, paved roads are generally considered to be among road classes A to D. Road class A corresponds to a very good road, which typically indicates a newly paved highway. An unpaved road where a truck would hardly be able to travel at a speed of 40 km/h corresponds to road class E or F. Thus, it is observed that the P1-profile is categorized as very good road according to the ISO 8608 code [5].

3.2 Verification of analytical dynamic wheel loads of two-axle vehicle

To verify the validity of analytical dynamic wheel loads of the two-axle cargo truck model, time histories of wheel loads, the dynamic load coefficient (DLC) [3, 4] and the dominant frequency of wheel loads at each tire are compared to the field-test data. The DLC is defined as the ratio of the root mean square (RMS) dynamic wheel loads to the mean wheel load where the RMS dynamic wheel load is essentially the standard deviation of the probability distribution as shown in Eq. (3.1). The DLC is hence the wheel load coefficient of variation. Since the DLC value has a limited role in validating models, the cumulative distribution function is also adopted as a function to analyze and validate the model.

$$DLC = \frac{\sigma_{dy}}{WL_{st}} \tag{3.1}$$

where, σ_{dy} is the RMS value of the dynamic component of the wheel load, and WL_{st} is the maximum static load (mean wheel load) over the component of the wheel load.

The measured dynamic wheel load of the two-axle vehicle running on the P1-profile is taken from the DIVINE (Dynamic Interaction Vehicle-INfrastructure Experiment) project developed by the OECD [3, 4]. A part of the project was coordinated by the TNO (Road-Vehicles Research Institute of Netherlands Organization for Applied Scientific Research) working under the auspices of the DIVINE joint research program [3].

Spring constants and damping coefficients of the two-axle vehicle shown in Table 3-1 are estimated in the DIVINE project [4]. In field-test, vehicle speeds were measured as 64.96km/hr, 75.68km/hr and 82.73km/hr. The sample rates were 100Hz during the experiment.

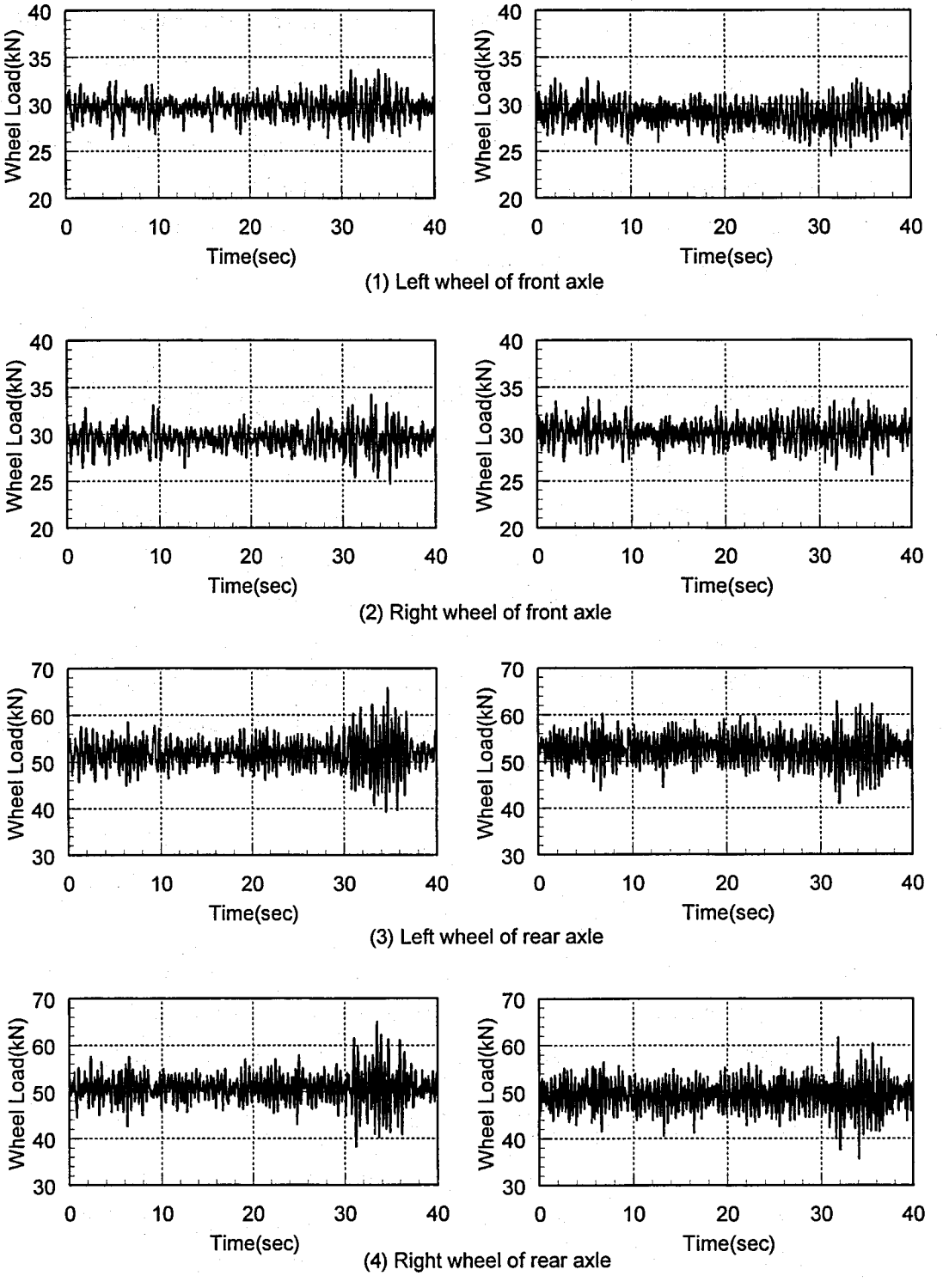

Fig. 3-3 Dynamic wheel loads of two-axle vehicle; v=82.73km/hr

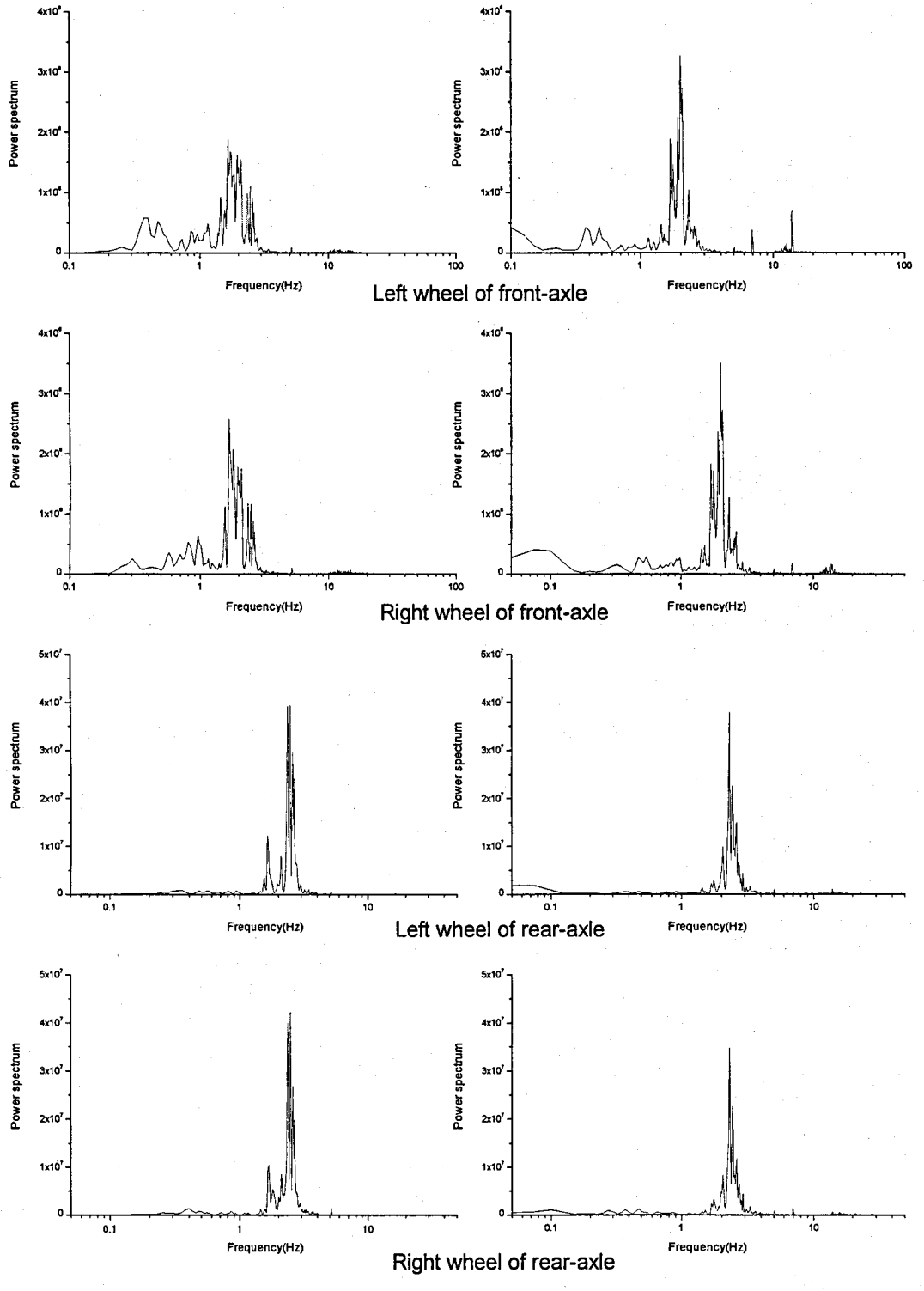

(b) Analysis (b) Experiment

Fig. 3-4 PSD curves of dynamic wheel loads; v=82.73km/hr

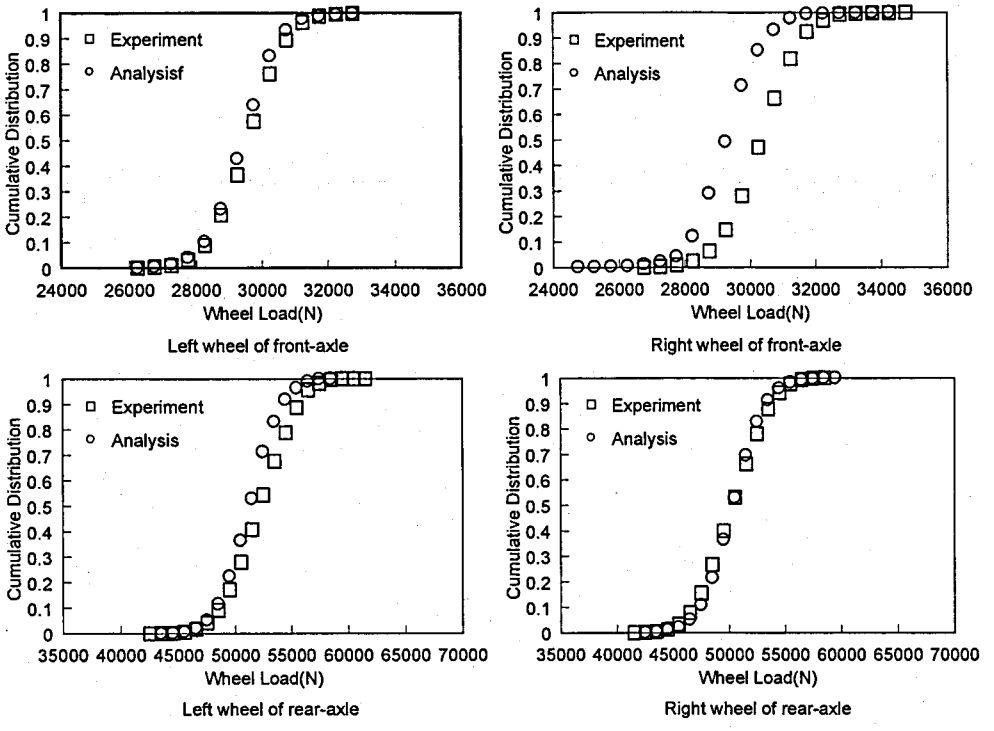

Fig. 3-5 Cumulative distributions of dynamic wheel loads of two-axle vehicle (I); *v=64.96km/hr*

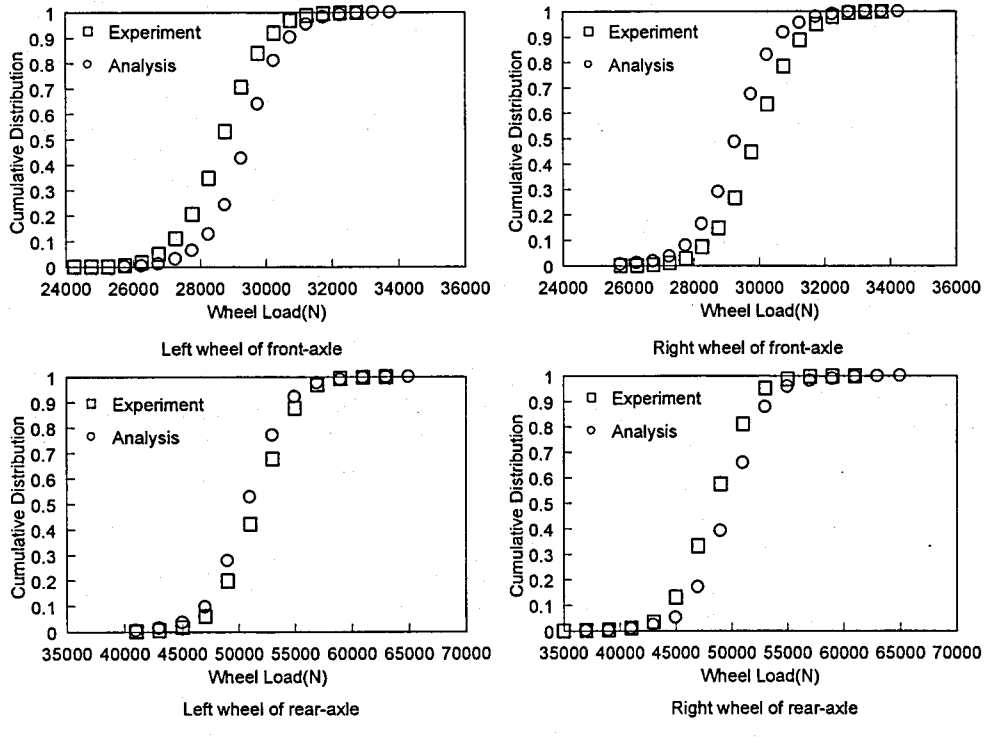

Fig. 3-6 Cumulative distributions of dynamic wheel loads of two-axle vehicle (II); *v=75.68km/hr*

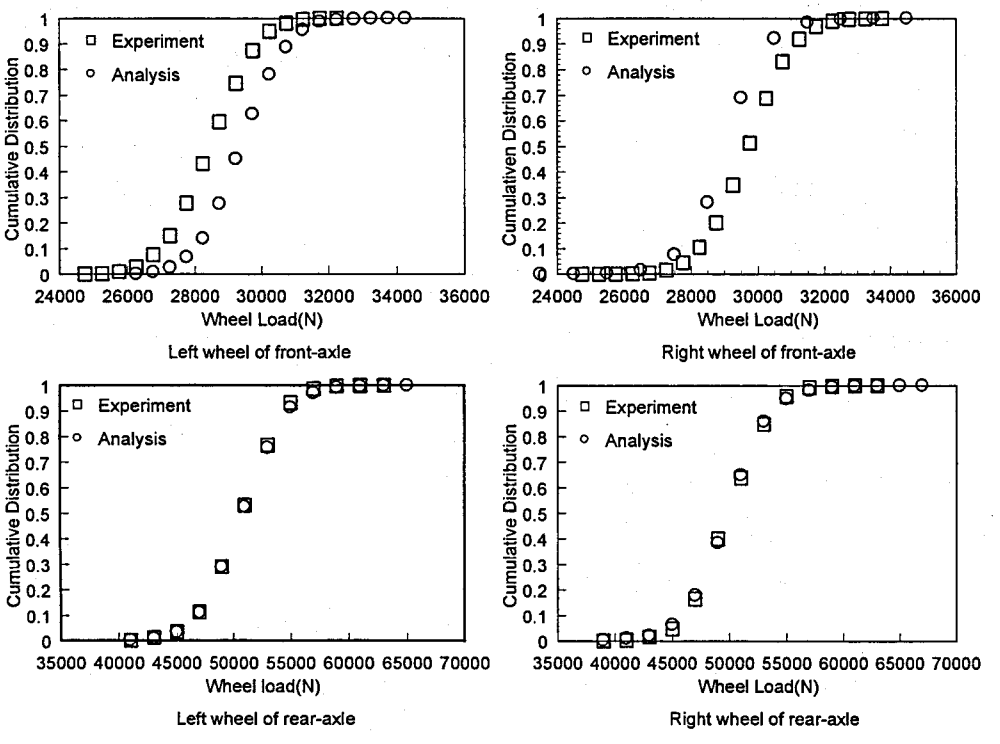

Fig. 3-7 Cumulative distributions of dynamic wheel loads of two-axle vehicle (III); *v=82.73km/hr*

Table 3-2 DLC values and dominant frequencies of dynamic wheel loads of two-axle vehicle

Speed (km/hr)	Wheel	DLC		Dominant frequency (Hz)	
		Experiment	Analysis	Experiment	Analysis
64.96	Front left	0.0309	0.0328	1.93	1.96
	Front right	0.0319	0.0337	1.93	1.96
	Rear left	0.0444	0.0511	2.53	2.58
	Rear right	0.0471	0.0531	2.53	2.58
75.68	Front left	0.0342	0.0394	1.88	1.93
	Front right	0.0357	0.0371	1.88	1.93
	Rear left	0.0579	0.0572	2.46	2.43
	Rear right	0.0582	0.0609	2.46	2.43
82.73	Front left	0.0384	0.0399	1.98	1.66
	Front right	0.0397	0.0377	1.98	1.66
	Rear left	0.0632	0.0598	2.31	2.48
	Rear right	0.0649	0.0601	2.31	2.48

Figures 3-3 and 3-4 show, respectively, time histories and PSD curves of dynamic wheel loads of the two-axle vehicle. A good agreement is observed between analysis and experiment.

To assess the validity of the analytical dynamic wheel load quantitatively, the cumulative distribution of wheel loads, the DLC value and the dominant frequency of the wheel loads are compared with experimental ones. Cumulative distributions of the dynamic wheel load at each wheel of the vehicle are shown in Figs. 3-5 to 3-7. The DLC value and dominant frequency are summarized in Table 3-2. The correlation between analysis and experiment shown in Figs. 3-5 to 3-7 and Table 3-2 shows that the model is capable of simulating the dynamic wheel loads to accuracy under 10 percent in average.

It is observed that the dominant frequency of dynamic wheel loads varies with respect to vehicle speeds as shown in Table 3-2. One of the reasons for the dominant frequency variation according to speed may be that the dominant space frequency of the roadway profile which can resonant with a vehicle system can change with respect to the vehicle speed. How travel speed and spatial frequency affect the vehicle dynamics can be determined from the relation shown in Eq. (3.2) [7].

$$f = \frac{v}{\lambda} = v\Omega \tag{3.2}$$

where, f is frequency in cycle/sec, v is vehicle speed in units of m/sec, Ω is the spatial frequency (wave number) in cycle/m, and λ is the wave length in m/cycle

3.3 Frequency relations between dynamic wheel load and vehicle motion

The dynamic response of the vehicle is investigated by using the experimentally verified two-axle vehicle. As parameters, the roadway roughness condition and the vehicle speed are considered. The roadway profile measured at Umeda entrance bridge, Osaka, Japan [8, 9] is used in analysis to examine the effect of roadway roughness condition. The profile is named as P2-profile is shown in Fig. 3-8. The PSD curve of the P2-profile is shown in Fig. 3-9, and shows the roughness condition can be categorized as very good according to the ISO estimate [5] like as the condition of the P1-profile. However, the roughness condition of the P2-profile is relatively worse than that of P1-profile.

Frequency relations between dynamic wheel loads and vehicle motion are shown in Fig. 3-10, and it is observed that there exists strong resemblance between frequencies of dynamic wheel load and bounce motion.

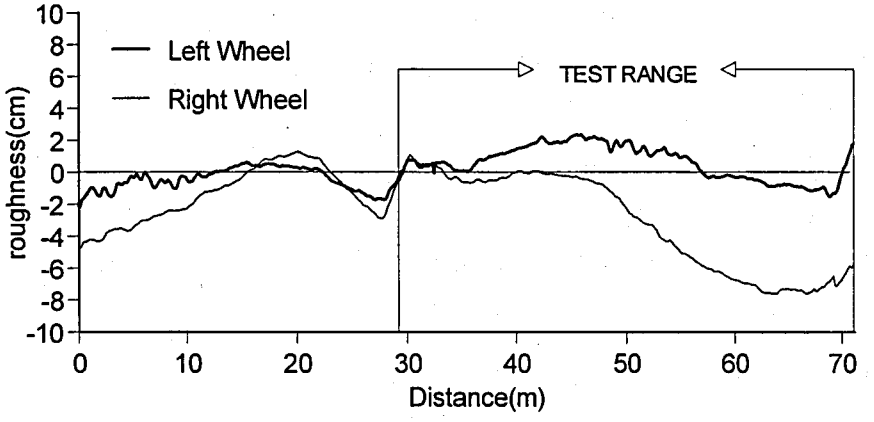

Fig. 3-8 Measured roadway surface profile under the wheel track of two-axle vehicle: P2-profile

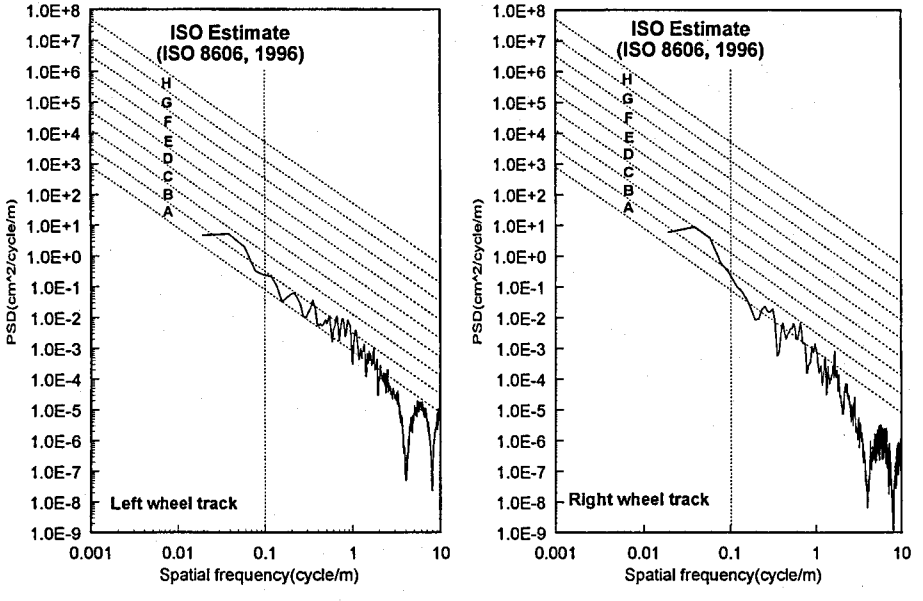

(a) Left wheel track (b) Right wheel track

Fig. 3-9 PSD curves of P2-profile shown in Fig. 3-8

Another interesting feature is appeared in Fig. 3-11, which show PSD curves of the dynamic wheel load while the two-axle vehicle running on P1 and P2 profiles, respectively with different speeds of *v=30km/hr, v=50km/hr* and *70km/hr*. From the figures, it is observed that the dynamic characteristic of wheel loads is dominated by the frequency of 2.4Hz corresponding to the bounce motion of the vehicle. The frequency near 14Hz corresponding

to the axle-hop motion of the vehicle is the secondary dominant frequency, even though the energy is very small compared with that of the bounce motion. However, the peaks of PSD curves of wheel loads near 14Hz become apparent with increasing speed. It means that those axle-hop motions with relatively high frequency can affect dynamic wheel loads with increasing speed. Moreover, those powers of PSD curves increase notably due to the roadway roughness condition.

It supports the fact that the deck slab with relatively higher frequency characteristic than that of the main girder can be easily damaged by the vehicle running on rough roadway surface with high speed.

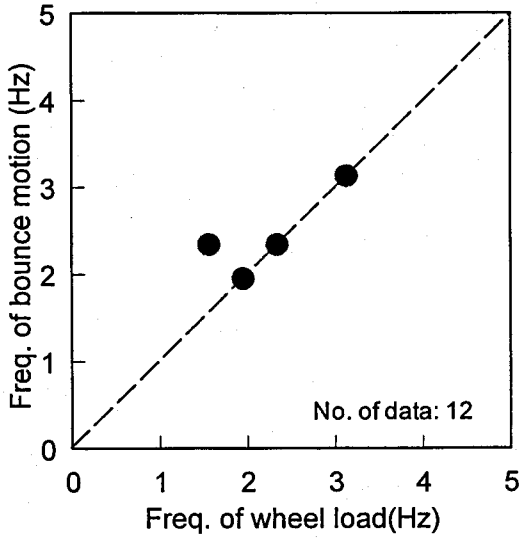

Fig. 3-10 Dominant frequency relation between wheel load and bounce motion

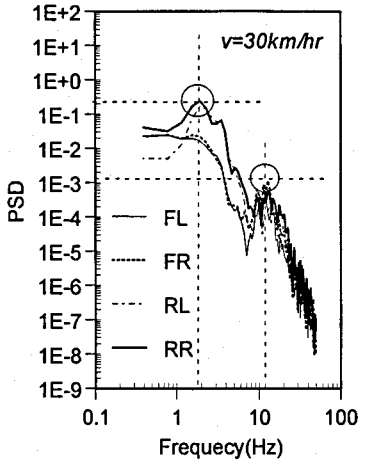

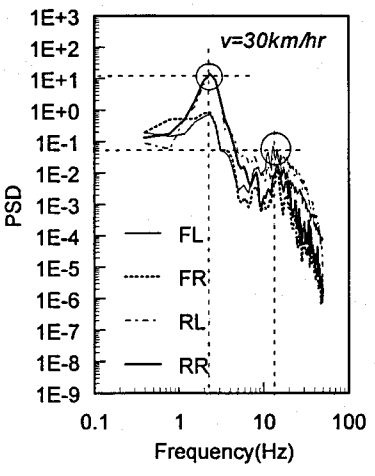

(1) *v=30km/hr*

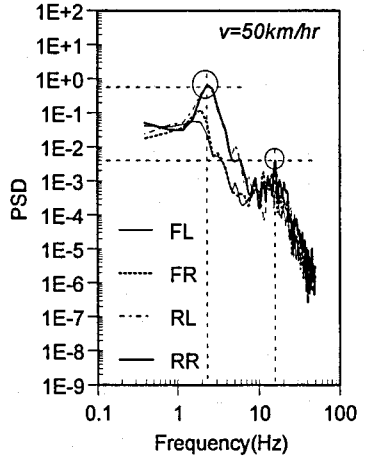

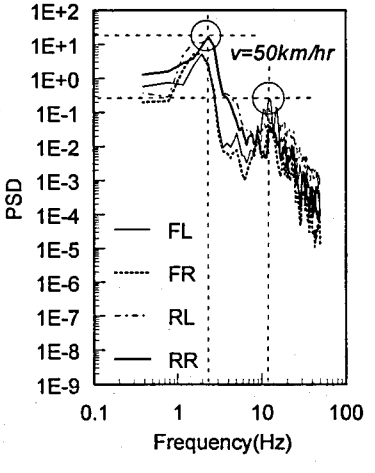

(2) *v=50km/hr*

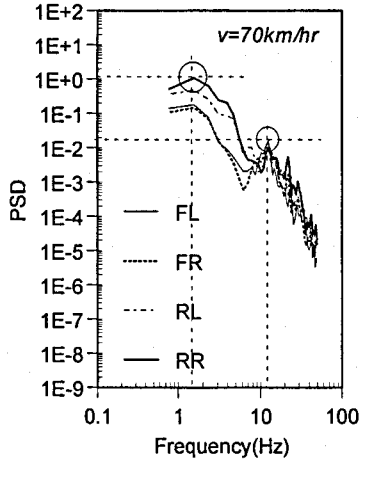

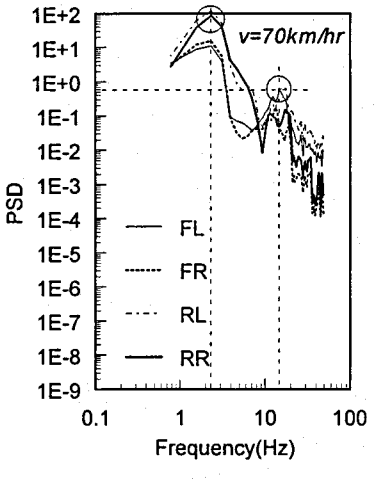

(3) *v=70km/hr*

(a) Running on P1-profile (b) Running on P2-profile

Fig. 3-11 PSD curves of wheel loads with respect to vehicle speed; two-axle vehicle

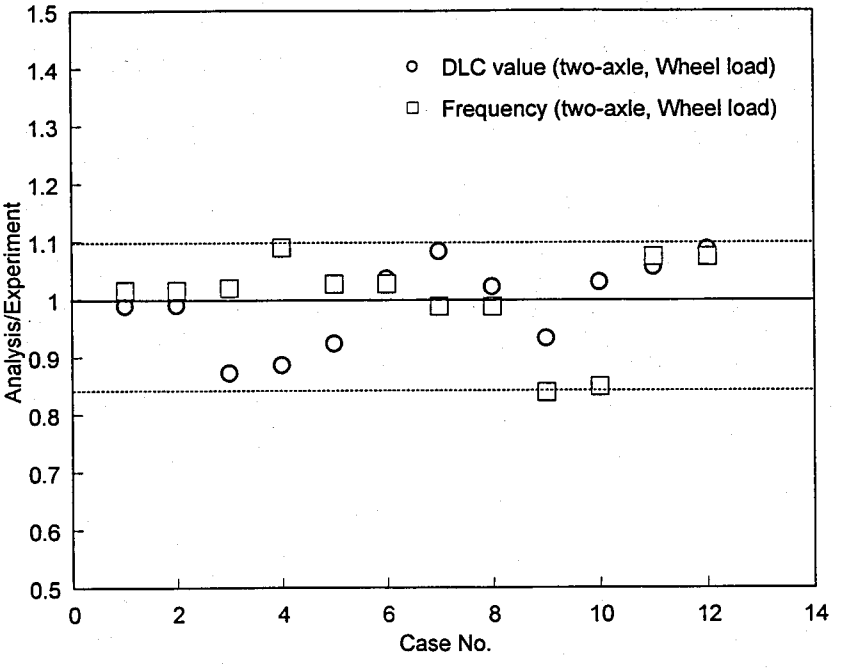

Fig. 3-12 Ratio of analytical results to experimental ones

3.4 Conclusions

In this chapter, the verification of analytical dynamic responses of a vehicle is carried out by comparing with field-test data. The major conclusions that can be drawn from the comparative investigation between the analysis and the experiment are as follows:

1. The data from field-test indicate that the analytical method is accurate for predicting the dynamic response as well as the wheel load of heavy vehicles.
2. It is observed that the dominant frequency of dynamic wheel loads varies with respect to vehicle speeds, and one of the reasons for the dominant frequency variation according to speed may be that the dominant space frequency of the roadway profile which can resonant with the vehicle system can change with respect to the vehicle speed.
3. The dominant frequency of the dynamic wheel load and the bounce motion of vehicle are strongly related with each other. The axle-hop motion, which has relatively high frequency characteristic compared to that of the bounce motion, can also influence to the dynamic wheel load with increasing speed. Therefore, the deck slab that has relatively higher frequency characteristic than that of the main girder can be easily damaged by the vehicle running on a rough roadway surface with high speed.
4. If the properties of the vehicle are well estimated or tested, then the analytical method

guarantees good simulation result. The analytical DLC values and dominant frequencies of wheel loads of the two-axle vehicle are scattered within 88% ~ 110% and 84% ~ 110% of the experiment, respectively (see Fig. 3-12).

References

[1] Page, J.: Dynamic wheel load measurements on motorway bridges, TRRL report No. 722, 1976.

[2] Cantieni, R.: Dynamic load testing of highway bridges, IABSE Proceedings, **P-75/84**, 57-72, 1984:

[3] Hoogvelt, R. B. J. and Ruijs, P. A. J.: OECD-IR6 DIVINE Element 4. Computer simulation of heavy vehicle dynamic wheel loads, TNO Report 97.OR.016.1/H/PR, TNO, Delft, The Netherlands, 1997.

[4] Technical Report, DSTI/DOT/RTR/IR6(98)1FINAL, OECD. 1998.

[5] ISO 8608: Mechanical Vibration – Road Surface Profiles – Reporting of Measured Data, British Standard, BS 7853, 1996.

[6] Kim, C. W. and Kawatani, M.: A comparative study on dynamic wheel loads of multi-axle vehicle and bridge responses, Proc. of DETC'01 ASME 2001 Design Engineering Technical Conference and Computers and Information in Engineering Conference Pittsburgh, USA, ASME, CD-ROM, 2001

[7] Sayers, M. W. and Karamihas, S. M.: The little book of profiling-Basic information about measuring and interpreting road profiles, http://www.umtri.umich.edu/erd/roughness /lit_book.pdf

[8] Technical report-Inspections on Umeda entrance bridge structures, Hanshin Expressway Public Corporation (HEPC), 1992. *(in Japanese)*

[9] Kim, C.W.: An experimental and analytical study for traffic-induced vibration on roadway bridges, Ph.D. Thesis, Chung-Ang University, Korea, 46-48, 1997.

Chapter 4

Dynamic responses of conventional type steel girder bridge

4.1 Introduction

The basic research topic on the traffic-induced vibration of bridges has been impact factor related problems, since the complicate vehicle-bridge-surface roughness interaction effect is determined by means of the impact factor in most of all the bridge design codes. In general, the impact factor taken from a field test has features that fluctuate with vehicle speeds. The reason for those phenomena is not clear so far though some research works related to the dynamic amplification factor such as the effect of moving mass on beam [1-3] have been investigated. Because, there are many factors that would affect the bridge-vehicle interaction such as roadway roughness, non-linearity of vehicle suspension system, vehicle axle spacing and frequency spectra of vehicle and bridge as well as moving speed [4].

One of the most important sources on the traffic-induced vibration of bridges is the dynamic wheel load that is the result of dynamic motions of vehicles, since, originally, the impact factor itself means the effect of the external dynamic load. Another important factor can be the relation of the frequency characteristic between bridge behaviors and vehicle motions as the Ontario bridge design code [5] define the impact factor (dynamic amplification factor) as a function of the frequency of the first bending mode to consider the possibility of the resonance between the vehicle motion and the bridge behavior. Therefore, the relationship between the dynamic response of bridges and the dynamic wheel load of vehicles is investigated by using the experimentally verified analytical model of a conventional type steel three-girder bridge [6] and vehicles [7].

The deck is another important member experiencing the dynamic wheel load, since the RC decks, being directly subjected to wheel loads of vehicles, are more easily damaged than other structural members in steel highway bridges [8]. Moreover, the wide spreading adoption of the steel two-girder bridge needs higher performance of deck slabs than those of conventional multi-girder bridges because of the adoption of wider girder spacing than conventional bridges.

The rational criterion of the performance level of reinforced concrete (RC) decks provides useful assessment tool for decision making related to the inspection, repair, upgrading and replacement of existing steel plate girder bridges based on life-cycle cost. It is clear that, except corrosion due to environmental factors, the traffic load or the dynamic wheel load plays an important role in the deterioration of RC decks. For the RC deck, the bump near

expansion joints is another important factor inducing the impulsive loading effect generated by a vehicle passing over the bump [9-11].

However, most of all the existing research topics related to the deck have been focused on static responses. The dynamic response of deck slabs due to moving vehicles has not been fully investigated, even though the fatigue problem for the RC deck as a part of dynamic problem has been wide spreading research theme. Moreover, in civil infra structures, the recent design concept trends reliability-based design to consider many sources of uncertainties in the structure design. However, researches on the impact factor of deck slabs based on probabilistic approach have not been advanced. Therefore, there is a need to fill this gap.

The dynamic increment factor (DIF) [12] is selected as a parameter for the quantitative investigation of bridge responses. The DIF is defined as the ratio of absolute maximum difference between dynamic and static responses during one major period of the dynamic response including maximum static response to the maximum static response as expressed in Fig. 4-1 [12]. The ΔY in Fig. 4-1 can be expressed as $\Delta Y=|Y_{dynamic}-Y_{static}|_{max}$.

The bridge considered is a steel plate girder bridge with span length of 40.4m, and composed of three girders and RC decks [6, 13]. The validity of analytical results is experimentally verified [6]. Sectional and plan views of the bridge are shown in Fig. 4-2. Details of the bridge model are summarized in Table 4-1.

The FE model of the conventional three-girder bridge is shown in Fig. 4-3. The solid circles at the center of the G1 and G2 girders indicate the noted nodes for the dynamic response of the bridge, and the DIF value at each node is compared with the DLC value of dynamic wheel loads. Solid circles denoted by P1, P2, P3, P4 and P5 are the node to consider the DIF value of decks.

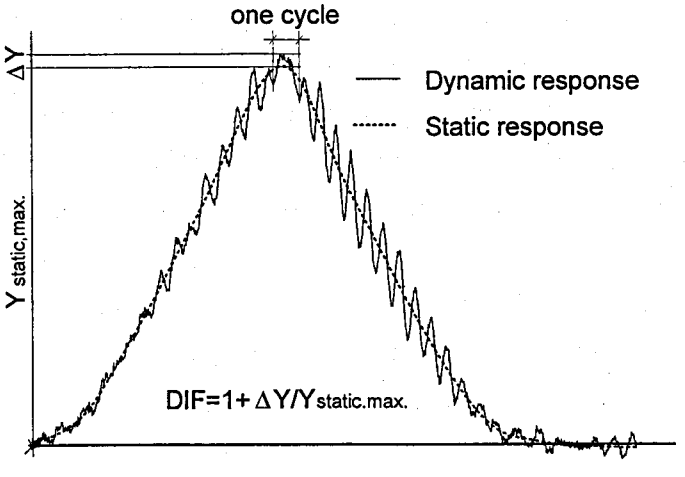

Fig. 4-1 Definition of DIF

Table 4-1 Properties of steel bridge

Mass per unit length (kg/m)		7,550
Section area of girders (m^2)		0.142
Moment of inertia (m^4)		0.212
Torsional constant (m^4)		0.0548
Damping constant(for 1st and 2nd modes)		0.0253
Fundamental frequency (Experiment/Analysis, Hz)	1st(Bending) 2nd(Torsion)	2.33/2.32 3.86/3.56

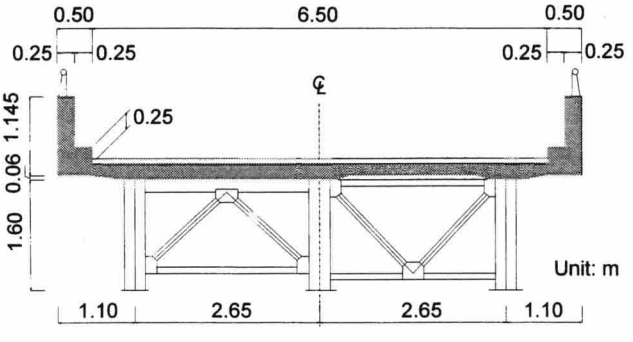

(a) Section view

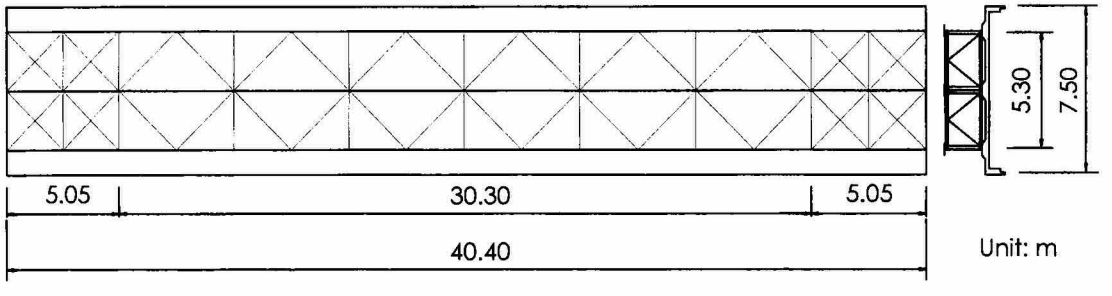

(b) Plan view

Fig. 4-2 Conventional steel girder bridge with three girders

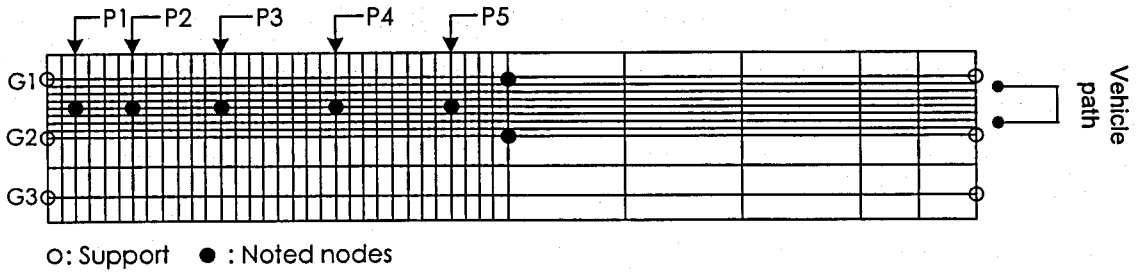

Fig. 4-3 FE model of bridge

Table 4-2 Properties of three-axle vehicle

Geometry (m)	Tread	1.80
	Distance between front and rear axle	3.99
	Distance of tandem axle	1.20
	Distance between front axle and center of gravity	2.99
Mass (kg)	Sprung mass including payload	18,500
	Steer axle un-sprung mass	500
	Drive axle un-sprung mass	1,450
Spring constant of suspension (*kN/m*)	Front leaf spring	1,577
	Rear leaf spring	4,724
Spring constant of tire (*kN/m*)	Front tire	3,146
	Rear tire	4,724
Damping coefficient of suspension (*kN·s/m*)	Front left	11.200
	Front right	11.200
	Rear left	33.420
	Rear right	33.420
Damping coefficient of tire (*kN·s/m*)	Front tire	13.300
	Rear tire	10.000

4.2 Dynamic relationship between vehicle and bridge

The impact factor taken from the field test has features fluctuating with respect to vehicle speeds. The reason for these phenomena is not clear so far though some research works related to the dynamic amplification factor such as the effect of moving mass on beam [1, 3-4] have been investigated, because of the coupled effect of factors that would affect the bridge-vehicle interaction such as roadway roughness, non-linearity of vehicle suspension system, vehicle axle spacing and frequency spectra of vehicle and bridge as well as moving speed [3].

To determine the relationship between vehicle motions and dynamic responses of bridges, the correlation between the vehicle speed to DLC of dynamic wheel load and DIF of bridge response are investigated. The parametric study is also focused on the effect of different vehicle types and roadway roughness conditions on the variation of DLC values of dynamic wheel loads and DIF of the bridges according to vehicle speed. The frequency relations between dynamic wheel loads and bridge responses are also investigated.

The roadway profiles used in the analysis are the P1- and P2-profile. The experimentally verified three-axle vehicle [13, 14] is also used in analysis to investigate the effect of vehicle type (or axle configuration type), and properties of the three-axle vehicle are summarized in Table 4-2.

4.2.1 DLC *vs.* (DIF-1)

To investigate the relation between DLC values (see, Eq. 3.1) of wheel loads and DIF values of the bridge responses, the traffic-induced vibration analysis of the conventional steel girder bridge is carried out. In the analysis, the effect of vehicle types by using the two-axle and three-axle vehicles under the condition of eight types of vehicle speeds (30km/hr, 40km/hr, ... , 90km/hr, 100km/hr) and two types of surface roughness condition (P1- and P2-profile) are considered.

The correlation between the two parameters DLC and (DIF-1) is determined, and summarized in Tables 4-3 and 4-4. In Tables 4-3 and 4-4, μ_{DLC}, $\mu_{(DIF-1)}$ and $\rho_{DLC,DIF}$ are the mean value of DLC, the mean of (DIF-1) and the correlation coefficient of DLC and DIF, respectively.

Table 4-3 Co-relation between DLC and DIF values; effect of roadway surface roughness

	Roadway Profile					
	P1-profile			P2-profile		
	μ_{DLC}	$\mu_{(DIF-1)}$	$\rho_{DLC,DIF}$	μ_{DLC}	$\mu_{(DIF-1)}$	$\rho_{DLC,DIF}$
Front axle	0.104	0.067	0.418	0.233	0.349	0.651
Rear axle	0.034		0.587	0.221		0.692

Table 4-4 Co-relation between DLC and DIF values; effect of vehicle type

	Vehicle type					
	Two-axle vehicle			Three-axle vehicle		
	μ_{DLC}	$\mu_{(DIF-1)}$	$\rho_{DLC,DIF}$	μ_{DLC}	$\mu_{(DIF-1)}$	$\rho_{DLC,DIF}$
Front axle	0.093	0.306	0.832	0.181	0.109	0.823
Rear axle	0.143		0.870	0.112		0.891

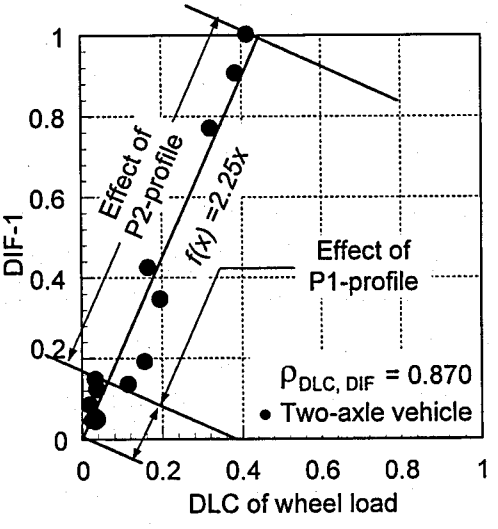

(a) Two-axle vehicle

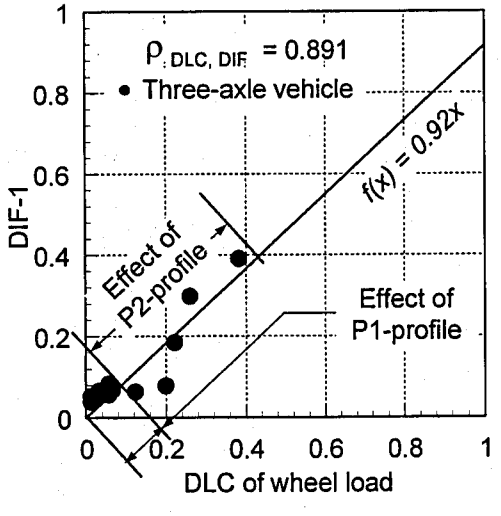

(b) Three-axle vehicle

Fig. 4-4 Relations between DLC of wheel load and (DIF-1) of bridge response

Table 4-5 Dominant frequencies of vehicle motion

Axle configuration type	Vehicle body			Front axle		Rear axle		
	Bounce	Pitching	Rolling	Parallel-hop	Tramp	Parallel-hop	Wind-up	Tramp
Two-axle	2.4Hz	2.4Hz	1.5Hz	11.8Hz	12.3Hz	13.9Hz	-	14.5Hz
Three-axle	3.4Hz	3.6Hz	3.5Hz	17.3Hz	13.9Hz	18.8Hz	17.1 Hz	18.3Hz

Analytical fundamental frequency for the first bending mode of the bridge: 2.32Hz

It is observed that the correlation between DLC and DIF values due to a vehicle running on the P1-profile is weaker than those due to vehicles running on the P2-profile as shown in Table 4-3. One reason of the phenomena may be that under the condition of vehicle running on smooth roadway like the P1-profile the vehicle motion or wheel load cannot fully stimulate the bridge, thus the DIF value of the bridge in this case will depend not on the weak external load but on the fundamental natural frequency or stiffness of bridge itself. It is observed that the DIF value of the bridge as well as the DLC value of dynamic wheel loads is affected by roadway surface conditions very severely as expected.

The effect of vehicle types on the DIF value of the bridge is summarized in Table 4-4, which shows the strong correlation between DLC and DIF values. As shown in the Table 4-4, the DLC value of wheel loads at the rear-axle is more strongly correlated with the DIF value of the bridge than that of the wheel load at the front axle. To investigate the correlation between DLC and DIF values with respect to vehicle types, the two corresponding parameters DLC and (DIF-1) are plotted with a curve fitted line as shown in Fig. 4-4. The $\rho_{DLC,\ DIF}$ is the correlation coefficient, and the $f(x)$ indicates the linear relation between DLC and DIF values.

It is observed in Fig. 4-4 that the slope due to the two-axle vehicle (Fig. 4-4 (a)) is steeper than that due to the three-axle vehicle, although similar strong correlations can be observed in both cases. It means that the dynamic response of the bridge is easily amplified by the small dynamic component of wheel loads of the two-axle vehicle. One of reasons for this result can be the existence of resonance between the vehicle motion and the bridge system. As shown in Table 4-5, the frequency characteristic of the bounce motion of the two-axle vehicle has about 2.4Hz, and it is very similar frequency of the first bending mode of the bridge like 2.32Hz (see Table 4-1). On the other hand the frequency for bounce motion of the three-axle vehicle is 3.4Hz, and DLC and DIF values are corresponding one to one with each other. Thus, it can be concluded that, despite of the strong correlation between DLC and DIF values, the frequency features of vehicles and bridges should be included to define dynamic effect due to vehicle loads.

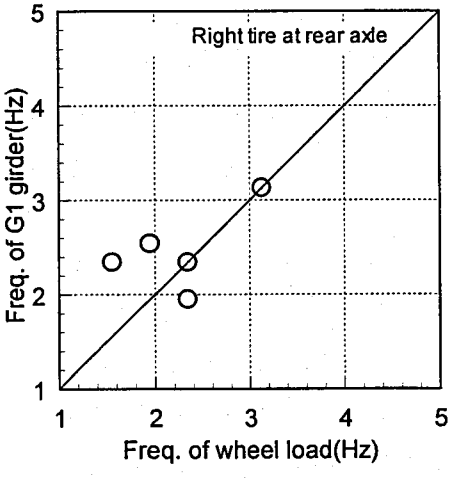

(1) Running on P1-profile

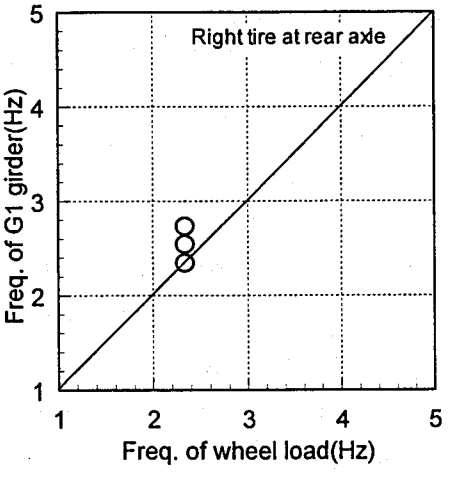

(2) Running on P2-profile

(a) Two-axle vehicle running

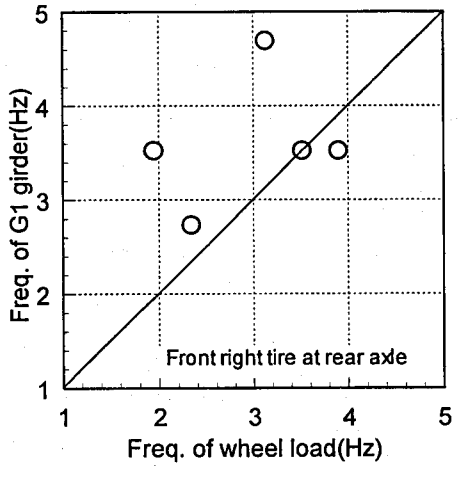

(1) Running on P1-profile

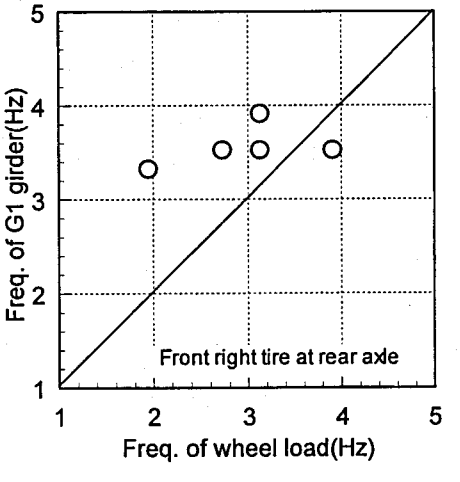

(2) Running on P2-profile

(b) Three-axle vehicle running

Fig. 4-5 Dominant frequency relations between dynamic wheel load and bridge response

4.2.2 Frequency relations between dynamic wheel load and bridge response

Figure 4.5 shows the frequency relation between dynamic wheel loads and bridge responses, and a good resemblance of the frequency relation between the dynamic wheel load and the bridge response is observed. It indicates that the dynamic characteristic of bridge is strongly affected by the bounce motion of vehicles, because the frequency feature of dynamic wheel loads is strongly correlated with that of the bounce motion.

As observed in Fig. 4-5, the best correlation can be seen in the case of the two-axle vehicle running on the P2-profile that has relatively worse surface than that of the P1-profile. On the other hand the worst correlation can be observed in the case of the three-axle vehicle running on the P1-profile that has smoother surface than that of the P2-profile. One of the reasons for the result can be that the dynamic characteristic of bridge responses is dominated by the natural frequency of bridges or bridge stiffness itself in the case of vehicles running on the very smooth roadway because of the weak external loading effect. On the other hand, when vehicles are running on relatively rough roadway that has enough ability to stimulate the vehicles, the dynamic characteristic of the bridge tends to be dominated by the dynamic characteristic of vehicles.

Another feature can be observed in Figs. 4-6 and 4-7, which show PSD curves of dynamic wheel loads (right wheel of rear axle for the two-axle vehicle and front right wheel of rear axle for the three-axle vehicle) and bridge responses according to vehicle speeds while the two-axle and the three-axle vehicles are running on P1- and P2-profile, respectively.

From the PSD curve, it is observed that the power of wheel loads and bridge responses increases according to the vehicle speed. Moreover, those powers of PSD curves increase notably due to roadway roughness conditions. Therefore, it is possible to conclude that the dynamic features of bridge responses can be more easily dominated by dynamic characteristics of vehicle system while vehicle running on rough roadway with high speed than running on smooth roadway with low speed.

The power of wheel loads and bridge responses at the frequency range between 10Hz and 20Hz, which can be the effect of axle-hop motion as summarized in Table 4-5, increases according to the vehicle speed, simultaneously. It indicates that the axle-hop motion with higher frequency characteristics than that of the bounce motion can influence to dynamic wheel loads and bridge responses with increasing speed.

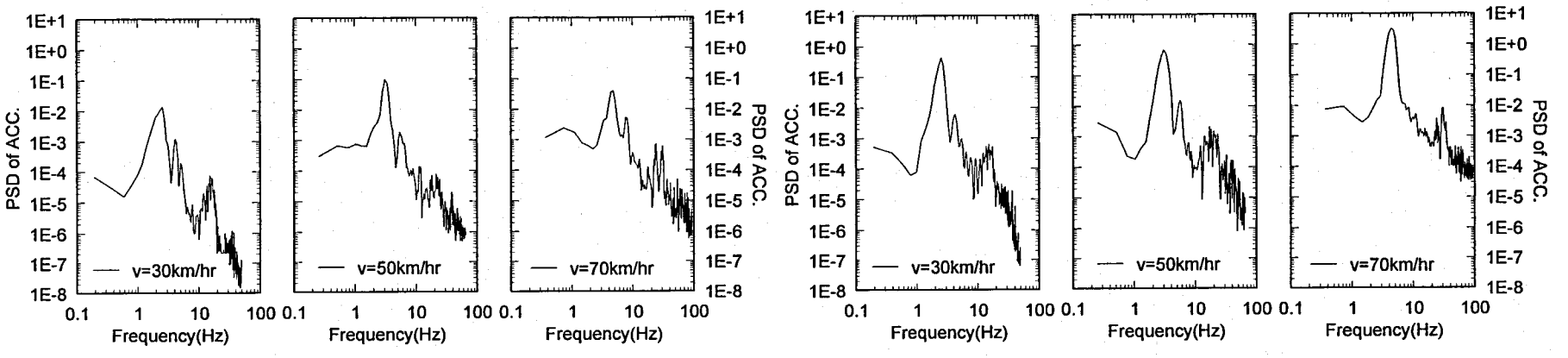

(1) Running on P1-profile (2) Running on P2-profile

(a) Bridge response

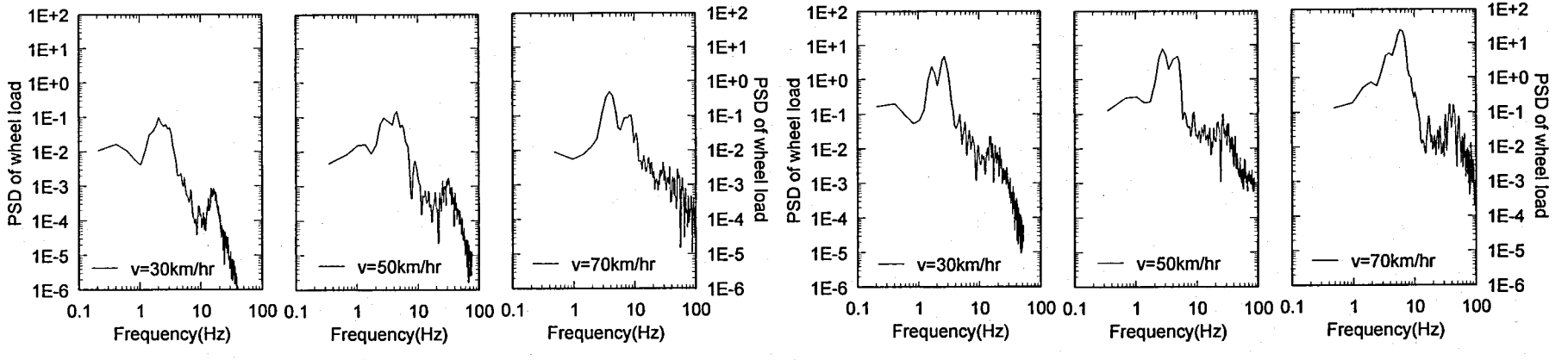

(1) Running on P1-profile (2) Running on P2-profile

(b) Wheel load

Fig. 4-6 Variation of PSD curves according to vehicle speed: two-axle vehicle running

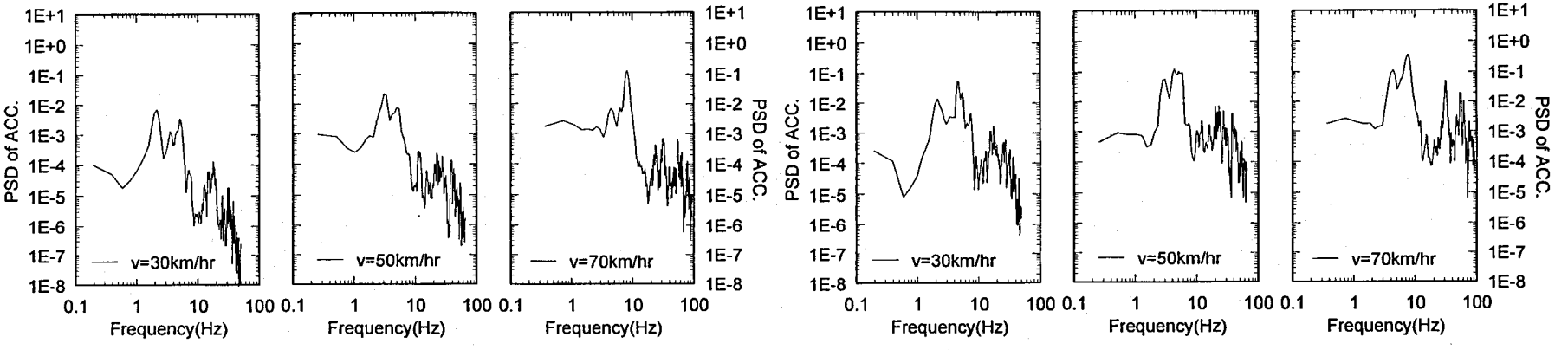

(1) Running on P1-profile (2) Running on P2-profile

(a) Bridge response

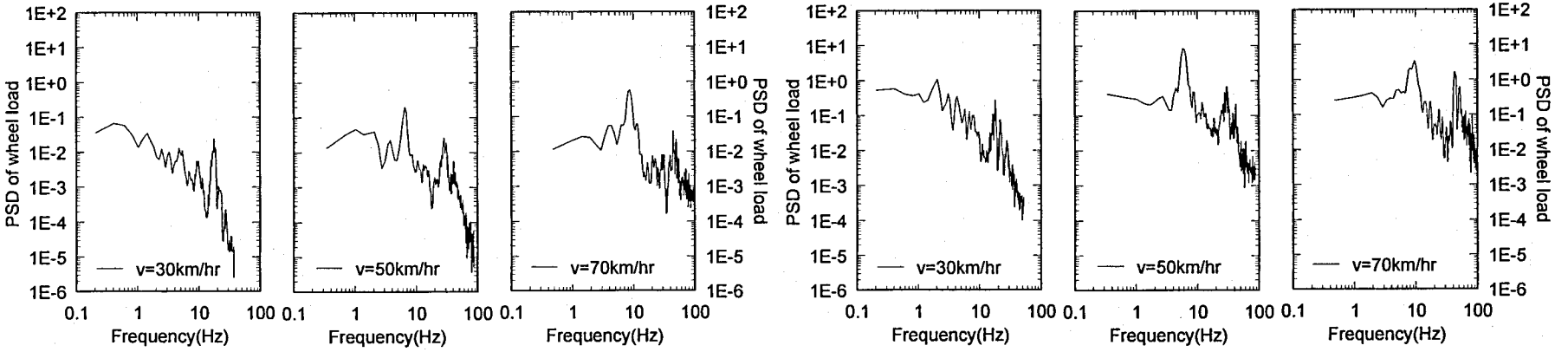

(1) Running on P1-profile (2) Running on P2-profile

(b) Wheel load

Fig. 4-7 Variation of PSD curves according to vehicle speed: three-axle vehicle running

4.3 Assessment of code specified impact factors of deck considering random variables

In this section, probabilistic assessment of code-specified impact factors for the deck slab of the steel girder bridge in Fig. 4-2 is carried out by means of three-dimensional traffic-induced vibration analysis of bridges combined with Monte-Carlo simulation (MCS) technique [17].

It has been reported that the most low reliability index can be expected on the RC deck near an expansion joint due to a bump and a vehicle with tandem axle [10, 11]. Therefore, the impact factor of decks are simulated by means of experimentally verified analytical model [18] in considering random variables such as bump heights, vehicle speeds, axle weights and traveling positions of vehicles as well as the roadway roughness under the condition of three-axle vehicles running.

4.3.1 Random variables

Roadway profile

Physical features of the roadway profiles and those stochastic models can be treated as a homogeneous Gaussian random process with zero mean [19] and the random characteristics can be defined by a power spectral density (PSD) function. The Eq. (4.1) is used as a PSD function of roadway roughness [20].

$$S(\Omega) = \frac{\alpha}{\Omega^n + \beta^n} \tag{4.1}$$

where, α is roughness coefficient, $\Omega(=\omega/2\pi)$ is spatial frequency (cycle/m), β designates shape parameter and n means parameter to express the distribution of power of the PSD curve.

As parameters in Eq. (4.1), $\alpha=0.001$, $\beta=0.05$ and $n=2.0$ [21] are used in this study based on measured data of Meishin Expressway in Japan, and the PSD curve is shown in Fig. 4-8 with ISO estimates [22]. If the PSD function for a roadway profile is defined, then, by means of MCS method, samples of roadway profiles can be obtained using the sampling function expressed as Eq. (4.2).

$$z_r(x) = \sum_{k=1}^{M} a_k \sin(\omega_k \cdot x + \varphi_k) \tag{4.2}$$

where, a_k is Gaussian random variable with zero mean and variance $\sigma_k^2=4S(\omega_k)\Delta\omega$; φ_k, a random variable having uniform distribution between 0 and 2π; ω_k, circular frequency of roadway surface roughness written as $\omega_k = \omega_L + (k-1/2)\Delta\omega$, $\Delta\omega = (\omega_U - \omega_L)/M$, ω_U and ω_L designate the upper and lower limit of the frequency, respectively; M means a large enough integer number and $S(\omega_k)$ is the PSD of a roadway profile.

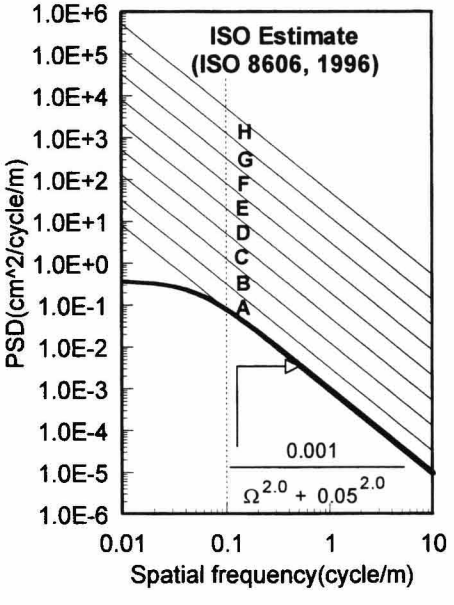

Fig. 4-8. PSD curve of roadway roughness.

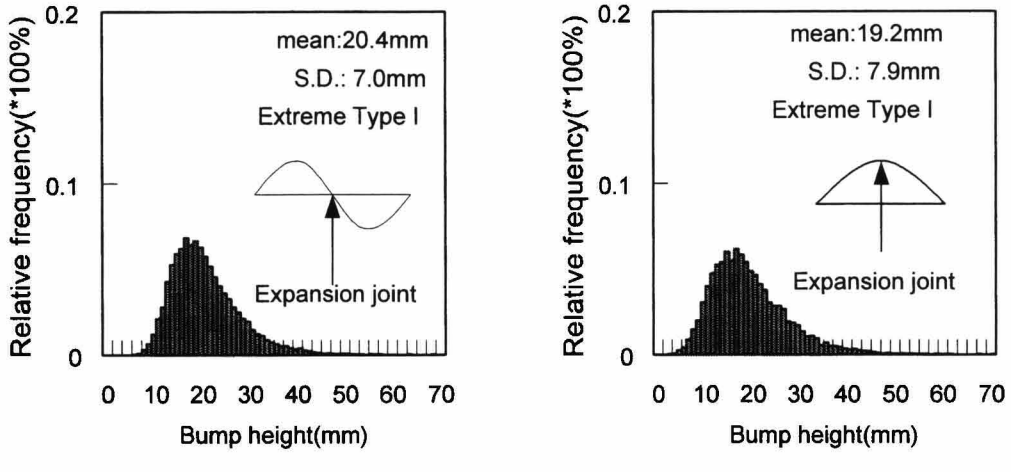

a) Bump: Pattern-A

b) Bump: Pattern-B

Fig. 4-9 PDF of bump height at expansion joint

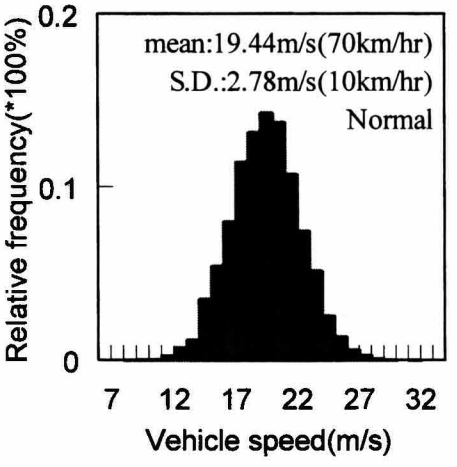

Fig. 4-10 PDF of vehicle speed

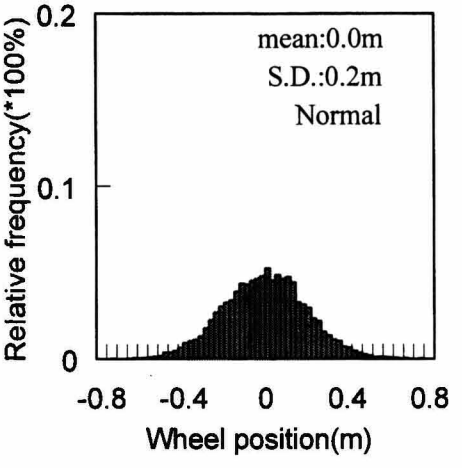

Fig. 4-11 PDF of vehicle path

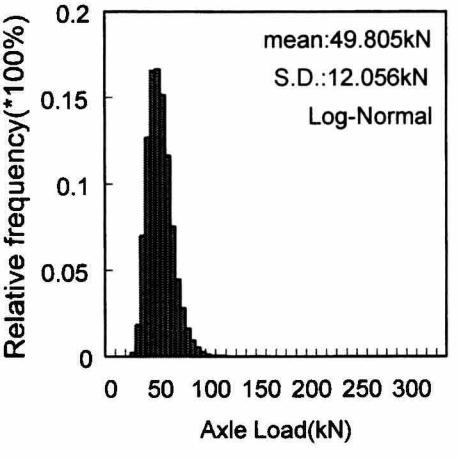

(a) Front axle

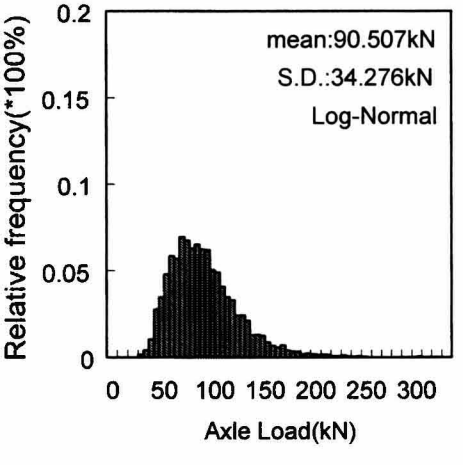

(b) Front wheel of rear axle

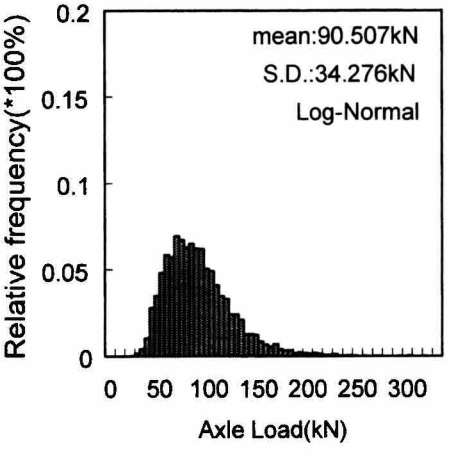

(c) Rear wheel of rear axle

Fig. 4-12 PDF of axle loads

Bump height near expansion joints

The extreme Type I distribution is assumed to describe bump heights at expansion joints of bridges based on the surveying results in Japan [23] as shown in Fig. 4-9(a) and Fig. 4-9(b). It was found, from the preliminary investigation, that the bump Pattern-B (Fig. 4-9(b)) gives greater effect on impact factors of decks than the Pattern-A (Fig. 4-9(a)) does. Thus the Pattern-B is adopted as a bump model.

Vehicle speed

The normal distribution is assumed for vehicle speed on a highway as shown in Fig. 4-10 [24].

Vehicle path

The position of a vehicle path from a target position is assumed to follow normal distribution with zero mean value and standard deviation of 0.2m as shown in Fig. 4-11 [25].

Axle weight

The lognormal distribution is assumed for axle loads of the three-axle vehicle based on the database measured on Hanshin Expressway, Japan [25] (see Fig. 4-12(a) to Fig. 4-12(c)).

4.3.2 Simulation of impact factor for deck

A number of sample roadway profiles, bump heights, vehicle speed, vehicle path and axle loads are generated by means of MCS method. Impact factors of each deck are analyzed according to each sample of the random variables by means of traffic-induced vibration analysis of bridges. In simulations, no correlation among the considered random variables is assumed.

A hundred samples of the simulated random variables are considered in analysis, since impact factors tend to converge within 100 samples as shown in Fig. 4-13.

Cumulative distribution functions of deck slab's impact factors

The preliminary investigation on the impact factor of the RC deck shows that the normal

distribution can represent the statistical characteristics of the impact factor by only considering randomness of roadway roughness [10, 11]. However, the histogram of the impact factor at each panel is shown in Fig. 4-14 indicates that the impact factor of decks is no longer idealized as a normal distribution.

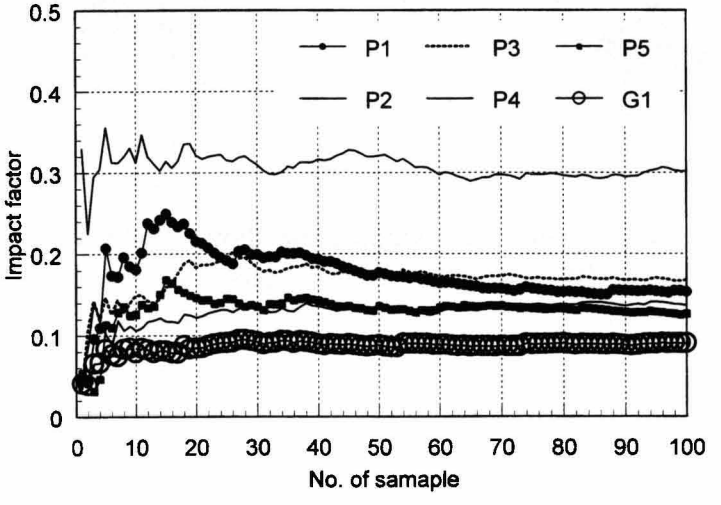

Fig. 4-13. Updated means of impact factors

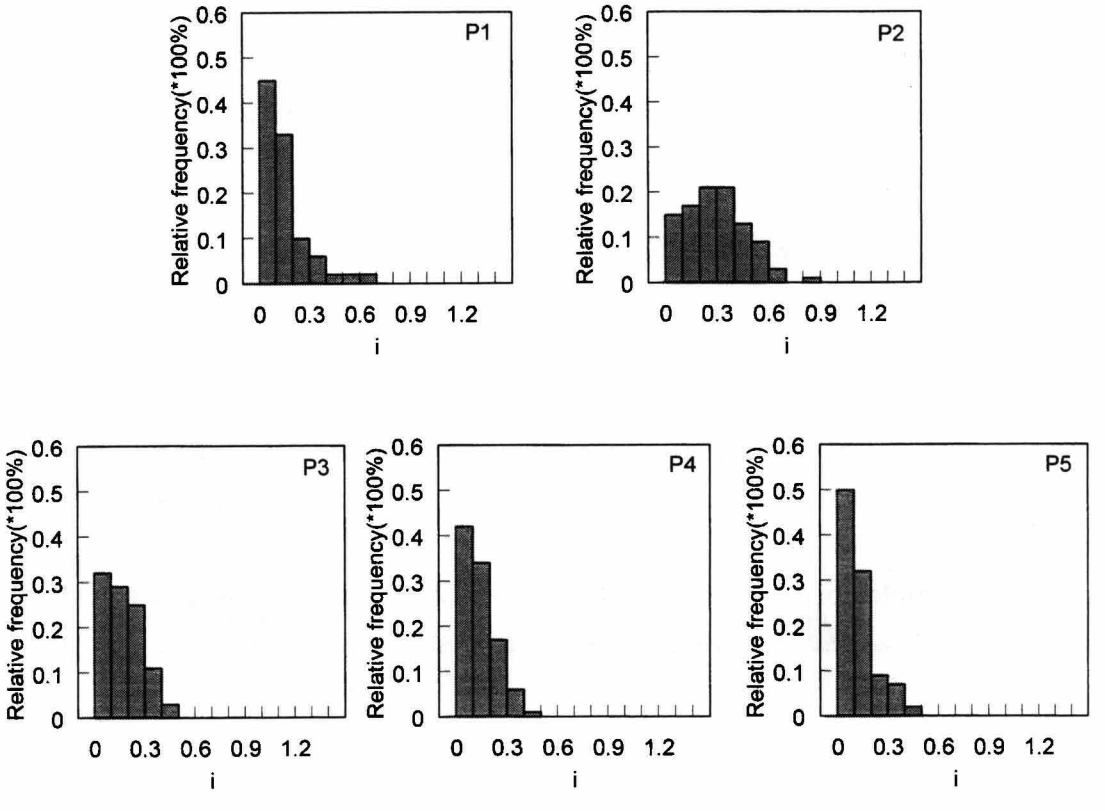

Fig. 4-14 Histogram of impact factors at each panel of the deck

To examine the probabilistic feature more clearly, simulated impact factors at each deck slab are plotted on the normal, lognormal and extreme Type I probability papers as shown in Fig. 4-15 to Fig. 4-17, and the straight lines on the lognormal and extreme Type I distribution paper can approximately represent the probabilistic property of the impact factor.

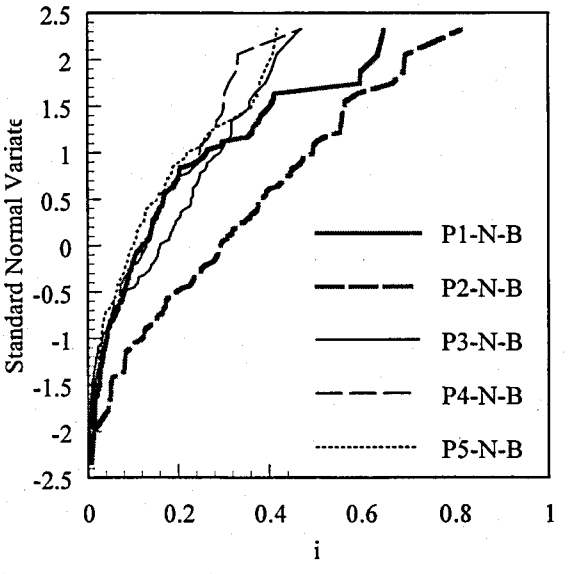

Fig. 4-15 Analytical impact factors of deck slabs on normal probability paper

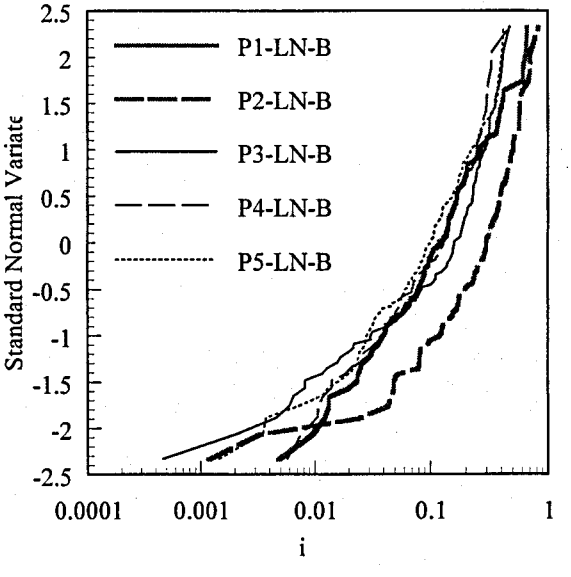

Fig. 4-16 Analytical impact factors of deck slabs on log-normal probability paper

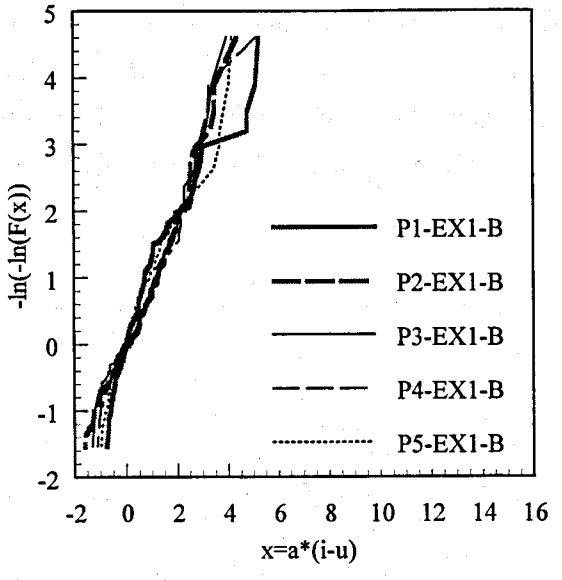

Fig. 4-17 Analytical impact factors of deck slabs on extreme Type I probability paper

Table 4-6 Code specified impact factors for deck slab

Code	Impact factor	i_{code}
AASHTO (USA)	$i=50/(3.3L+125)\leq 0.3$	0.300
DIN1072 (German)	$i=0.4-0.008L$	0.379
JSHB (Japan)	$i=20/(L+50)$	0.380
OHBDC (Ontario, Canada)	$i=0.4$	0.400

$L=2.65m$: Span length in meter

Probability exceeding codes specified impact factors

The probabilities of exceeding the impact factors specified in AASHTO standard, Japanese Specifications of Highway Bridges (JSHB), Ontario Highway Bridge Design Code (OHBDC) and DIN1072 are examined. The impact factors specified in the codes are shown in Table 4-6. The probabilities of exceeding the code specified impact factors are determined according to the relations in Eqs. (4.3) to (4.5).

Normal distribution ; $P(i > i_{code}) = 1 - \Phi\left(\frac{(i_{code} - \mu_i)}{\sigma_i}\right)$ (4.3)

Lognormal distribution ; $P(i > i_{code}) = 1 - \Phi\left(\frac{(y - \mu_y)}{\sigma_y}\right)$ (4.4)

Extreme Type I distribution; $P(i > i_{code}) = 1 - F(i) = 1 - e^{-e^{-\alpha(i_{code} - u)}}$ (4.5)

where, i is the impact factor assumed as a general normal random variable, i_{code} is the code specified impact factor, μ_i, a mean value of the impact factor, σ_i, a standard deviation of the impact factor, y indicates $ln(i)$, μ_y, a mean of $ln(i)$ and σ_y, a standard deviation of $ln(i)$. α and u are distribution parameters of the extreme Type I distribution.

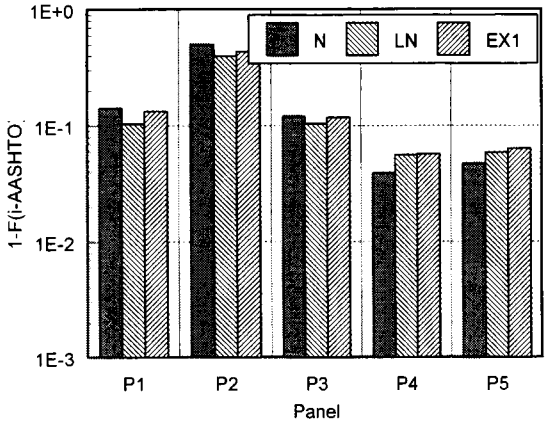

(a) AASHTO (USA)

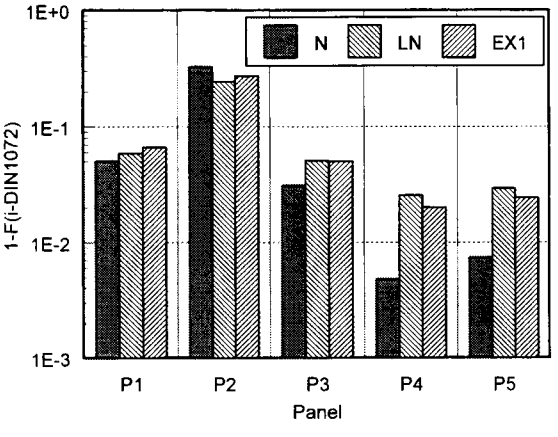

(b) DIN1072 (Germany)

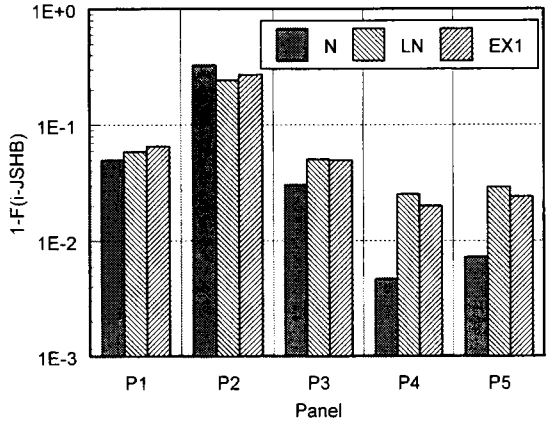

(c) JSHB (Japan)

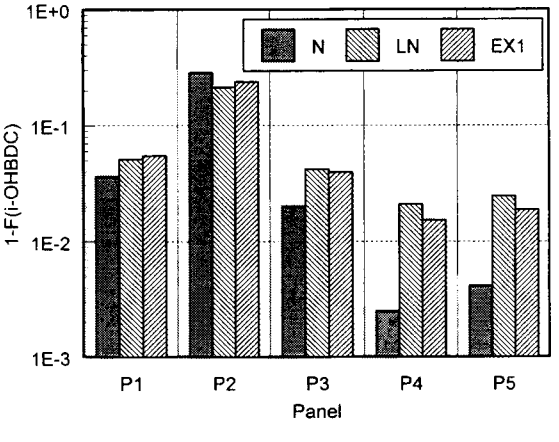

(d) OHBDC (Ontario, Canada)

Fig. 4-18. Probability of exceeding code specified impact factors

The probability of exceeding the code-specified impact factors is summarized in Fig. 4-18 with respect to each panel. It shows that the impact factor of the deck near the expansion joint (P2 panel) dominates the design impact factor under the conditions considered in this study. The symbols N, LN and EX1 in Fig. 4-18 indicate the probability determined from the impact factor assumed as normal, lognormal and extreme Type I distribution, respectively.

For the P2 panel experiencing the maximum impact factor, the probability exceeding the code-specified impact factors is the order of 10^{-1} under the assumption of following the lognormal distribution of the impact factor, on the other hands those for P1 and P3 ~ P5 panels are the order of 10^{-2} as shown in Table 4-7.

As an example, for the bridge with two lanes on Hanshin Expressway (see Fig 4-2), if the traffic volume per hour in one lane is assumed to be 862 vehicles, 20% of the traffic volume to be the heavy trucks, 30% of the heavy trucks to be the three axle truck [26] and the probability exceeding the code specified impact factor to be 10^{-1} as shown in Table 4-7, then the number that the deck experiences the dynamic effect greater than that considered in designing stage becomes more than one hundred per day.

The reliability index of the code specified impact factor under the assumption of log-normal distribution is summarized in Table 4-8, the value in the parenthesis indicates the reliability index of the code specified impact factor under the condition of no bump at the expansion joint.

The target reliability index proposed in Eurocode is also summarized in the Table 4-8 and Fig. 4-19: target reliability index for serviceability limit state (SLS) is 1.5; for the ultimate limit state (ULS), 3.8; for the fatigue limit state (FLS), 1.5~3.8 [27, 28]. The G1 in Table 4-8 indicates the reliability index of code specified impact factor for the G1-girder (see, Fig. 4-3), which is adopted to compare with the impact factor of decks.

If the impact factor can be classified in the serviceability limit state then reliability index for the P2 panel is lower than that of the target reliability index for the SLS, although what kind of limit state the impact factor is classified in has not been defined yet. On the other hand the reliability considering the condition of no bump at the expansion joint satisfies the SLS. The reliability index for the SLS of the G1-girder satisfies the target reliability index regardless of the existence of bump at the expansion joint except the DIN1072. It indicates that the bump is one of important factors for impact factor of decks. It is noteworthy, however, that the probability of exceeding code specified impact factors is overestimated since the bump in real highway bridges is expected to have better condition than that measured at national roadway bridges which used in this study.

To investigate the effect of vehicle speed on the DIF value of decks, except the vehicle speed the random variables mentioned above are considered. The deterministic vehicle speed of 40km/hr and 80km/hr is considered, and the probabilities of exceeding the code-specified

impact factor are summarized in Table 4-9.

The probability becomes the order of 10^{-1} for P1 and P2 panels and the order of 10^{-2} for P3 ~ P4 panels under vehicle speed of 80km/hr, on the other hand that probability becomes the order of 10^{-2} for the P1 panel, the order of 10^{-3} for P2~ P4 panels and the order of 10^{-4} for the P5 panel under the speed of 40km/hr. It means that the impact factor of the deck has tendency to increase according to the vehicle speed. One of the reasons for increasing possibility to exceed the code specified impact factor according to vehicle speeds may be that the impulsive wheel load generated by passing the bump tends to travel far from the expansion joint even under the condition of large damping of the vehicle and affect the dynamic response of deck slabs. Therefore, the vehicle speed should be considered as a random variable in the simulation.

Table 4-7. Probability of exceeding code specified impact factors

Panel / Code	P1	P2	P3	P4	P5
AASHTO	10^{-1}	10^{-1}	10^{-1}	10^{-2}	10^{-2}
DIN1072	10^{-2}	10^{-1}	10^{-2}	10^{-2}	10^{-2}
JSHB	10^{-2}	10^{-1}	10^{-2}	10^{-2}	10^{-2}
OHBDC	10^{-2}	10^{-1}	10^{-2}	10^{-2}	10^{-2}

* The probabilities are calculated based on the assumption of following lognormal distribution

Table 4-8. Reliability index of the code specified impact factors

Panel / Code	P1	P2	P3	P4	P5	G1
AASHTO	1.3 (2.1)	0.3 (2.4)	1.3 (2.5)	1.6 (2.7)	1.6 (2.7)	1.6 (2.5)
DIN1072	1.6 (2.5)	0.7 (2.7)	1.7 (2.7)	2.0 (2.9)	1.9 (2.9)	0.5 (1.0)
JSHB	1.6 (2.5)	0.7 (2.7)	1.6 (2.7)	2.0 (2.9)	1.9 (2.9)	1.8 (2.7)
OHBDC	1.6 (2.5)	0.7 (2.7)	1.7 (2.7)	2.0 (2.9)	2.0 (3.0)	2.8 (3.7)

( ): Reliability index of the code specified impact factor in the case of no bump

β_T for SLS: 1.5, β_T for ULS: 3.8, and β_T for FLS: 1.5~3.8

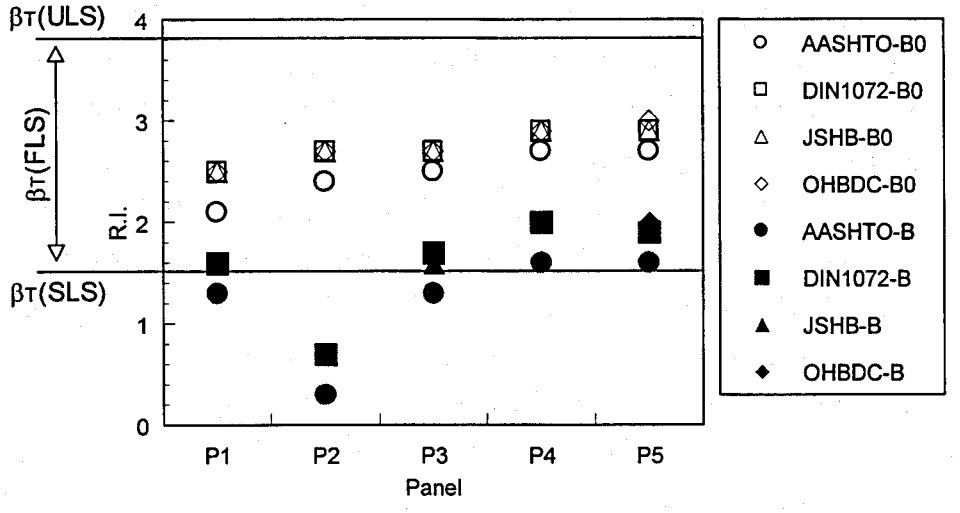

Fig. 4-19 Reliability index of code specified impact factors with target reliability indices

Table 4-9. Probability of exceeding code specified impact factors at different speeds

Panel	P1		P2		P3		P4		P5	
Speed / Code	40km/hr	80km/hr	40km/hr	80km/hr	40km/hr	80km/hr	40km/hr	80km/hr	40km/hr	80km/hr
AASHTO	10^{-2}	10^{-1}	10^{-3}	10^{-1}	10^{-3}	10^{-2}	10^{-3}	10^{-2}	10^{-3}	10^{-2}
DIN1072	10^{-2}	10^{-1}	10^{-3}	10^{-1}	10^{-3}	10^{-2}	10^{-3}	10^{-2}	10^{-4}	10^{-2}
JSHB	10^{-2}	10^{-1}	10^{-3}	10^{-1}	10^{-3}	10^{-2}	10^{-3}	10^{-2}	10^{-4}	10^{-2}
OHBDC	10^{-2}	10^{-1}	10^{-3}	10^{-1}	10^{-3}	10^{-2}	10^{-3}	10^{-2}	10^{-4}	10^{-2}

* The probabilities are calculated based on the assumption of following lognormal distribution

4.4 Conclusions

It is not possible to generalize the vehicle-bridge interaction problems because of its complicate dynamic interaction system. Nevertheless of its complicate dynamic relations between vehicle motions and bridge responses with roadway roughness, if some effects of influence factors are defined, it can be seen that the variation is not purely random but must follow a certain physical law. Therefore, in this chapter, to investigate to a certain physical law of the vehicle-bridge interaction problem, a computer simulation on dynamic responses of bridges and wheel loads of heavy vehicles idealized as 7DOF and 8DOF vehicle systems is carried out.

The probabilistic features of RC decks' simulated impact factors are also examined in this chapter. The reliability evaluation of code-specified impact factors is carried out considering randomness of roadway roughness, bump heights, vehicle speeds, traveling position of vehicles and axle weights.

The summarized result can be described as follows;

1. A strong correlation between DLC and DIF values is observed. The dynamic feature of bridge responses is dominated by the natural frequency of bridge itself for vehicles running on the very smooth roadway. On the other hand, the dynamic feature is dominated by vehicle's dynamic characteristics for vehicles running on the relatively rough roadway which has enough ability to stimulate vehicles. Moreover, the dominant frequencies of dynamic wheel loads, bounce motions of vehicles and bridge responses are strongly related with each other.
2. The axle-hop motion with relatively high dominant frequency compared to those of vehicle wheel loads and bridge responses can also influence to the dynamic wheel load and the bridge response with increasing speed. Thus, despite of the strong correlation between DLC and DIF values, the frequency features of vehicles and bridges should be included to define dynamic effect of vehicle loads on bridges.
3. The lognormal distribution can approximately represent probabilistic properties of the impact factor for the RC deck slab.
4. The impulsive wheel load effect on decks due to the bump tends to travel far from the expansion joint even under the condition of large damping of the vehicle, and the impact factor has tendency to increase according to the vehicle speed. That is, the probability can be greatly affected by the vehicle speed, thus the vehicle speed must be considered as a random variable to assess the impact factor more rationally.
5. The impact factor of the deck near expansion joints dominates the design impact factor under the conditions considered. For the panel experiencing the maximum impact factor, the probability exceeding the code-specified impact factors is the order of 10^{-1} under the assumption of following lognormal distribution of the impact factor. Thus, if the impact factor of the deck near an expansion joint of approaching side of a bridge satisfies a given reliability due to a vehicle with tandem axle running on a bump, those reliabilities of other deck slabs are satisfied automatically.
6. It is noteworthy that the probability of exceeding code specified impact factors is overestimated since the bump in real highway bridges is expected to have better condition than that measured at national roadway bridges which used in this study. The advanced study considering a real condition on highway bridges remains to be studied until measured data for highway bridges are acquired.

References

[1] Biggs, J. M.: Introduction to structural dynamics, McGraw-Hill, 315-327, 1982.

[2] Billing, J. R.: Dynamic loading and testing of bridges in Ontario, CSCE J. of Civ. Eng., **II**, 833-843, 1984.

[3] Cantieni, R.: Dynamic load testing of highway bridges, IABSE Proceedings, P-75/84, 57-72, 1984.

[4] Cantieni, R.: Dynamic behavior of highway bridges under the passage of heavy vehicles, EMPA report, No.220, 1992.

[5] ONTARIO Highway Bridge Design Code 1983, Highway Engineering Division, Ministry of Transportation and Communications, OTM, 1983.

[6] Kim, C.W.: An experimental and analytical study for traffic-induced vibration on roadway bridges, Ph.D. Thesis, Chung-Ang University, Korea, 54-61, 1997.

[7] Kawatani, M. and Kim, C.W.: Computer simulation for dynamic wheel loads of heavy vehicles. Int. J. of Structural Engineering and Mechanics, **12**(4), 409-428, 2001.

[8] Furuta, H, Tsukiyama, I., Dogaki, M. and Frangopol, D.M.: Maintenance support system of steel bridges based on life cycle cost and performance evaluation, Reliability and optimization of structural systems; Proceedings of the 10th IFIP WG7.5 Working Conference on Reliability and Optimization of Structural Systems Osaka, Japan, 25-27 March 2002.

[9] Yokoyama, K., Inoue, J. and Nagahara, T.: Field test on the impact coefficient of steel deck and reinforced concrete slab of highway bridges, JSCE Structural Engineering Vol.35A, 749-756, 1989. *(in Japanese)*

[10]Kim, C.W. and Kawatani, M.: A probabilistic investigation on impact factor of deck slabs of highway bridges, Reliability and optimization of structural systems; Proc. of the 9th IFIP WG7.5 Working Conference on Reliability and Optimization of Structural Systems, Ann Arbor, Michigan, USA, 2000.

[11]Kim, C.W. and Kawatani, M.: Probabilistic investigation on impact factor of deck slabs due to truck configuration type, Reliability and optimization of structural systems; Proceedings of the 10th IFIP WG7.5 Working Conference on Reliability and Optimization of Structural Systems, Osaka, Japan, 25-27 March 2002.

[12]Kawatani, M., Nishiyama, S. and Yamada, Y.: Dynamic response analysis of highway bridges under moving vehicle, Technical Report of the Osaka Univ., 43(2137), 109-118, 1993.

[13]Technical report-Inspections on Umeda entrance bridge structures, Hanshin Expressway Public Corporation (HEPC), 1992. *(in Japanese)*

[14]Kim, C.W.: An experimental and analytical study for traffic-induced vibration on

roadway bridges, Ph.D. Thesis, Chung-Ang University, Korea, 46-48, 1997.

[15]Kim, C. W. and Kawatani, M.: A comparative study on dynamic wheel loads of multi-axle vehicle and bridge responses, Proc. of DETC'01 ASME 2001 Design Engineering Technical Conference and Computers and Information in Engineering Conference Pittsburgh, USA, 2001

[16]Hoogvelt, R. B. J. and Ruijs, P. A. J.: OECD-IR6 DIVINE Element 4. Computer simulation of heavy vehicle dynamic wheel loads, TNO Report 97.OR.016.1/H/PR, TNO, Delft, The Netherlands, 1997.

[17]Nowak, A.S. and Collins, K.R.: Reliability of structures, McGraw-Hill International Edition, 69-90, 2000

[18]Kawatani, M., Yamada, Y., Kim C.W. and Kawaki, H.: Estimtion of slab's response in traffic-induced vibration of highway bridge by three-dimensional analysis, JSCE Structural Engineering Vol.44A, 827-834, 1998. *(in Japanese)*

[19]Dodds, C.J. and Robson, M.M.: The description of road surface roughness, Sound and Vibrations, **31**(2), 175-183, 1973.

[20]Honda, H., Kajikawa, Y. and Kobori, T.: Spectra of road surface roughness on bridges, ASCE Structural Division, **108**, No.ST9, 1956-1966, 1982.

[21]Kawatani, M, Kobayashi, Y. and Takamori, K.: Nonstationary random analysis with coupling vibration of bending and torsion of simple girder bridges under moving vehicles, JSCE J. of Structural Engineering and Earthquake Engineering, **15**(1), 107s-114s, 1998.

[22]ISO 8608. Mechanical Vibration – Road Surface Profiles – Reporting of Measured Data, 1995; British Standard, BS 7853, 1996.

[23]Honda, H., Kajikawa, Y. and Kobori, T.: Roughness characteristics at expansion joint on highway bridges, Proceedings of JSCE, No.328, 173-176, 1982. *(in Japanese)*

[24]Sakano, M., Mikami, M. and Miyagawa, K.: Simultaneous loading effect of plural vehicles on fatigue damage of highway bridges, Reliability and optimization of structural systems V; IFIP Transactions B-12, Takamatsu, Kagawa, Japan, 1993.

[25]Hanshin Expressway Management Technology Center, HEPC, Crack damage of RC deck slabs of highway bridges and its resistance, 1991. *(in Japanese)*

[26]Hanshin Expressway Public Corporation (HEPC), JSSC, Fatigue design live load for urban highway bridges (III), 1995. *(in Japanese)*

[27]Dowling, P.J. and Chryssanthopoulos, M.K.: EC3: The new Eurocode for steel structures; Review of design philosophy and limit state principles, JSCE J. of Structural Engineering and Earthquake Engineering, **10**(3), 105s-116s, 1993.

[28]Eurocode 1: Basis of design and action on structures, Part 1: Basis of design, Sixth draft, March 1993.

Chapter 5

Dynamic responses of two-girder bridges with PC deck

5.1 Introduction

In the last two decades, there has been a significant increase in the number of new bridge constructions due to rapid urban development and economical growth in many areas of the world. Consequently, the challenges to state-of-practice of bridge engineering are becoming broader range. While bridge engineers still stride to build safe and economical bridges to meet the transportation needs of the public by using innovative techniques, many countries are now faced with the problem of developing innovative solutions to enhance the performance level of existing bridges. [1, 2]

Among the innovative design strategy to make steel bridges more economical, one of the most popular design concepts in short and medium span bridges has been the two-girder steel bridge using simplified structural system because of advantages it offers with regard to fabrication, maintenance, etc. [2~5]

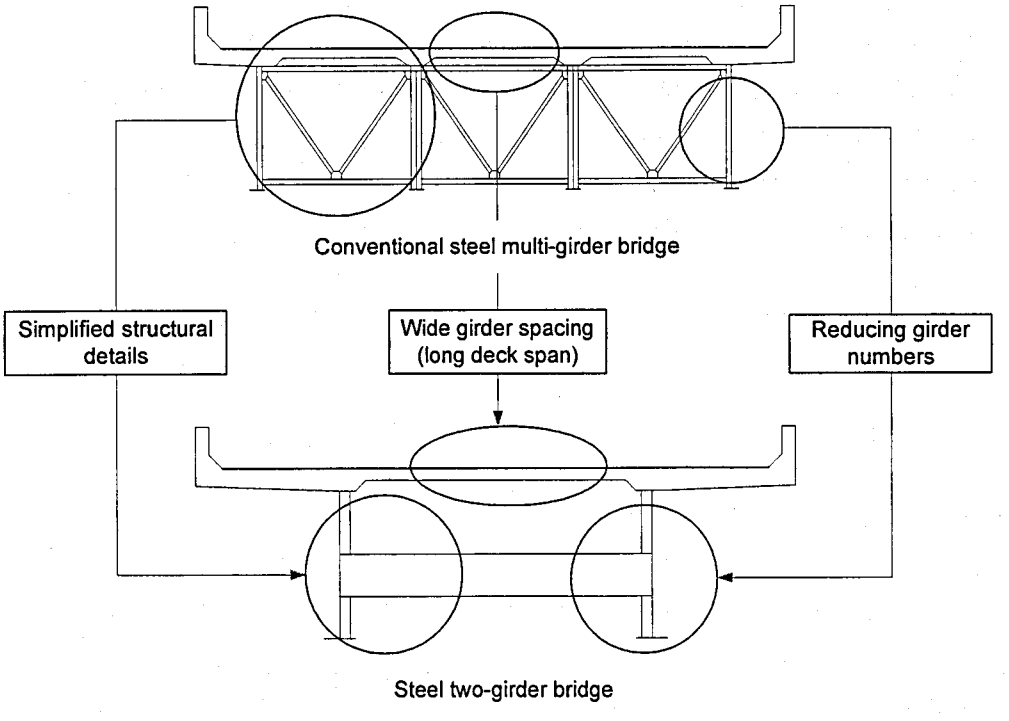

Fig. 5-1 Structural features: two-girder bridge vs. multi-girder bridge

However, as shown in Fig. 5-1, the wider girder spacing and more simplified structural system of the twin-girder bridges than conventional multi-girder bridges can give rise to change of dynamic characteristics of the bridge. It makes the bridge to be easily vibrated by external dynamic loads like wind, vehicle loads, etc. Questions that remain unanswered for the two-girder bridge are the dynamic behavior caused by the structural features under moving vehicles. Furthermore, it is expected that the large deflection of decks due to wide girder spacing can affect the vibration of web plates, which can be linked with fatigue problems as well as low frequency noise from the web plate.

Moreover, to minimize the seismic load on bridges, elastomeric bearings have been equipped in many bridges. The elastomeric bearing works as a soft part between sub- and superstructure and allows movements in all directions by elastic displacements or rotations. Despite of its excellence against seismic loads, larger vertical displacement of the elastomeric bearing than the steel bearing can occur undesirable vibration under moving vehicular loadings.

The dynamic responses of the two-girder bridge due to moving vehicles, however, have not been studied and reported so far as the author knows. Moreover, few investigations on the bridge vibration including local members due to the elastic deformation of elastomeric bearings have been reported, although Harada et al. [6] reported a three-dimensional traffic-induced vibration of a bridge including vibrations of local members of the bridge idealized by means of flat elements for decks and web plates due to moving vehicles.

Therefore, in this chapter, a three-dimensional dynamic response analysis due to moving vehicles is carried out to investigate not only dynamic responses of a two-girder bridge but the effect of the elastic deformation at an elastomeric support on the dynamic response of local members such as web plates and decks. To verify the validity of the analytical response, analytical acceleration responses and Fourier amplitudes of the bridge members are compared with field test data.

5.2 Analytical models

5.2.1 Bridge models

A two-span continuous steel two-girder bridge in service with total length of 106m (53m+53m), girder spacing of 6.0m and width of 11.4m is adopted as a bridge model. Figure 5-2 shows the plan view and the cross-section of the bridge. The bridge model is assumed as a straight bridge, even though it is a curved bridge with radius of curve R=1000m. The deck slab is made of a prestressed concrete of 31cm thick, and is assumed to act compositely with

main girders. The properties of the bridge are shown in Table 5-1.

Two kinds of bridge models can be used in the analysis according to the problem to be solved. The full 3-D model can be adopted to determine the behavior of local members like web plates of a main girder, on the other hand the 3-D plane model is widely used in investigating the vertical dynamic responses of the bridge.

The full 3-D FE model of the bridge is shown in Fig. 5-3, which consists of flat shell elements [7, 8] for decks, guardrails, cross beams, web plates and upper and lower flanges of main girders and beam elements for stiffeners. V1, V2, V3 and V4 in Fig. 5-3 indicate the noted nodes adopted to compare with experimental responses; The location of the point V1 is top of the guardrail on the abutment A1; V2, center of the deck at the center of the first span; V3, upper flange of girder at the center of the first span; V4, center of the deck on the abutment A2. H1, H2, H3 and H4 are the nodes to investigate the dynamic response of web plates; H1 is the node connected with cross beam at the center of the first span; H2, the node located at 2.65m from the P1 support to the first span; H3, the node located at 2.65m from the P1 support to the second span; H4, the connected point with cross beam at the center of the second span.

The FE bridge model consists of 1003 nodes including double nodes. The bridge has elastomeric bearings at the supports on abutments A1 and A2 and pier P1, and thus the double node with springs at each direction including rotation is considered to idealize the elastomeric bearing.

Details for the spring constants of elastomeric bearings are summarized in Table 5-2. In modeling a prestressed concrete deck, the assumption of isotropic plate is adopted. Young's modulus for steel and prestressed concrete are assumed as $E_c=3.04*10^6 N/cm^2$ and $E_s=2.06*10^7 N/cm^2$, respectively. In modal analysis, the consistent mass is considered, and the mass of asphalt pavement is also considered.

Table 5-1 Properties of bridge model

Span length (m)	53m+53m=106m
Width (m)	11.4m
Thickness of deck (cm)	31cm (45cm at bridge end)
Girder depth (m)	3m
Weight of super-structure (kN/m)	175kN/m
σ_{ck} (N/mm^2)	39.2 N/mm^2
Dimensions of the main girder (mm): at center span	WEB 3000X23
	Up. FLG. 960X44
	Lw. FLG. 970X40

The damping ratio of the bridge is determined from test results based on logarithmic decrements of the bridge response; the logarithmic decrements for the first and the second modes are 0.045 and 0.040, respectively. Thus, the damping constant of the bridge is assumed to have 0.7 % for the first and second modes.

A 3-D plane FE model for the bridge is shown in Fig. 5-4, and it consists of 231 nodes, 192 flat elements for decks and 159 beam elements for girders, cross-beams and guard-rails. The properties of the structural members are the same as those of the full 3-D model.

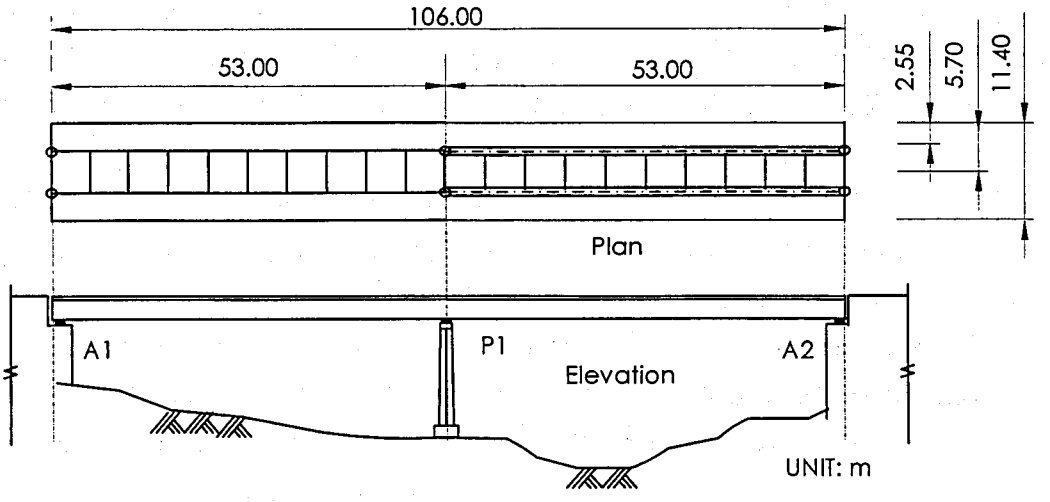

(a) Plan view

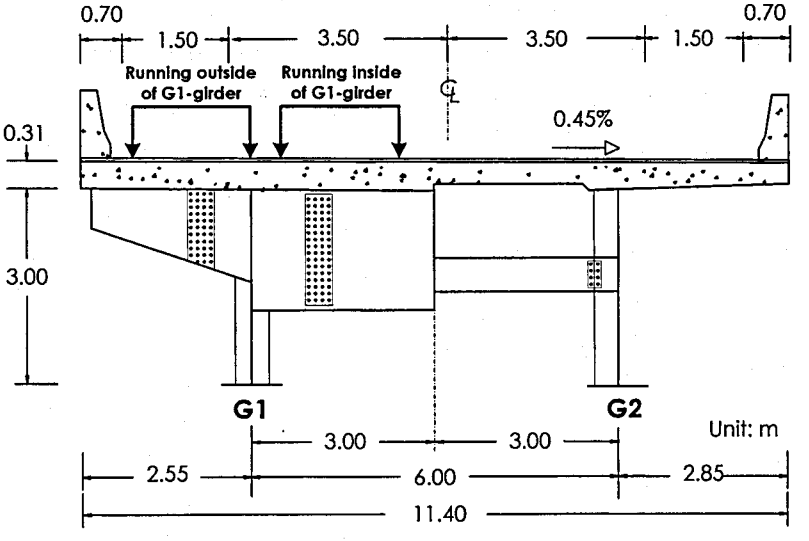

(b) Cross sectional view and vehicle paths adopted in analysis

Fig. 5-2 Steel two-girder bridge with PC deck

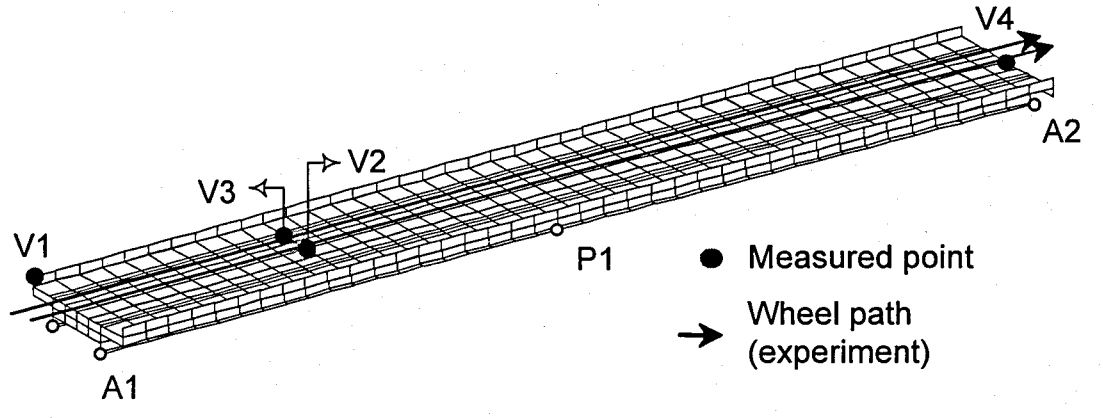

(a) Measured point on full 3-D FE model

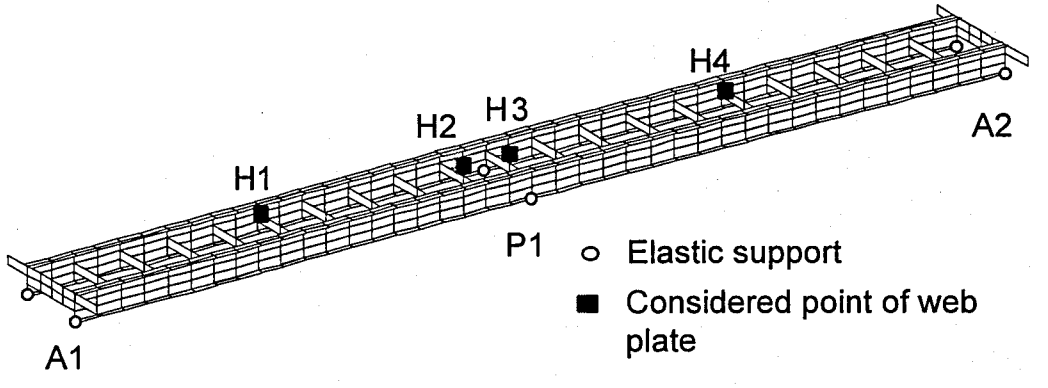

(b) Analyzed points on web plate of the main girder

Fig. 5-3 Full 3-D FE model for steel two-girder bridge with PC deck

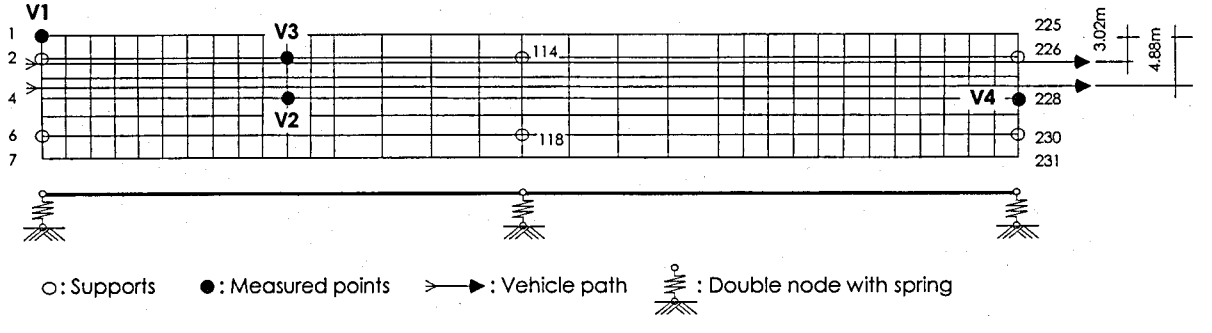

Fig. 5-4 3-D plane FE model for steel two-girder bridge with PC deck

Table 5-2 Spring constants of elastomeric bearing (kN/m)

	A1	P1	A2
Longitudinal	4.4718 E+02	9.806 7E+02	4.4718 E+02
Transverse	6.4332 E+02	7.3746 E+02	6.0409 E+02
Vertical	1.4834 E+06	1.0564 E+07	5.5547 E+06

Table 5-3 Properties of vehicles

Properties			Vehicle	VEH-EX	VEH-1
Gross weight (kN)				196.03	194.86
Axle weight (kN)	Front			42.95	49.92
	Rear			153.08	144.94
Natural frequency (Hz)	Bouncing	Front		2.35	1.90
		Rear		3.00	3.30
	Axle-hop	Front		8.54	16.35
		Rear		9.75	19.16
Logarithmic decrement	Front			0.81	0.66
	Rear			0.14	0.33
Tread (m)	Front			1.86	2.05
	Rear			1.86	1.86
Axle distance (m)	Front-Front tire of tandem axle			3.21	3.35
	Front-Rear tire of tandem axle			4.50	4.65

5.2.2 Vehicle model and roadway profile

A three-axle dump truck with gross weight of 196kN idealized as 8DOF model [9] as shown in Fig. 2-1 (b) is used in field test and analysis as a heavy vehicle model running on the bridge. Details of the vehicle model are in Table 5-3. The vehicle model denoted as VEH-EX in Table 5-2 is the vehicle used in the field test; VEH-1, the vehicle having tires of higher frequency characteristics than that of the VEH-EX vehicle.

The roadway roughness is measured every 50cm within the range of 10m at each supports. The roadway surface profile considered in the analysis is, however, simulated based on the PSD function in Eq. (2.65) [10], because the sampling rate is too rough and the measured range is too confined within a small area to apply to the analysis of the traffic-induced vibration of bridges. In dynamic response analysis, on the other hand, measured bumps assumed to have a shape of the half sine curve at expansion joint of A1 abutment under the vehicle path are considered: depth of 16mm with width of 780mm for left wheel track; 14mm

with 780mm for right wheel track.

The roughness coefficient α is assumed as $0.001cm^2/c/m$. The values of β and n of the PSD curve are assumed as β=0.05 and n=2.0, respectively, to fit the measured PSD of Meishin expressway in Japan [11]. The PSD curve assumed in numerical analysis is the same as the PSD curve appeared in Fig. 4-8.

5.3 Eigen-value analysis

5.3.1 Fundamental frequencies

Typical fundamental frequencies and mode shapes taken from the eigen-value analysis are compared with experimental results as shown in Fig. 5-5 and Fig. 5-6 of the full 3-D and 3-D plane models, respectively. It verifies the validity of two analytical bridge models for dynamic response analysis.

The natural frequency related to the bending mode of the 3-D plane model has greater value than that of full 3-D model. On the other hand, for the first torsional mode, the natural frequency of the 3-D plane model is lower than that of the full 3-D model, and the second torsional mode of the two models show similar frequency features with each other. It indicates that the stiffness for bending of the 3-D plane model is overestimated compared with the full 3-D model. On the other hand the torsional rigidity of the 3-D plane model is underestimated.

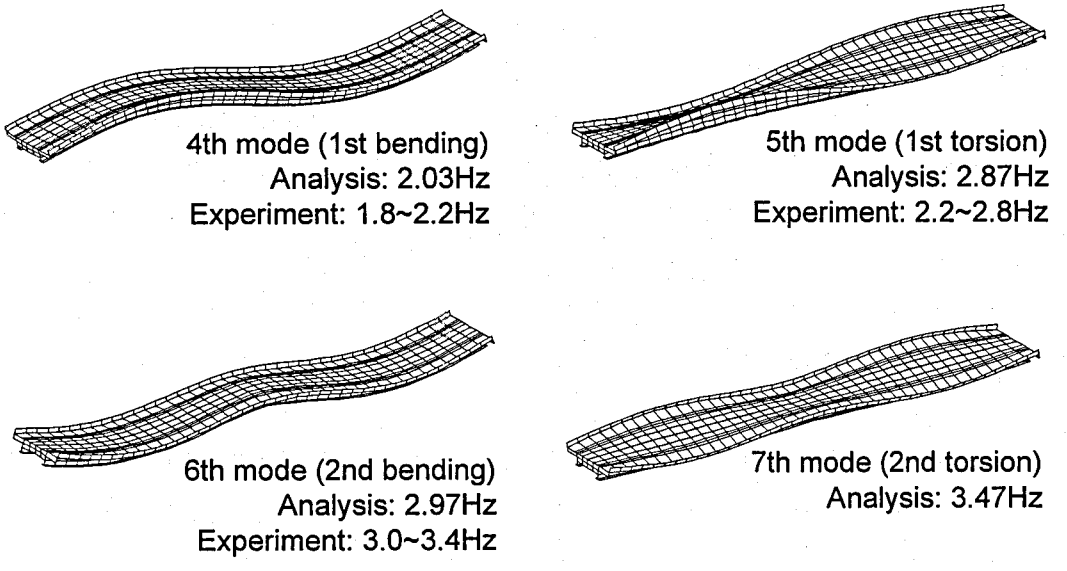

Fig. 5-5 Mode shapes and natural frequencies: Full 3-D model

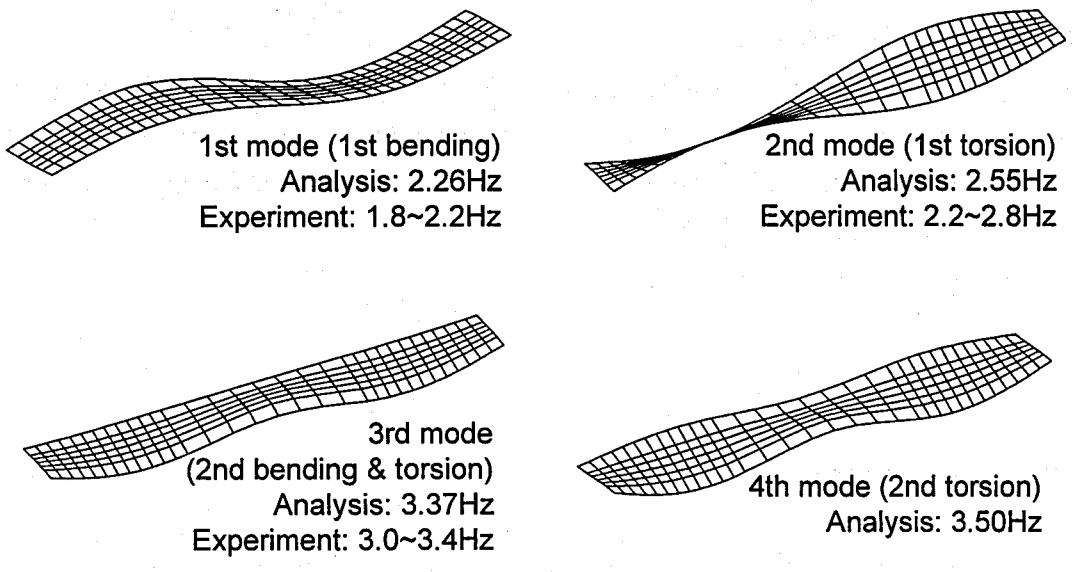

Fig. 5-6 Mode shapes and natural frequencies: 3-D plane model

5.3.2 Natural modes of local members

To investigate the dynamic characteristic of local members such as decks and web plates, typical mode shapes of the full 3-D model are summarized in Fig. 5-7. It is observed that the natural frequencies related to the bending of decks and out-of-plane deformation of web plates are distributed near 7Hz and 8Hz (see Fig. 5-7(a) and Fig. 5-7(b)) and 16Hz (Fig. 5-7(d)), respectively. The frequency related to vertical deformation of elastomeric bearings can be observed near 14Hz as shown in Fig. 5-7(c).

Those modes taken from the 3-D plane model corresponding to the bending of decks and the vertical deformation of elastomeric bearings of the full 3-D model are shown in Fig. 5-8. The mode shapes and the natural frequencies related to the bending of decks of the 3-D plane model are very similar to those of the full 3-D model. On the other hand, the natural frequency related to the vertical deformation of elastomeric bearings due to the 3-D plane model reveals quite difference, although the same properties for elastomeric bearings are used in analysis. One of the reasons may be the difference in modeling of the main girder directly linked with the bearings at the supports.

Dynamic characteristics of the two-girder bridge indicate that the natural frequency of the bending of decks is less than that of the conventional multi-girder bridges (e.g., the natural frequency of a deck of a conventional three-girder bridge is about 20Hz [12]).

In dynamic response analysis by using the full 3-D model, acceleration responses of the bridge are estimated by superposing up to 200th mode (f_{200}=30.54Hz).

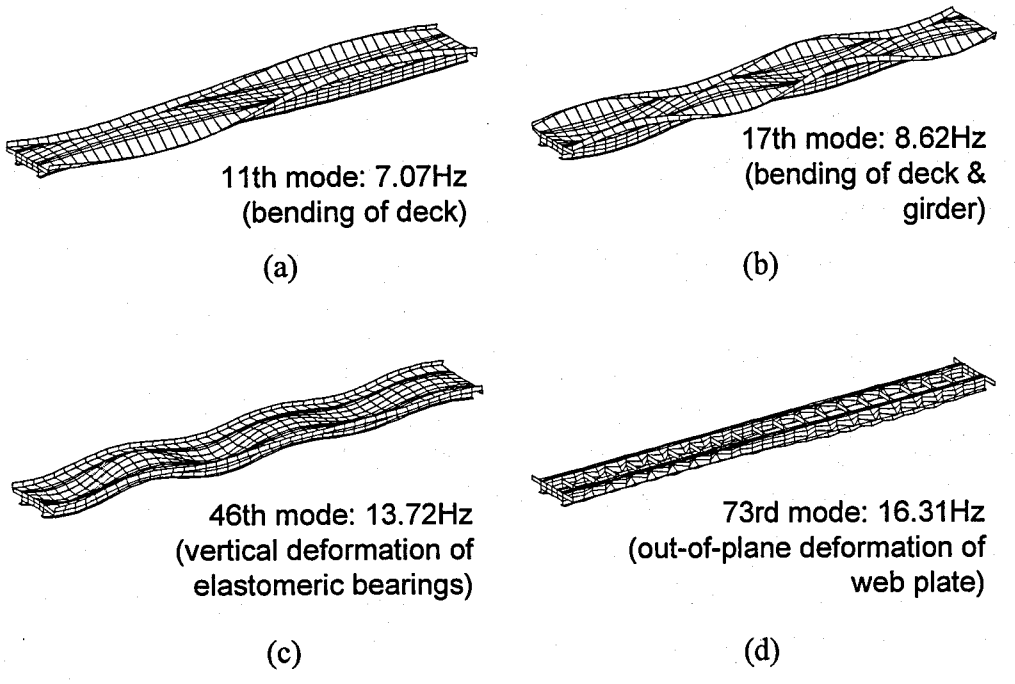

Fig. 5-7 Mode shapes and natural frequencies of local members: full 3-D model

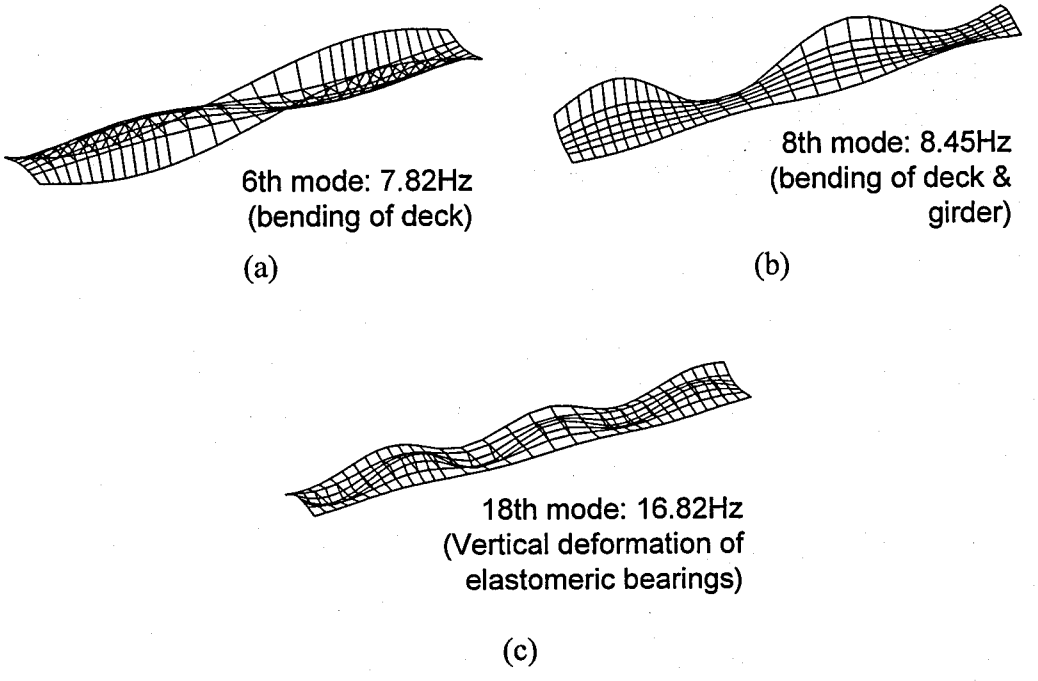

Fig. 5-8 Mode shapes and natural frequencies of local members: full 3-D model

5.4 Verification of the analytical acceleration responses

To verify the validity of the analytical responses of the noted nodes shown in Fig. 5-3, the analytical acceleration responses as well as the Fourier amplitude of the acceleration responses are compared with those of experimental results. The vehicle speed in analysis and experiment is 100km/hr. Experimental acceleration responses and Fourier amplitudes of the noted nodes are compared with those of analytical ones determined from the full 3-D model as well as the 3-D plane model, and the result is shown in Fig. 5-9 and Fig. 5-10.

Although the roadway surface profile used in the analysis of the full 3-D model is the assumed one, the trends, maximum amplitudes and overall responses and the Fourier amplitude of the analytical response match quite well with experimental ones.

The responses of the 3-D plane model have tendency to have smaller amplitude than that of the full-3D model. However, in general, the quality of the agreement between the experimental and analytical results is considered extremely encouraging and quite acceptable in the light of potential sources of error.

The most dominant acceleration responses due to the impulsive load as vehicle passing over bumps can be found at the guardrail on A1 (node V1) among the acceleration responses appeared in Fig. 5-9. The dominant frequency over 15Hz may be the effect of the axle-hop motion amplified by bumps combined with the elastic deformation of elastomeric bearings. The dominant frequency near 3Hz is found in the Fourier amplitudes of the acceleration responses of nodes V2 and V3 (Fig. 5-9 (b) and Fig. 5-10 (a)). It can be explained as the combined effect of the torsional and bending modes of the bridge as well as the bounce motion of the vehicle.

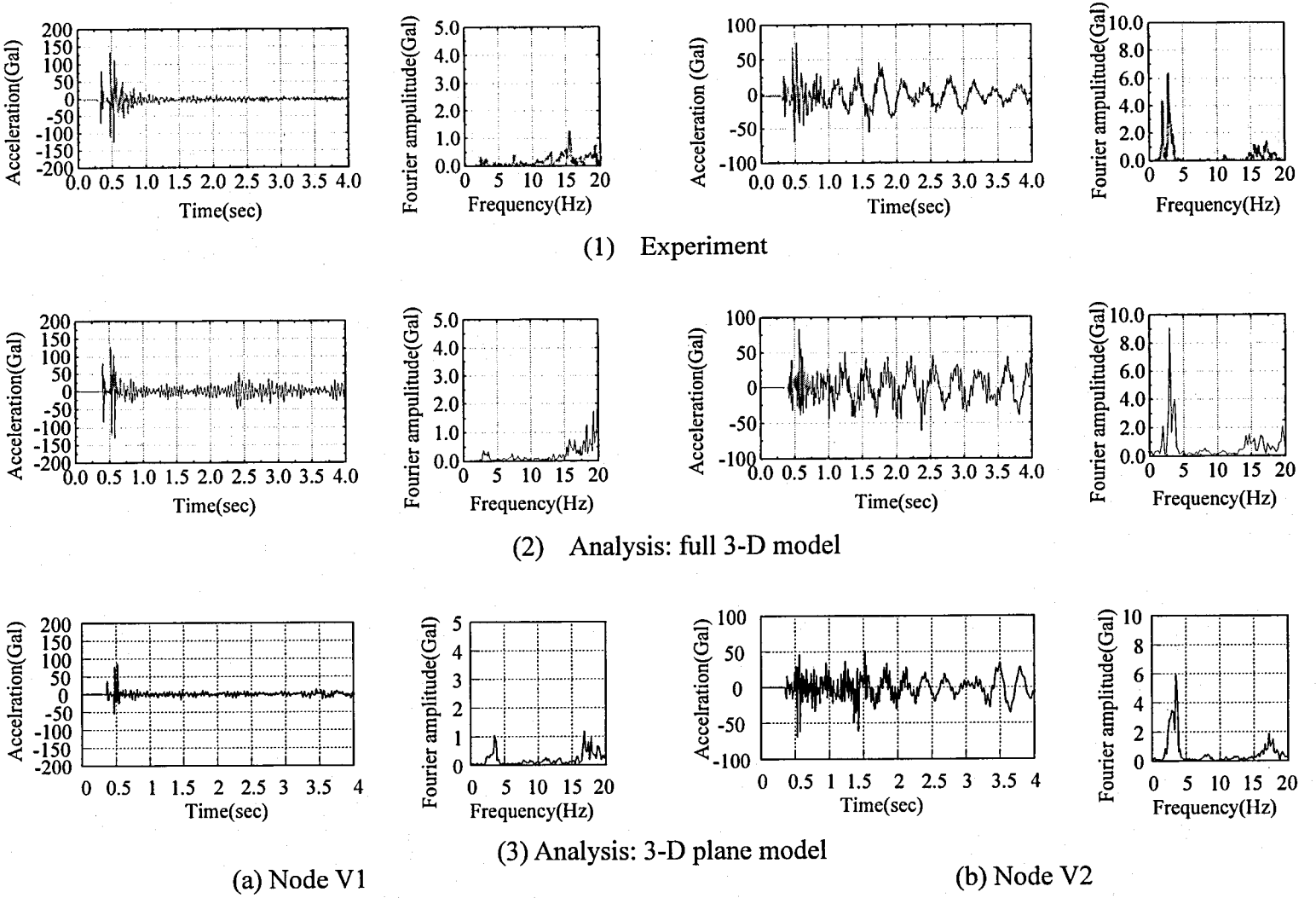

Fig. 5-9 Experimental and analytical acceleration responses and their Fourier amplitudes under single VEH-EX vehicle running (I): v=100km/hr;

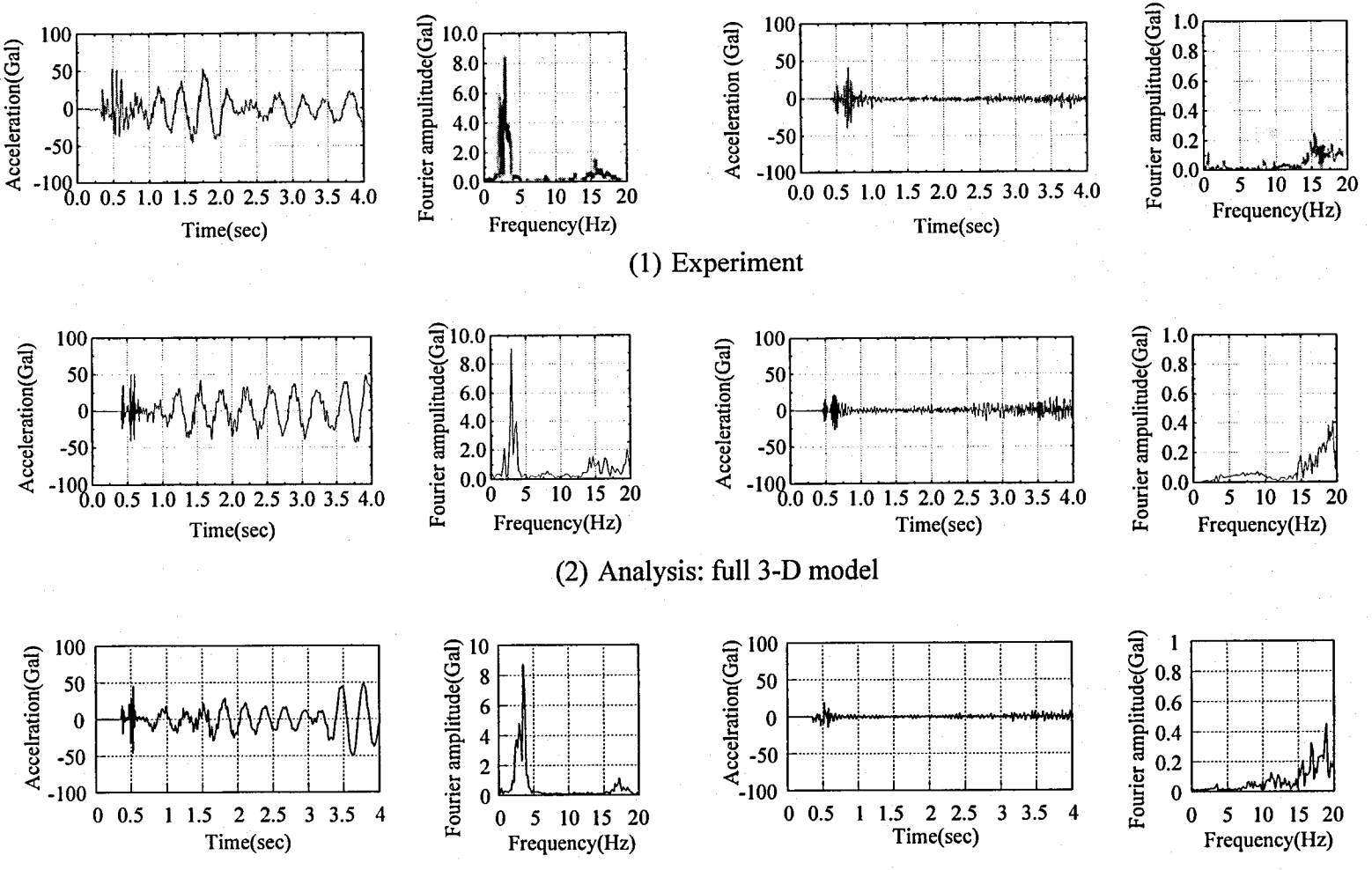

Fig. 5-10 Experimental and analytical acceleration responses and their Fourier amplitudes under single VEH-EX vehicle running (II): v=100km/hr;

5.5 Parametric study for dynamic responses of full 3-D model

In the field test of the bridge, only the case of a vehicle running on the lane located at inside of the G1-girder was considered. However, the vehicle running on biased position of the bridge or outside of the G1-girder (cantilevered part of the deck) will be expected to give critical effects, since the simplified lateral bracing system of the steel two-girder bridge makes the bridge have less torsional rigidity than that of the conventional multi-girder bridge. The additional bump effect due to the elastic deformation of the bearings will give rise to greater impulsive loads to the vehicle followed by the head vehicle.

Therefore, the vehicle type, the vehicle running position, the vehicle speed and the existence of following vehicle are considered as parameters. The critical headway of traveling vehicles can be estimated from the relationship between the vehicle speed and the natural period of a bridge as shown in Eq. (5.1).

$$L_{cr} = n \cdot v \cdot T_i \quad (n: \text{integer}) \tag{5.1}$$

where, L_{cr} is critical headway(m); v, vehicle speed(m/s); T_i, *i-th* natural period of bridge (sec).

5.5.1 Effects of vehicle types on dynamic responses

The vehicle used in the experiment (VEH-EX) has natural frequencies of 8~10Hz for the axle-hop motion. On the other hand, in Japan, it has been reported that dump trucks generally in service have natural frequency of 15Hz to 16Hz about the axle-hop motion [13]. It means that the vehicle used in the experiment (VEH-EX) does not guarantee the critical situation, since the first out-of-plane mode of the web plate occurs at 16.31Hz as shown in Fig. 5-7 (d). The VEH-1 vehicle with higher frequency than that of the VEH-EX vehicle is thus adopted to investigate the response of local members of the steel two-girder bridge. Dominant frequencies of axle-hop motions are summarized in Table 5-3.

The effect of vehicle type to acceleration responses of the bridge is demonstrated in Fig. 5-11. As expected, the peak amplitude of the acceleration response as well as the Fourier amplitude near 20Hz due to the VEH-1 vehicle is greater than that of the VEH-EX.

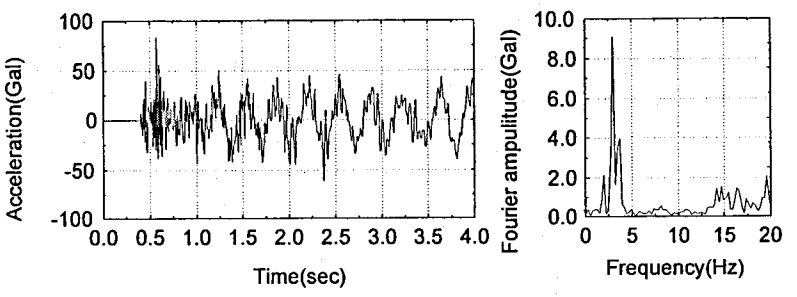

(a) VEH-EX

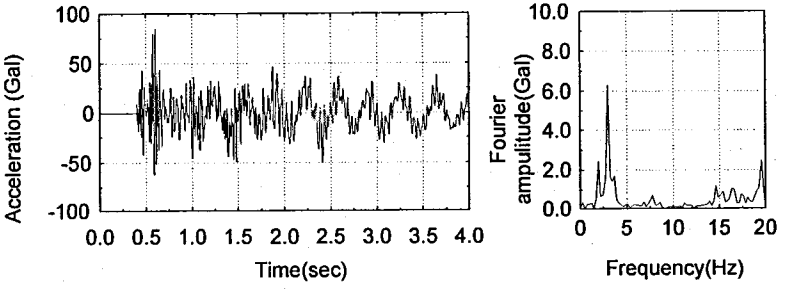

(b) VEH-1

Fig. 5-11 Acceleration responses and Fourier amplitudes of node V2 w.r.t. vehicle type: v=100km/hr; running inside of G1-girder

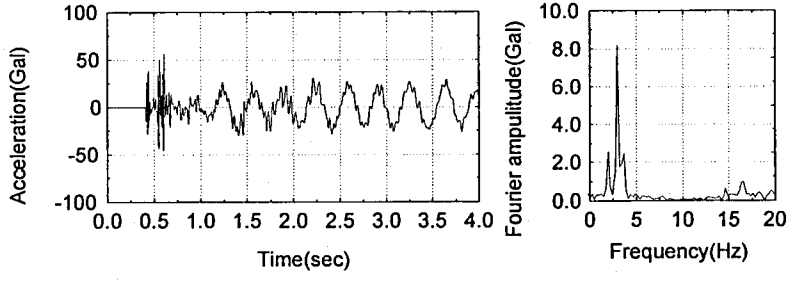

(a) Vehicle running inside of G1-girder

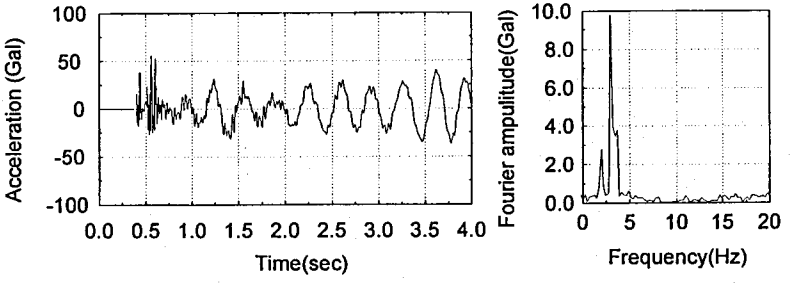

(b) Vehicle running outside of G1-girder

Fig. 5-12 Acceleration responses and Fourier amplitudes of node V3 w.r.t. vehicle path: v=100km/hr; VEH-1 vehicle

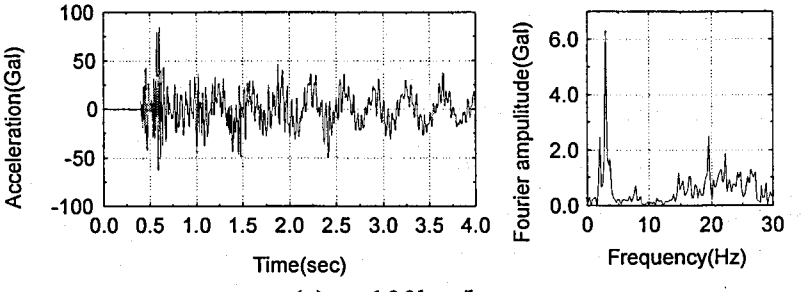

(a) v=100km/hr

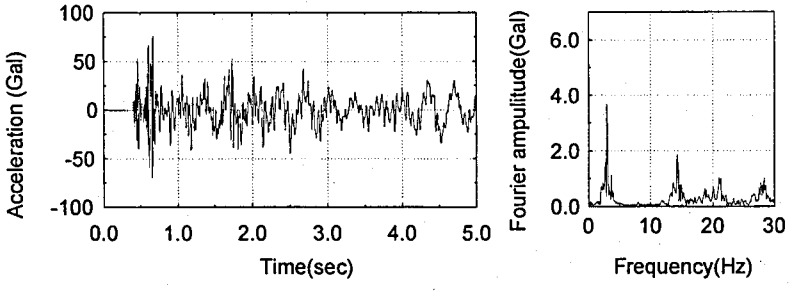

(b) v=80km/hr

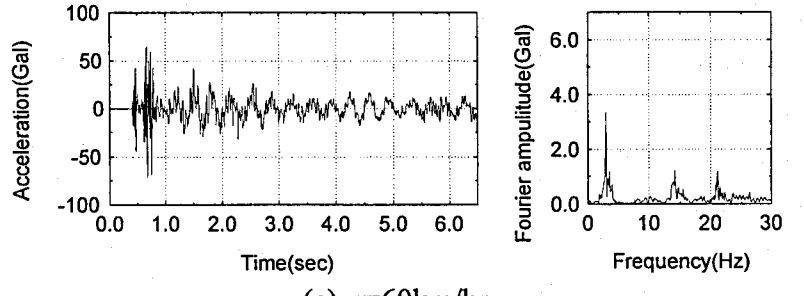

(c) v=60km/hr

Fig. 5-13 Acceleration responses w.r.t. vehicle speed: node V2; VEH-1 vehicle running

5.5.2 Effects of vehicle running position on dynamic response of main girder

The running position of a vehicle (running on inside of the G1-girder and/or on outside of the G1-girder (see Fig. 5-2 (b))) is considered as a parameter to investigate the effect of vehicle running position on dynamic responses of the two-girder bridge. The vehicle model used is the VEH-1, and considered node is the V3. Acceleration responses of the node V3 with respect to running positions of the vehicle are shown in Fig. 5-12.

In considering peak acceleration responses at the moment of vehicle entering the bridge, the peak acceleration response and the Fourier amplitude at 16Hz due to the vehicle running inside of the G1-girder are greater compared with those responses and amplitudes induced by

the vehicle running outside of the G1-girder. It indicates that at the moment of a vehicle entering the bridge the response can be strongly affected by vertical deformations caused by the bending of a deck and the elastic deformation of elastomeric bearing of the support.

On the contrary, when the impulsive loading effect induced by vehicles running on the bump on the expansion joint is damped, the amplitude of acceleration responses as well as the Fourier amplitude of the main girder is more easily affected by the vehicle running outside of the G1-girder because of the coupled effect between torsional modes and vehicle loadings as shown in the Fourier amplitude near 3Hz of Fig. 5-12(a) and (b).

5.5.3 Effects of vehicle speed and vehicle series

Acceleration responses and those Fourier spectra of the noted node V2 under the condition of the VEH-1 vehicle running are shown in Fig. 5-13 with respect to running speed. It is observed that amplitudes of responses tend to decrease as the vehicle speed decrease. Moreover, the Fourier spectra indicate that both Fourier amplitudes near 3Hz and over 10Hz also have tendency to decrease as vehicle speed decrease. It is noteworthy that the amplitude near 19Hz become dominant according to vehicle speed, and it can be the effect of the axle-hop motion of 19.16Hz as shown in Table 5-3.

The effect of vehicle series (two vehicles with critical headway of 46.63m) on dynamic responses is summarized in Fig. 5-14. It shows that the amplitude of the acceleration response of decks is more easily amplified by passage of traveling vehicles than by single vehicle running. As shown in Fig. 5-14(b), the amplitude of the second peak at the moment of 2.2 second is greater than that of the first peak, although the two vehicles having the same properties are used in analysis. One of the reasons for the result can be that the impulsive wheel load of the second vehicle becomes amplified by the additional bump height generated by the elastic deformation of the elastomeric bearing and decks under the load of the head vehicle. On the other hand, amplitudes of the Fourier spectrum tend to decrease over the frequency range in considering except near 8Hz related to bending mode of decks.

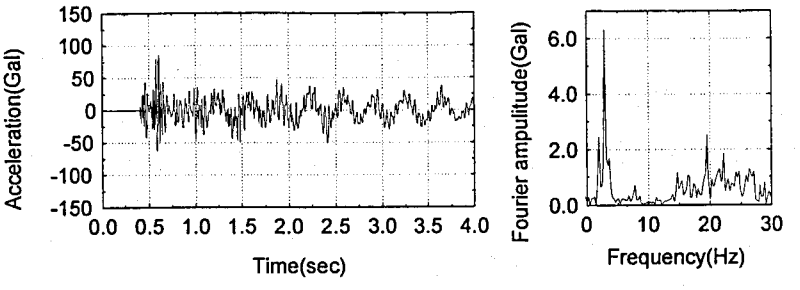

(a) Single vehicle running

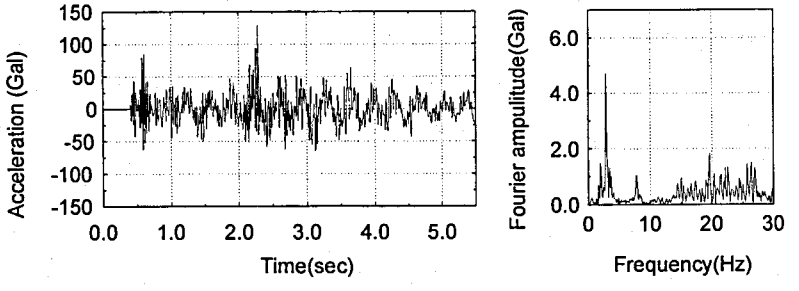

(b) Two vehicles running

Fig. 5-14 Acceleration responses due to number of traveling vehicles on a lane: node V2; v=100km/hr

5.6 Acceleration responses of web plates

To investigate the response characteristics of web plates, numerical analyses are carried out under conditions of different vehicle type, running position and number of vehicles. Acceleration responses of H1, H2, H3 and H4 nodes (see Fig. 5-3(b)) under the condition of the vehicle VEH-EX running with speed of 100km/hr are considered as a prototype for the response of web plates, and are summarized in Fig. 5-15. The acceleration responses of the nodes on the web plate that is connected with a cross beam (H1 and H4 nodes) is observed to have relatively small amplitudes compared with those of the nodes on the web plate (H2 and H3 nodes) that is distant from cross beams.

In considering the dynamic characteristics from Fourier spectra, the dynamic characteristics of the web plates connected with a cross beam (H1 and H4) are dominated by the frequency of about 3Hz. On the other hand, those dynamic characteristics of the web plates apart from the connection point with a cross beam (H2 and H3) is dominated by

frequency of about 25Hz (14~25Hz). Typical mode shapes related to the frequency of 25Hz are shown in Fig. 5-16. It indicates the existence of a strong relationship between the dominant frequency of near 25Hz and modes related to the out-of-plane mode of web plates.

The results demonstrate that the dynamic properties of the web plates that connected with a cross beam can be easily affected by dynamic characteristics of the bounce motion of heavy vehicles. On the other hand, the responses of web plates apart from the cross beam can be dominated by dynamic sources with higher frequency features like axle-hop motion of vehicles, etc.

The simulation for dynamic response of web plates due to the VEH-1 vehicle is carried out to investigate the effect of the vehicle type on the dynamic response of web plates by comparing the responses shown in Fig. 5-15 (b). In here, the vehicle VEH-1 is used as the vehicle having higher frequency axle-hop motion than that of the VEH-EX vehicle. Typical acceleration responses at the H2 node due to VEH-1 vehicles running on inside as well as out side of the G1-girder are shown in Fig. 5-17.

It is observed, by comparing the response of Fig. 5-17(a)(1) and that of Fig. 5-15(b)(1), that the Fourier amplitude at 25Hz as well as the amplitude of acceleration responses produced by the VEH-1vehicle running become larger than those responses induced by the vehicle VEH-EX running. It demonstrates the importance of assuming the spring constant of tires of vehicles in simulating the critical response. That is, if the main object of an analysis is the response of local members, the use of tire property well defined is necessary.

The effect of vehicle series on the dynamic response of web plates is examined by comparing Fig. 5-17 (a) with Fig. 5-17 (b). It is also observed that, at the moment of the second vehicle entering, acceleration responses of the web plate are amplified like the responses of decks shown in Fig. 5-14.

Interesting phenomena are observed by comparing responses induced by different vehicle paths (running inside of the G1-girder and outside of the G1-girder); that is, as shown in Figs. 5-17 (a)(1) and (2) as well as Figs. 5-17(b)(1) and (2), the Fourier amplitude at 25Hz and acceleration responses produced by vehicles running on inside of the G1-girder is greater than those amplitudes induced by vehicles running on outside of the G1-girder. It means that the out-of-plane dynamic response of web plates is more easily affected by deformations of deck slabs between girders than by deformations due to vehicles running on the cantilevered part of decks.

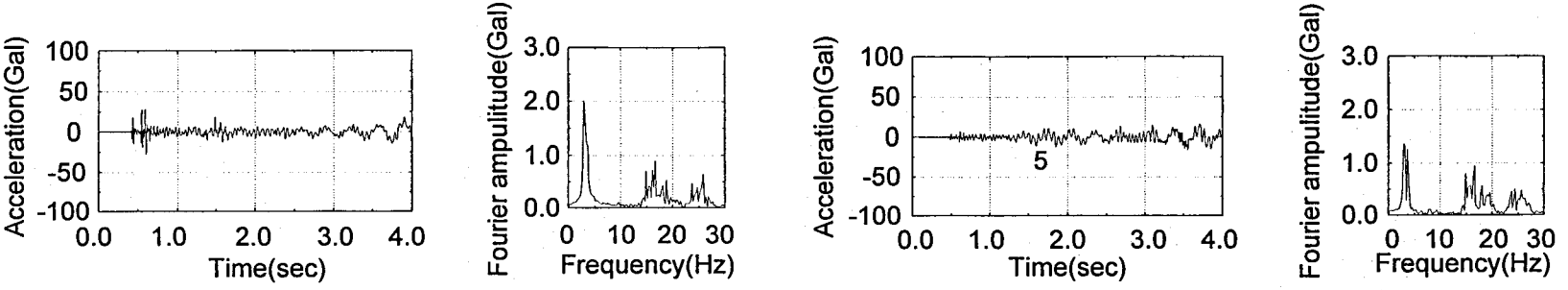

(1) node H1 (2) node H4

(a) Web plate connected with cross beam

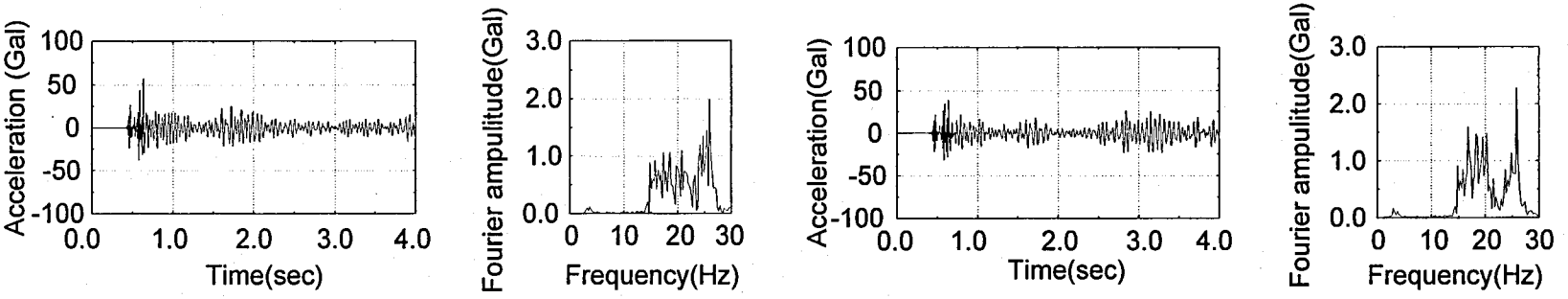

(1) node H2 (2) node H3

(b) Web plate apart from cross beam

Fig. 5-15 Acceleration response and Fourier amplitudes of web plates due to VEH-EX vehicle running on inside of the G1-girder: v=100km/hr

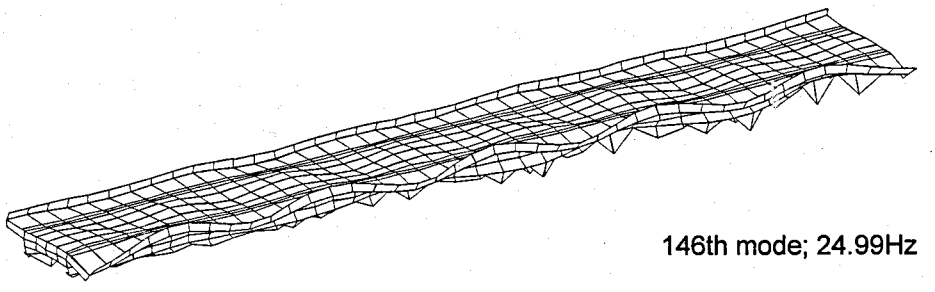

(a) 146th mode

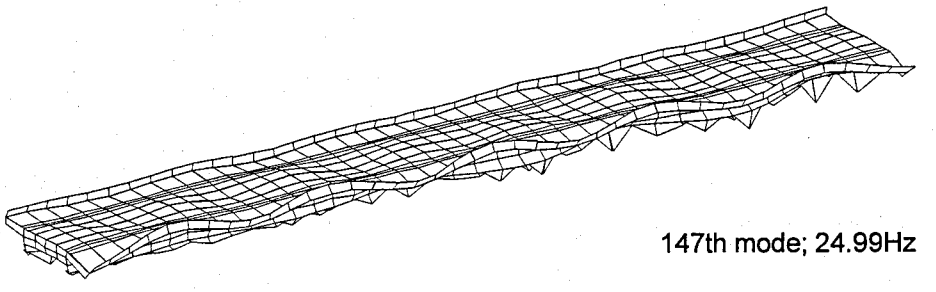

(b) 147th mode

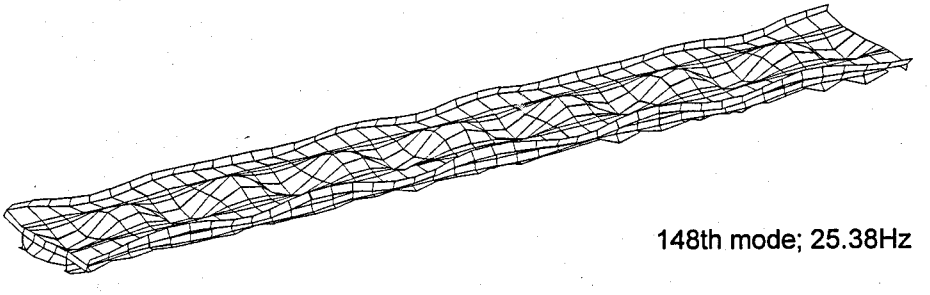

(c) 148th mode

Fig. 5-16 Modes corresponding to the frequency of near 25Hz included in the responses of web plates

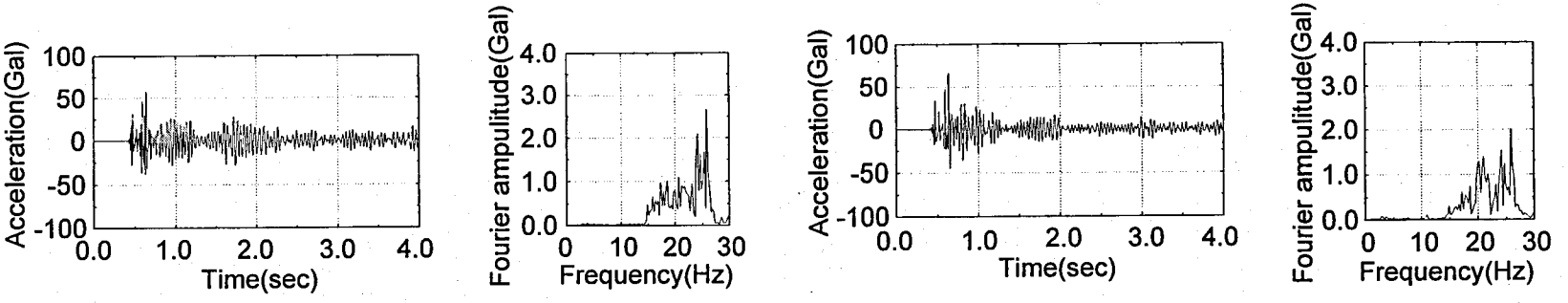

(1) Vehicle running on inside of G1-girder (2) Vehicle running on outside of G1-girder

(a) Single vehicle running

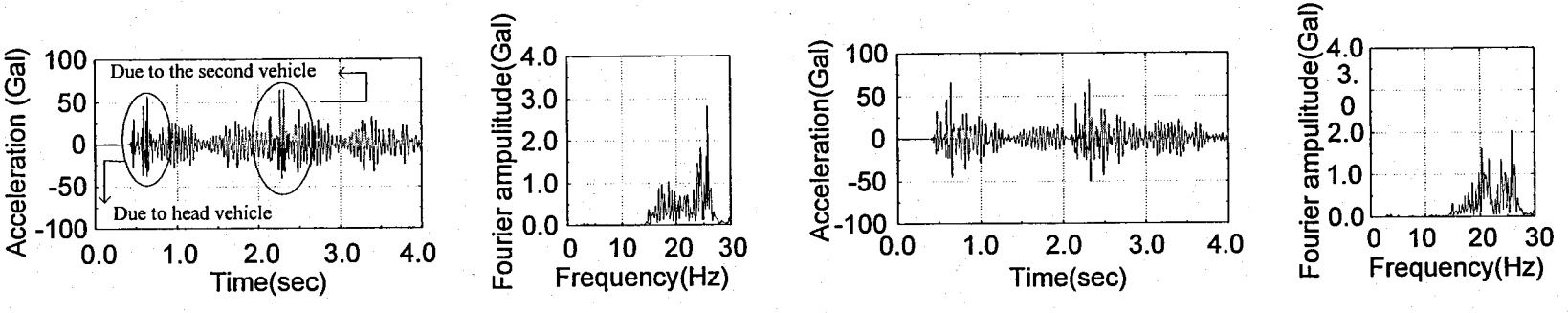

(1) Vehicle running on inside of G1-girder (2) Vehicle running on outside of G1-girder

(b) Two vehicles running with headway of 46.63m

Fig. 5-17 Acceleration response and Fourier amplitudes at node H2 of web plates due to number of traveling vehicles VEH-1: v=100km/hr

5.7 Conclusions

In this chapter, a three-dimensional traffic-induced dynamic response analysis due to moving vehicles is carried out to investigate not only dynamic responses of a two-span continuous steel two-girder bridge but the effect of the elastic deformation at an elastomeric support to dynamic responses of local members like web plates and decks. The summarized result of this chapter is as follows:

1. Although the roadway surface profile used in analysis of the full 3-D model is the assumed one, the trends, maximum amplitudes and overall responses and the Fourier amplitude of the analytical response match quite well with experimental ones.
2. In general, the quality of the agreement between the experimental and analytical results is considered extremely encouraging and quite acceptable in the light of potential sources of error, even though responses of the 3-D plane model have tendency to have smaller amplitude than that of the full-3D model.
3. At the moment of a vehicle entering the bridge the response of the main girder can be strongly affected by vertical deformations due to the bending of a deck and the elastic deformation of elastomeric bearings at the support. The amplitude of the acceleration response of the main girder as well as the Fourier amplitude is more easily affected by the vehicle running outside of the G1-girder because of the coupled effect between torsional modes and vehicle loadings.
4. On the other hand, the out-of-plane dynamic response of web plates is more easily affected by deformations of deck slabs between girders than by deformations produced by vehicles running on the cantilevered part of decks.
5. It is observed that the response amplitude of decks tends to decrease as the vehicle speed decrease, and the Fourier spectrum indicates that both Fourier amplitudes near 3Hz and over 10Hz also have tendency to decrease as vehicle speed decrease.
6. The amplitude of the acceleration response of decks is more easily amplified by passage of vehicle series than by single vehicle running, since the impulsive wheel load of the following vehicle is amplified by the additional bump height generated by the elastic deformation of elastomeric bearings and decks under the load of the head vehicle. The acceleration responses of the nodes on the web plate that is connected with a cross beam (H1 and H4 nodes) is observed to have relatively small amplitudes compared with those of the nodes on the web plate (H2 and H3 nodes) that is apart from cross beams. The appearance of the dominant frequency near 3Hz of the web plate connected with a cross beam demonstrates that the dynamic property of the web plate connected with cross beams can be easily affected by dynamic characteristic of the bounce motion of heavy

vehicles. On the other hand, the response of web plates apart from the cross beam can be dominated by dynamic sources with higher frequency features like the axle-hop motion of vehicles. Thus, if the main object of an analysis is the response of local members, the use of tire property well defined is necessary.

References

[1] Kulicki, J. M.: The once and future steel bridge, Journal of The Transportation Research Board-Fifth International Bridge Engineering Conference, Transportation research board, National research Council, 1(1696), 219-237, 2000.

[2] Yamagata, K.: Simplified bridge structure for less manpower-Special theme: The rationalization of bridge structures, JSSC Bulletine, **13**, 2-11, 1994. (*in Japanese*)

[3] Takahashi, S., Tachibana, Y., Shimura T. and Konishi, T.: Design and study of structural performance for the two-girder bridge "Horonai river bridge", Bridge and Foundation Engineering, 2, 23-30, 1996. (*in Japanese*)

[4] Survey examination report regarding the simplification of bridges, Express Highway Research Foundation of Japan (EHRF), 1993. (*in Japanese*)

[5] Eurocode4: Design of composite steel and concrete structure-Part2: Bridges, 1996.

[6] Harada, M., Kajikawa, Y. and Fukada, S.: The Strengthened Effect of Endurance in Existing Steel Bridge, J. of Structural Mechanics and Earthquake Engineering, JSCE, I-60(710), 129-139, 2002. (*in Japanese*)

[7] Bathe, K. J.: Finite element procedures in engineering analysis, Prentice-Hall, 1982.

[8] Zienkiewicz, O.C. and Taylor, R.L.: The finite element method, Vol.2, Butterworth-Heinemann, Oxford, 2000.

[9] Kawatani, M. and Kim, C.W.: Computer simulation for dynamic wheel loads of heavy vehicles, Int. J. of Structural Engineering and Mechanics, **12**(4), 409-428, 2001.

[10]Honda, H., Kajikawa, Y. and Kobori, T.: Spectra of road surface roughness on bridges, J. of Structural Division, ASCE, **108**(ST9), 1956-1966, 1982.

[11]Kawatani, M, Kobayashi, Y. and Takamori, K.: Nonstationary random analysis with coupling vibration of bending and torsion of simple girder bridges under moving vehicles, JSCE J. of Structural Engineering and Earthquake Engineering, **15**(1), 107s-114s, 1998.

[12]Research group of bridge vibration: Measurement and Analysis of Bridge Vibration, Gihodo, 1993. (*in Japanese*)

[13]Yokoyama, K and Inoue, J.: Traffic mode and impact coefficients of highway bridges, J. of Structural Mechanics and Earthquake Engineering, JSCE, I-14(422) (Note), 391-394, 1990. *(in Japanese)*

Chapter 6

End-cross beam reinforcement of two-girder bridges

6.1 Introduction

Bridges that equipped the two-girder system have been adopted as one of the most common structural types for the bridge with span length of about 50m because of advantages they offer with regards to fabrication, erection, etc. However, the structural characteristics of the two-girder bridge makes the bridge to be easily vibrated by external dynamic loads like wind, moving vehicles, etc., since the simplified structural system and the wide girder spacing make the bridge more sensitive to vibrations.

Steel plate girder bridges with span length of 30m to 60m usually have fundamental frequencies about 2Hz to 4Hz [1, 2]. Heavy vehicles on highway bridges, generally, have the dominant frequency of about 3Hz related to the bounce motion and the frequency of about 10Hz related to the axle-hop motion. The dynamic characteristic of dynamic wheel loads is mainly affected by the bounce-motion [3]. It means that the bounce motion of vehicles influences greatly to dynamics of the bridges. The axle-hop motion affects dynamic responses of local members of bridges with higher frequency characteristics than that of girders. Thus, in here, the terminology "high-frequency" is adopted to indicate the frequency related to that of local members.

The bump at the expansion joints is another important factor that causes excessive impulsive dynamic wheel loads with the high frequency characteristic. Because of the large damping property of vehicles that makes the impulsive wheel load dissipated within a short period, the impulsive dynamic wheel load will give severe influences on the members located near the bump [4]. The impulsive wheel load at the expansion joint can also be a source to cause undesirable noises and vibrations, and, what is worse, the impulsive wheel load has tendency to travel farther from the expansion joint according to the vehicle speed [4].

The undesirable vibration occurred at the members located near the expansion joints of steel bridges will influence to nearby grounds and buildings through supports and piers [5], and also give rise to complaints related to the infra-sound [6]. The undesirable vibration, so called an environmental vibration, has been one of major technical problems because of its high possession rates of viaducts in land scarce major cities.

To reduce the traffic-induced vibration, Yamada and Kawatani [7] investigated the effect of girder-end reinforcement on reducing the traffic-induced vibration of a conventional steel multi-girder bridge by the dynamic response analysis. Chubb and Kennedy [8] observed reduction effects on dynamic responses after stiffening the sway bracing at the end part of an

existing steel bridge from the field-test. A few studies on reinforcing the end part of steel bridges have been performed to prevent the undesirable vibration and enhance the resistance of the expansion joints and decks located near the expansion joints.

Nanjo et. al [9] have been reported that the end-cross beam reinforcement can extend life cycle of the deck and of the expansion joints of steel girder bridges. Nanjo et al. [9] also suggested the possibility that suppress the traffic-induced vibration. However, few investigations on the vibration reduction of the local member of the steel two-girder bridge due to the end-cross beam reinforcement have been reported. Therefore, in this chapter, the traffic-induced vibration of the steel two-girder bridges is investigated after reinforcing the end-cross beam. In addition, the method of removing bumps is considered as another method to reduce the traffic-induced vibration.

6.2 Does the dynamic response affected by types of bridge and bearing?

To investigate the effect of the bridge type and the bearing type to the traffic-induced vibration of bridges, the dynamic responses of a conventional steel girder bridge and a steel two-girder bridge is determined under the same conditions of vehicle, roadway roughness, speed, running position and start position of the vehicle.

Figure 6-1 shows the acceleration responses of the conventional steel multi-girder bridge (see, Fig. 4-2) and the steel two-girder bridge with respect to bearing types (see Fig. 5-2). The weight and properties of vehicle used in the analysis is the same as the three-axle vehicle shown in Table 4-2, and the vehicle is assumed to travel center of the two girders (G1 and G2 girders) with the speed of 100km/hr. The responses of decks and main girders are determined. One of the analyzed points of decks is the node of deck on the expansion joint of the bridge-entrance, and another is the center of deck located away from the expansion joint. The acceleration of the span center of the main girder G1 is considered.

It is observed that the deck of the steel two-girder bridge is more severely affected than that of the conventional steel multi-girder bridge by the traffic-induced vibration. Moreover, the two-girder bridge with elastomeric bearings is relatively easily vibrated by moving vehicles in comparing with the bridge with steel pin supports as shown in Figs. 6-1(b-1, 2) and 6-1(c-1, 2). However, the response of the main-girder of the three-girder bridge is more amplified by the moving vehicle than that of the two-girder bridge. It supports the need of the end-cross beam reinforcement for the steel two-girder bridge with wide girder spacing.

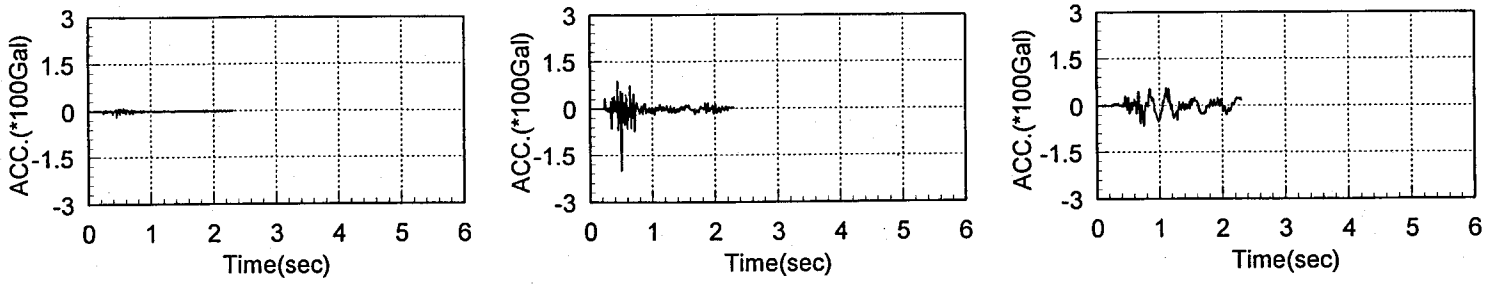

(1) Conventional steel three-girder bridge (Fig. 4-2)

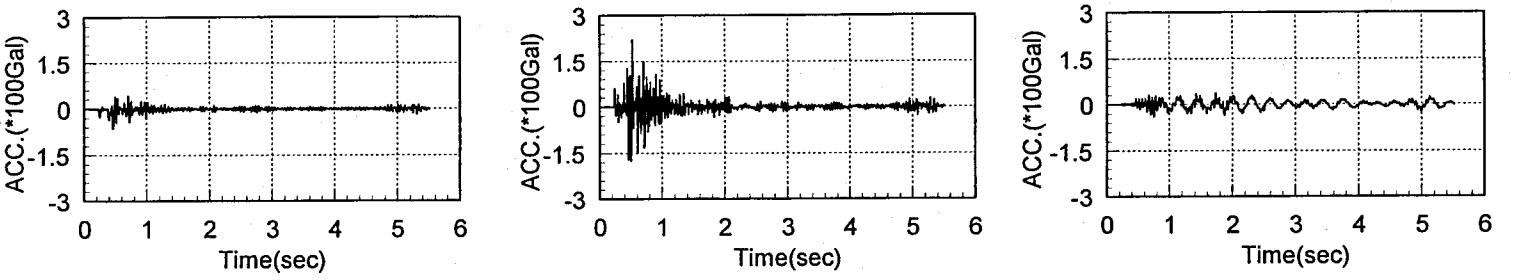

(2) Steel two-girder bridge with (Fig. 5-2) steel pin bearings

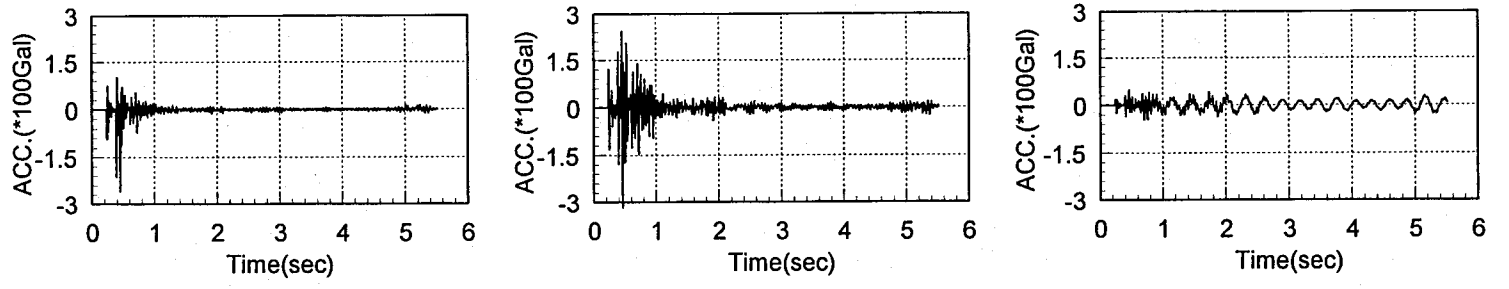

(3) Steel two-girder bridge (Fig. 5-2) with elastomeric bearings

(a) Node at bridge entrance (b) Node 2.5m away from bridge entrance (c) Center of G1-girder

Fig. 6-1 Dynamic responses of conventional steel three-girder bridge and of steel two-girder bridge: v=100km/hr

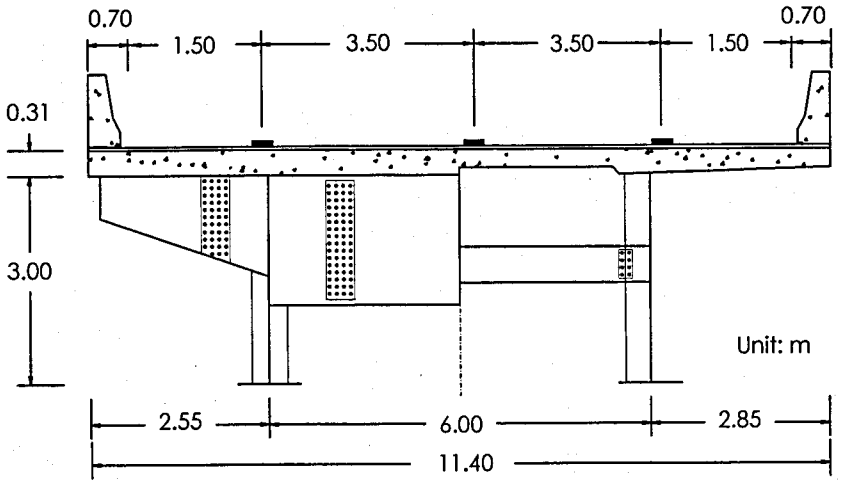

(a) Cross section before reinforcing: Section WO

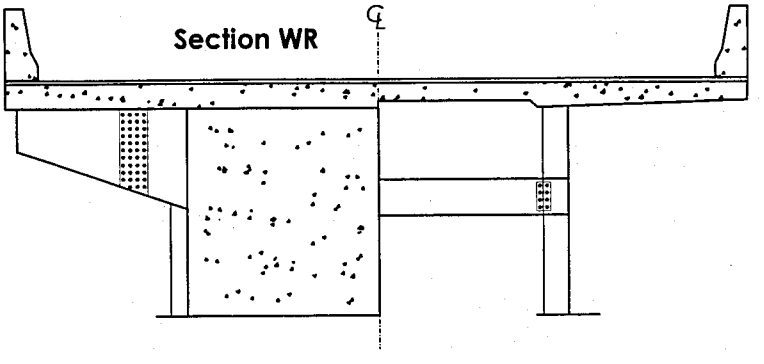

(b) Cross section after reinforcing: Section WR

Fig. 6-2 Cross section of bridge model

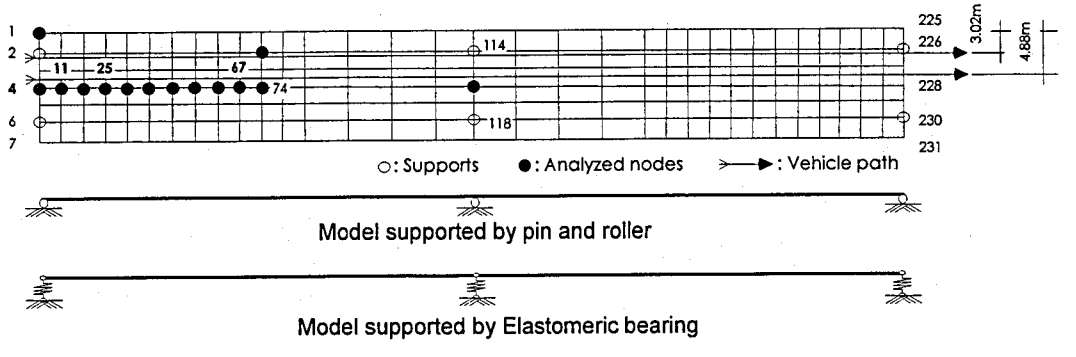

Fig. 6-3 FE model

6.3 End cross-beam reinforcement of steel two-girder bridge with PC deck

6.3.1 Analytical models

The two-span continuous steel two-girder bridge with PC deck shown in Fig. 5-2 of Chapter 5 is adopted as a bridge model for an analytical example. The reinforced section of the bridge is shown in Fig. 6-2 with the section before reinforcing. The symbols WO and WR in the Fig. 6-2 indicate sections in accordance with existence of reinforcement at the end-cross beams and the intermediate-cross beam on the pier P1; WO indicates the section before reinforcing; WR, the section after reinforcing with thickness of 50cm. Reinforced concrete blocks at the cross beams located at abutments A1 and A2 and the pier P1 are assumed to completely link with deck slabs.

A FE model for the bridge is again appeared in Fig. 6-3, which consists of 231 nodes, 192 flat elements and 159 (163 for the bridge model with WR section) beam elements. The number of each node is used for indicating the analyzed point, as it is. The VEH-1 vehicle shown in Table 5-3 of Chapter 5 is adopted as the heavy vehicle on the bridge. As a roadway model, the PSD curve ($S(\Omega_r)=0.001/(\Omega^2+0.05^2)$) defined in Fig. 4-8 of Chapter 4 is used to generate samples of roadway profiles. In dynamic response analysis, as shown in section 5.2.2, measured bumps at expansion joint of A1 abutment under the vehicle path are considered.

6.3.2 Vibration reduction effect due to end-cross beam reinforcement

Acceleration responses

Typical vertical accelerations at decks of the bridge with respect to the bearing type, the existence of reinforcement at the abutment A1 and A2 as well as at the pier P1 and bumps at expansion joint on A1 are shown in Fig. 6-4 to Fig. 6-5. Acceleration responses of the deck located 2.65m away from the A1 joint are shown in Fig. 6-4, the response of the deck at the center of the first span is shown in Fig. 6-5. The peak amplitude generated at the moment of a vehicle entering is reduced by both the end-cross beam reinforcement and removing bumps, regardless of bearing types.

Symbols following the WO and WR indicate the existence of the bump and the bearing type; B indicates the response considering the **B**ump at the expansion joint at A1; NB, the response considering **N**o **B**ump at the expansion joint at A1; PIN, the response of the bridge with pin supports; ELASTO, the response of the bridge with elastomeric bearings.

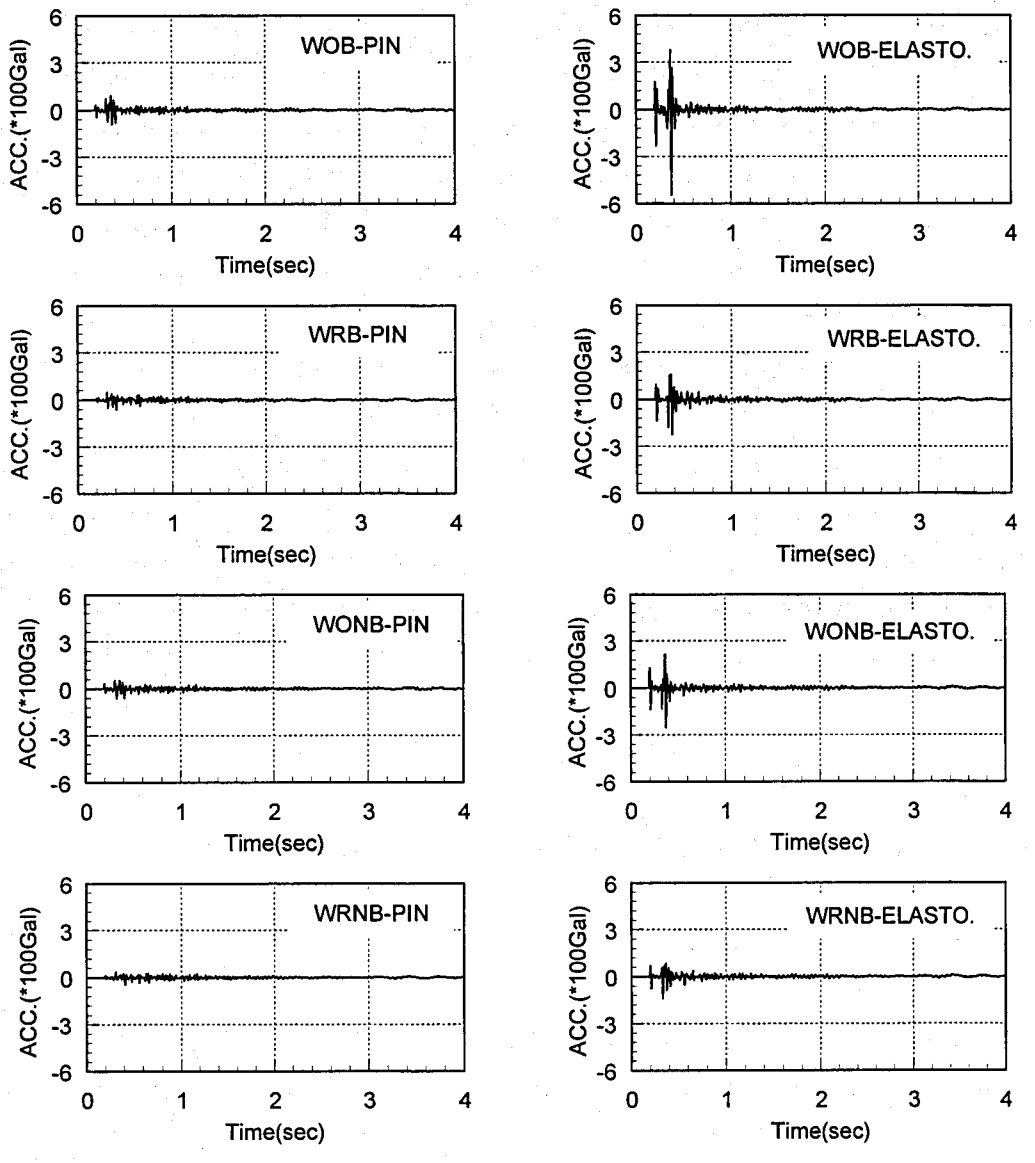

(a) Pin supported bridge (b) Bridge with elastomeric bearings

Fig. 6-4 Acceleration responses according to reinforcement and removing bump; v=100k/hr; at the deck located 2.65m away from the A1 joint

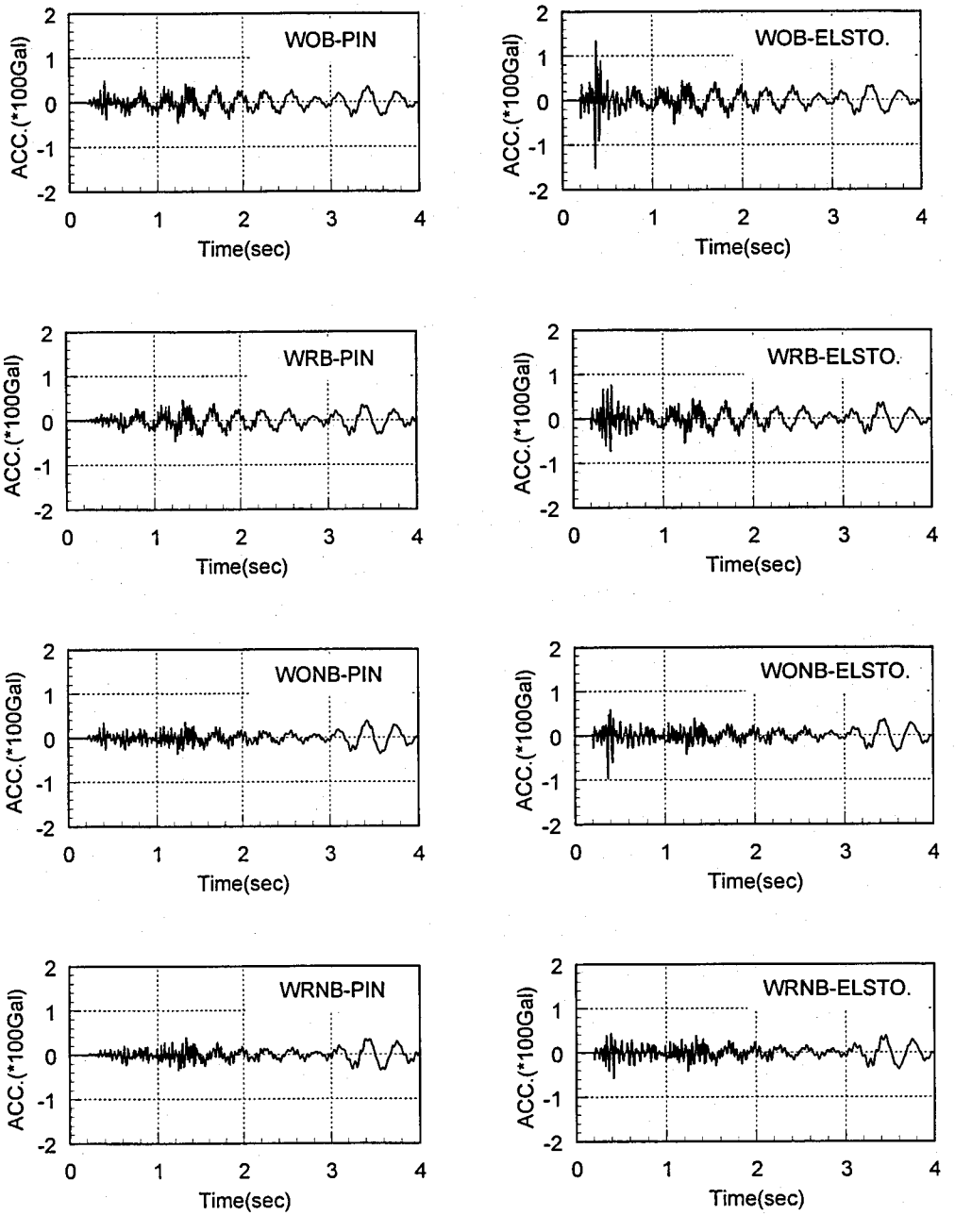

(a) Pin supported bridge (b) Bridge with elastomeric bearings

Fig. 6-5 Acceleration responses according to reinforcement and removing bump; v=100k/hr; at the deck located 26.5m (center of the 1st span) away from the A1 joint

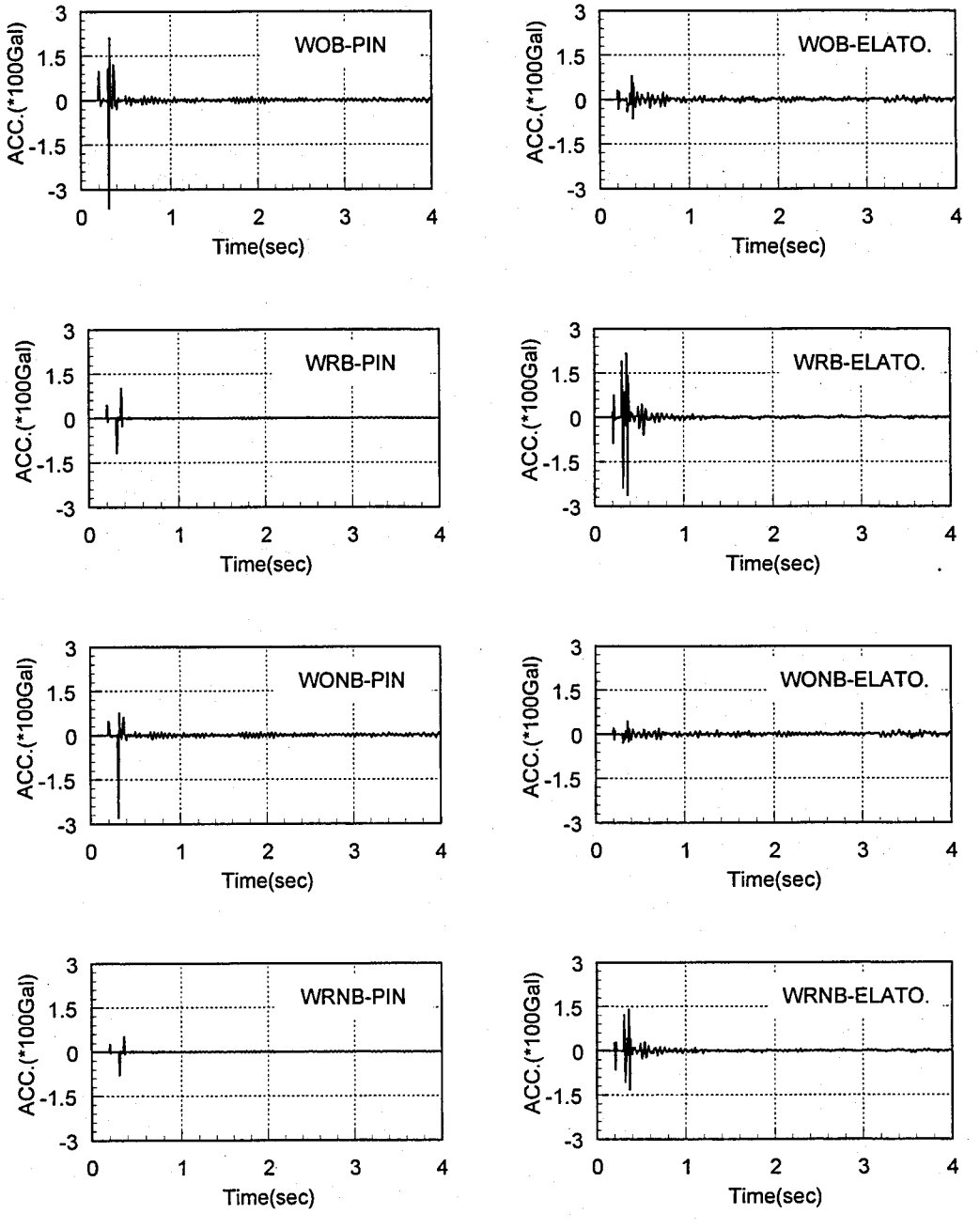

(a) Pin supported bridge (b) Bridge with elastomeric bearings

Fig. 6-6 Acceleration responses according to reinforcement and removing bump; v=100k/hr; at guard-rail on the A1 joint

It is noteworthy that even the deck at span center of the bridge supported by elastomeric bearings is experiencing the impulsive loading effect induced by the bump at the expansion joint, on the other hand those effects on the deck of the pin supported bridge are very small.

Interesting results can be observed from the Fig. 6-6, which shows the acceleration response of the node at the guard-rail on the A1 joint. It is observed that, for the pin supported bridge, the peak responses are reduced most effectively by the end-cross beam reinforcement. However the removing bump is the most effective countermeasure against the impulsive vibration in the case of the bridge with elastomeric bearings. On the contrary, the end-cross beam reinforcement magnifies the peak vibration of the node at the guard-rail of the bridge with elastomeric bearings. One of the reasons may be the inertia effect of the additional mass due to the reinforcement on the elastomeric bearings. It is noteworthy that, except the node at the guard-rail of the bridge, the dynamic response of nodes in considering can be reduced by the reinforcement.

Thus it can be concluded that the end-cross beam reinforcement is effective to curtail the impulsive response in the case of the pin supported two-girder bridges. On the other hand, although the end-cross beam reinforcement is also effective to buffer the impulsive vibration for the two-girder bridge with elastomeric bearings, the end-cross beam reinforcement using in combination with removing bumps is recommended.

Since the energy related with human perception in question is contained within the 1 to 80Hz band [10, 11], useful observations have been made mainly in the frequency range between 1 and 100Hz. Vertical accelerations are thus estimated by superposing up to the mode corresponding to 100Hz.

Vibration level

To assess the effect of vibration on human perception, in general, the vibration level (VL) is considered as a measure. The VL can be determined by comparing root mean squares (RMS) of accelerations and the standard acceleration defined by the least value of acceleration that human can perceive as

$$VL(dB) = 20\log_{10}\frac{a}{a_0} \tag{6.1}$$

where, a and a_0 indicate RMS values of acceleration responses and the standard acceleration defined by the least acceleration that human can perceive, respectively. $a_0=0.001Gal$ is used as the standard acceleration.

Typical results of VL taken from 1/3 octave band spectral analysis at the noted nodes according to the vibration reducing method are shown in Fig. 6-7, for the bridge supported by pin bearings under condition of single vehicle running. Those for the bridge supported by elastomeric bearings under condition of single vehicle running are shown in Fig. 6-8. The vertical and horizontal scales in the figures indicate VL (dB) and 1/3 octave band central frequency (Hz), respectively.

Figure 6-7 demonstrates that, for nodes located near the A1 joint of the bridge with pin bearings, the vibration level decreases through the entire frequency range due to the end-cross beam reinforcement as well as by the removing bumps. For the deck at the span center of the first span of the pin-supported bridge, the vibration reduction becomes very small. It is observed that the VL value at the 3Hz increases as the position located away from the A1 joint.

For nodes located near the A1 joint of the bridge supported by elastomeric bearings (Fig. 6-8 (a) and (b)), the VL of the bridge is dominated by the dynamic characteristic of high-frequency range (20Hz ~ 30Hz). It is observed that VLs at the frequencies over 3Hz tend to be reduced by the reinforcement as well as removing bumps.

Although the VL of the deck at the span center of the first span is dominated at the frequency of near 3Hz, those VLs at the frequency of near 20Hz increases due to the adoption of elastomeric bearings instead of pin bearings as shown in Fig. 6-8 (c). It supports the result concluded in section 6.2 that the bridge supported by elastomeric bearings is more easily vibrated by the impulsive wheel load generated by vehicles at the moment of passing over a bump.

From the 1/3 octave spectral analysis, it is observed that the reinforcing the end-cross beam can suppress high-frequency vibrations.

The over all acceleration level (OAL) (Eq. 6-2) with respect to each node is summarized in Fig. 6-9, to assess the vibration level along the bridge quantitatively. The additional bump effect due to the elastic deformation of elastomeric bearings can give rise to greater impulsive loads to the vehicle following the head vehicle as explained in the Chapter 5. Therefore, the effect of a vehicle series is considered. The critical headway of traveling vehicles of 42.21m is used in the analysis based on Eq. (5-1) and the dominant frequency of near 3Hz as shown in Fig. 5-10 (a)(1) of the previous chapter, which is similar with the second bending mode of 3.37Hz from the analysis.

$$OAL(dB) = 10\log_{10}(10^{VAL_1/10} + \cdots + 10^{VAL_{21}/10}) \qquad (6\text{-}2)$$

where, $VAL_1 \sim VAL_{21}$ indicate the central frequencies of the 1/3 octave band frequency.

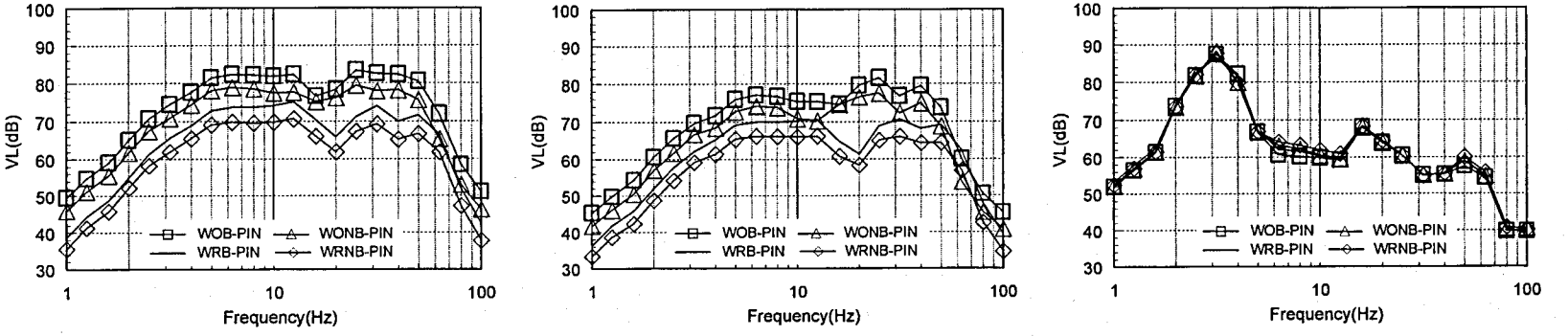

(a) Node at bridge entrance (b) Node 2.5m away from bridge entrance (c) Center of G1-girder

Fig. 6-7 1/3 octave band spectra of bridge with pin bearings

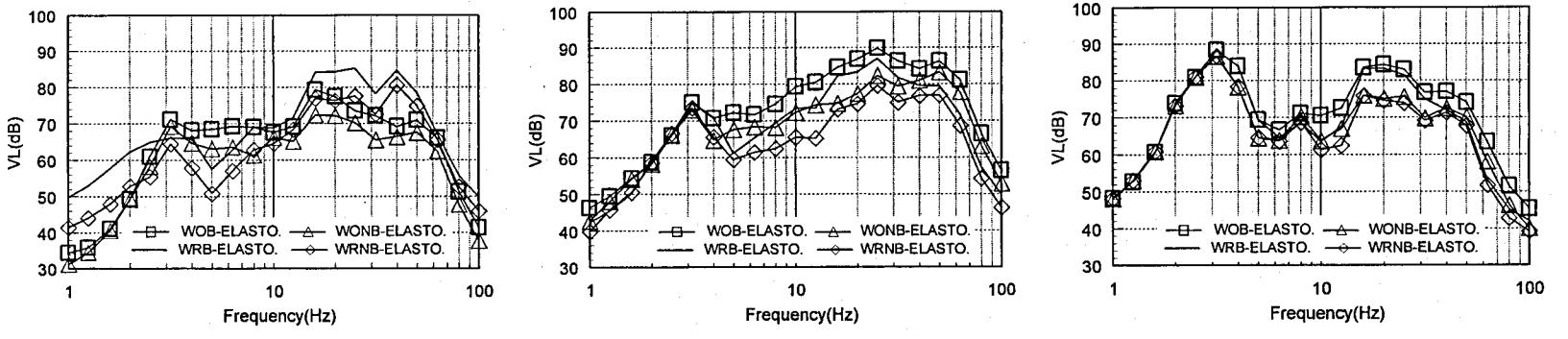

(a) Node at bridge entrance (b) Node 2.5m away from bridge entrance (c) Center of G1-girder

Fig. 6-8 1/3 octave band spectra of bridge with elastomeric bearings

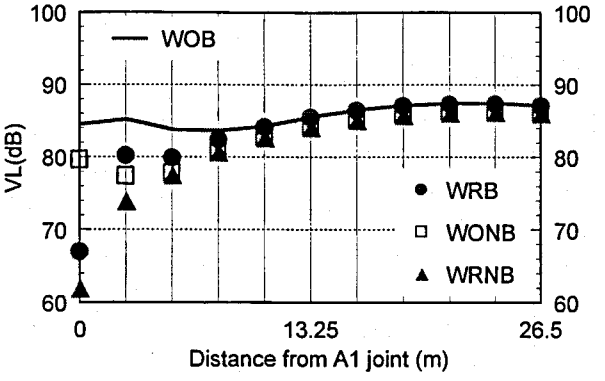

(a) Bridge with steel bearings under single vehicle running

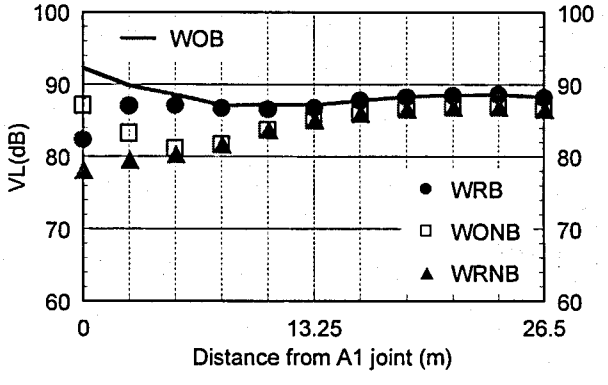

(b) Bridge with elastomeric bearings under single vehicle running

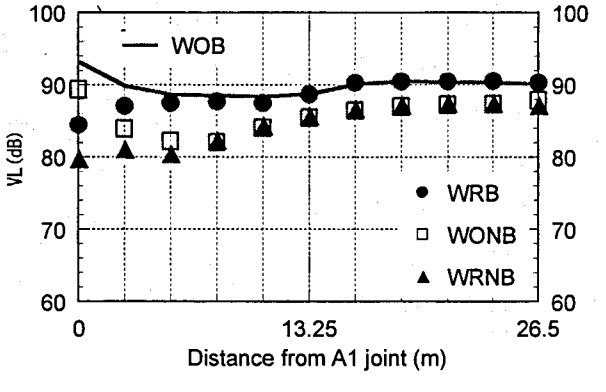

(c) Bridge with elastomeric bearings under two vehicles running

Fig. 6-9 Over all pass vibration level w.r.t countermeasures against vibration at each node of bridge; v=100km/hr

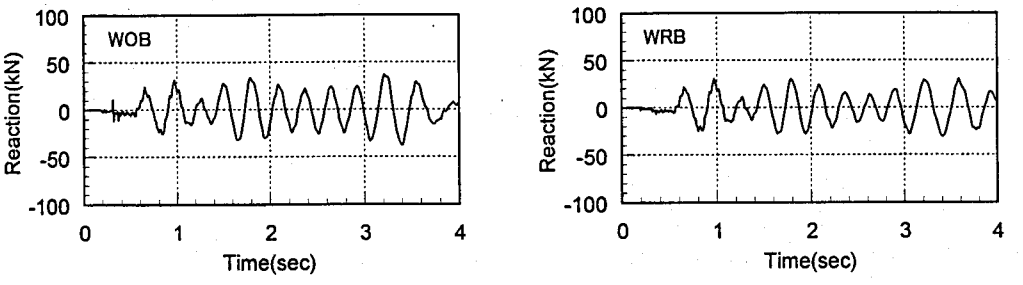

(a) Pin bearing

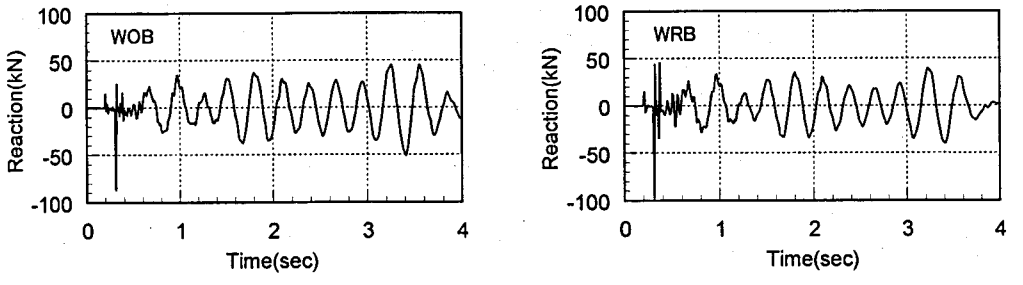

(b) Elastomeric bearing

Fig. 6-10 Dynamic reaction due to inertia effect of bridge at A1 joint of G1-girder

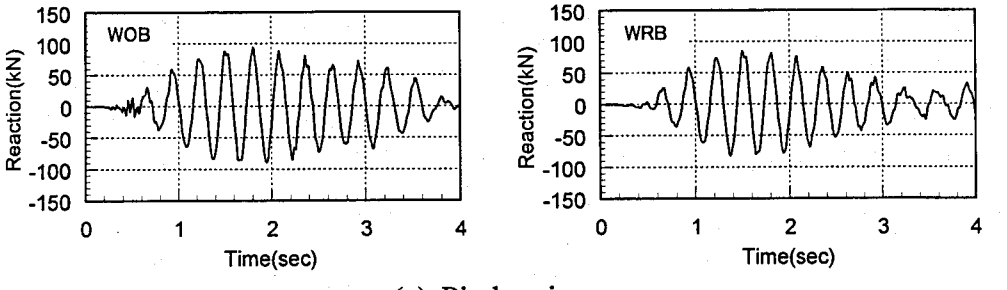

(a) Pin bearing

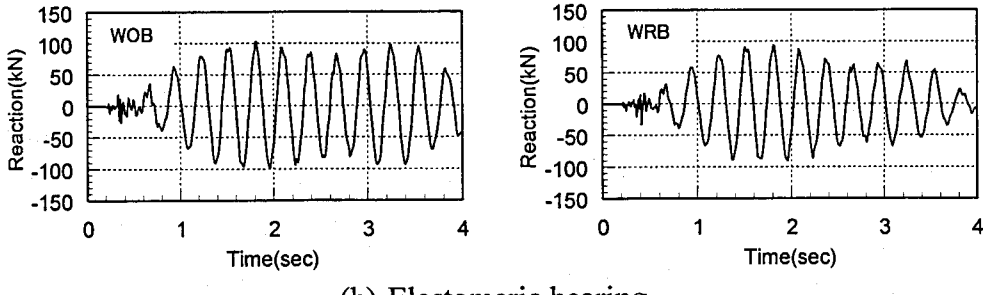

(b) Elastomeric bearing

Fig. 6-11 Dynamic reaction due to inertia effect of bridge at P1 joint of G1-girder

Figure 6-9 shows that the bridge with elastomeric bearings (87dB~92dB without any reinforcement) is more easily vibrated than the bridge with steel bearings (84dB~88dB without any reinforcement). Under the condition of two vehicles running on the bridge with elastomeic bearings, the VL at the span center of the bridge increases about 3dB compared with that of bridge under the condition of single vehicle running. Interesting results are that, for bridge with steel bearing, the dominated vibration level occurs at the members near span centre.

On the other hand, for bridge with elastomeric bearing, the dominated vibration level occurs at the members near the expansion joint. It means that the vibration near the expansion joint can be one of sources for an environmental vibration in steel two-girder bridges with elastomeric bearings. It is also observed that removing bumps, if possible, at the joint can guarantee effective vibration reduction regardless of bearing types of bridges, even though the reinforcement is an effective countermeasure against the vibration of two-girder bridges.

Reaction responses

Dynamic reaction forces of bridges can transfer around structures through piers and abutments, and become one of major sources that can occur undesirable vibrations of buildings nearby bridges [5, 6]. Thus, the reduction of dynamic reaction forces due to the end-cross beam reinforcement is examined.

The dynamic reaction forces of a bridge can be defined as a sum of static reaction of moving wheel loads and dynamic one generated by the inertia force of bridges and dynamic components of vehicle's wheel loads or contact forces. In general, the static and dynamic reaction forces due to wheel loads of a vehicle are difficult to be controlled by reinforcing the structural system of bridges. On the other hand, the dynamic reaction due to an inertia force of a bridge can be expected being suppressed by the reinforcement.

Figures 6-10 and 6-11 show typical time histories of dynamic reactions due to an inertia force of a bridge. Reactions at the G1 girder of A1 and P1 joints are considered because the maximum reaction occurs under the running condition shown in Fig. 6-3. It demonstrates the dynamic reaction due to the inertia effect of the bridge can be reduced by the end-cross beam reinforcement.

To investigate the reduction effect more clearly, the RMS value of dynamic reactions due to the inertia effect of the bridge is shown in Fig. 6-12. It is observed that the elastomeric bearings are one of the sources to magnify the dynamic reaction due to the inertia effect of bridge itself. The dynamic reaction due to the inertia effect of the bridge can be reduced by reinforcement as well as removing bumps, and the most effective result is obtained by combining the two methods.

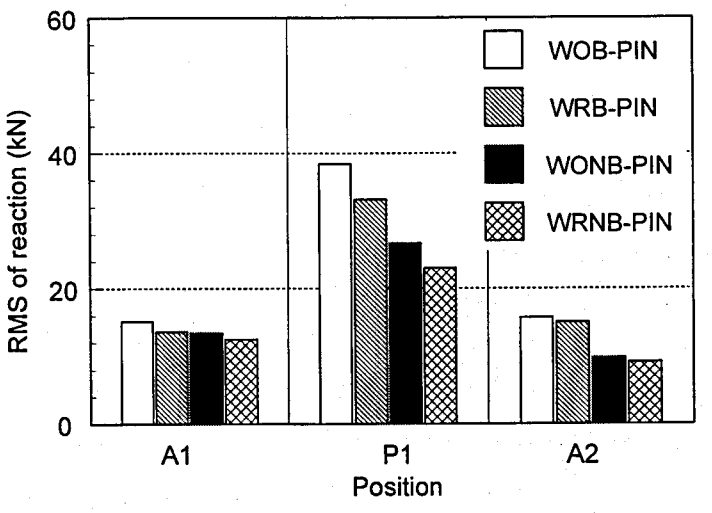

(a) Pin bearing

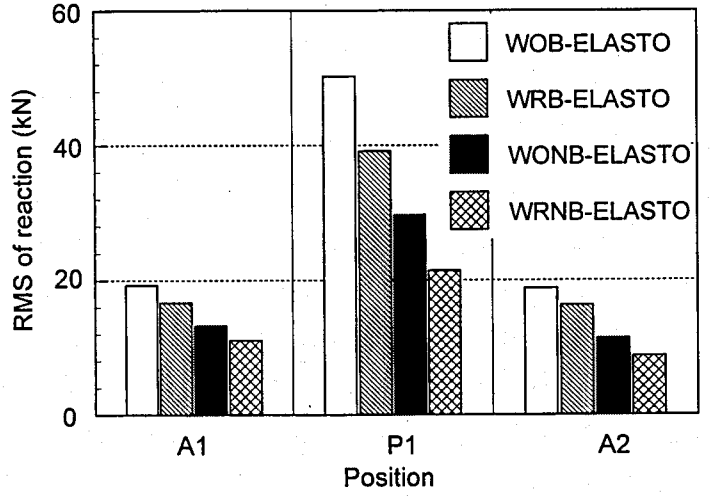

(a) Elastomeric bearing

Fig. 6-12 RMS values of dynamic reaction due to inertia effect of bridge

6.4 End cross-beam reinforcement of steel two-girder bridge with RC deck

6.4.1 Analytical models

Bridge Model

One of six-continuous spans idealized as a bridge with one end roller supported and other end fixed is considered as an analytical bridge model to investigate the effectiveness of the reinforcement on traffic-induced high-frequency vibration of the steel two-girder bridge with RC deck. The bridge has 50m span-length with 5.4m girder-spacing, and the width of the bridge is 12.5m wide. It adopts wide cantilevered decks (about 3.5m) supported by brackets. The bridge has the stringer to restrain the large deflection of the RC deck.

The general layout, typical cross section and devised end-cross beam reinforcing patterns are shown in Fig. 6-13, and the end-cross beam is assumed as reinforced by a RC block with thickness of 50cm. The symbols WO, WG and WB in Fig. 6-13c) indicate the reinforcing patterns; 1) WO indicates the section without any reinforcement; 2) WG is the section with reinforcing between two girders; 3) WB is the section with reinforcing up to the bracket. The RC block at the end-cross beam is assumed to completely link with decks. The damping constant of the bridge is assumed as 2 % for the first mode and the second one.

The FE model for the entire bridge is appeared in Fig. 6-14(a). The single span model adopted to increase calculation efficiency is shown in Fig. 6-14(b), which consists of 225 nodes, 196 plate elements and 158 beam elements. The symbols N1, N2 and N3 are the nodes whose responses are compared with the response of the single span model to verify the validity of the single span model. The symbols GD1, C2, C8, C14, GD15, D48, D52, D54 and D58 in the Fig. 6-14 (b) indicate the noted nodes for dynamic response analysis. The GD, C and D in Fig. 6-14 (b) denote the guide-rail, the cross beam and the deck slab, respectively. The numbers following the symbols coincide with the node number of the FE model. Running case 1 and running case 2 indicate, respectively, the vehicle paths on the central lane and the low speed lane considered in the analysis.

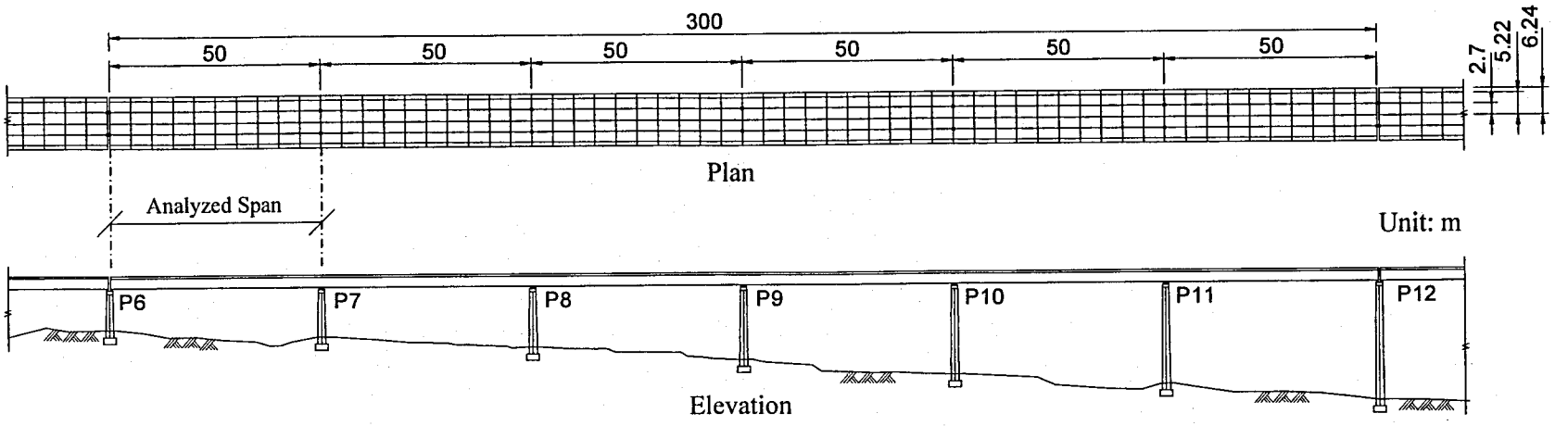

(a) General view of bridge

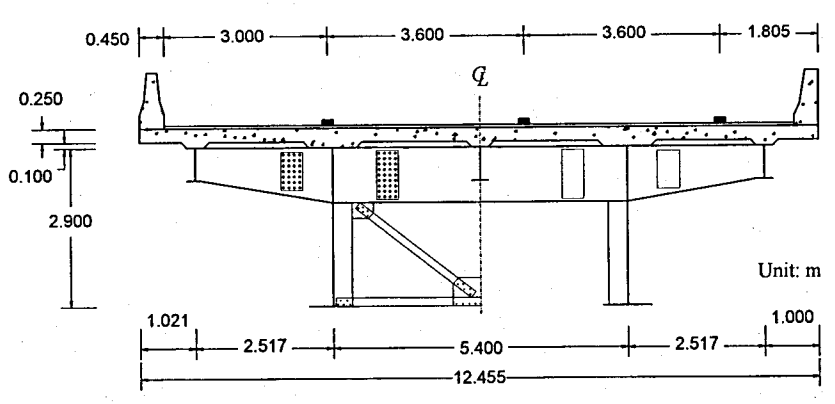

(b) Typical cross section

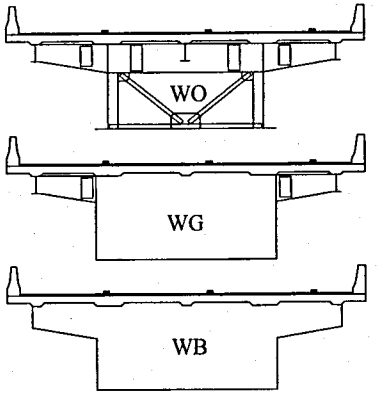

(c) Reinforcing patterns

Fig. 6-13 Bridge and reinforcing patterns

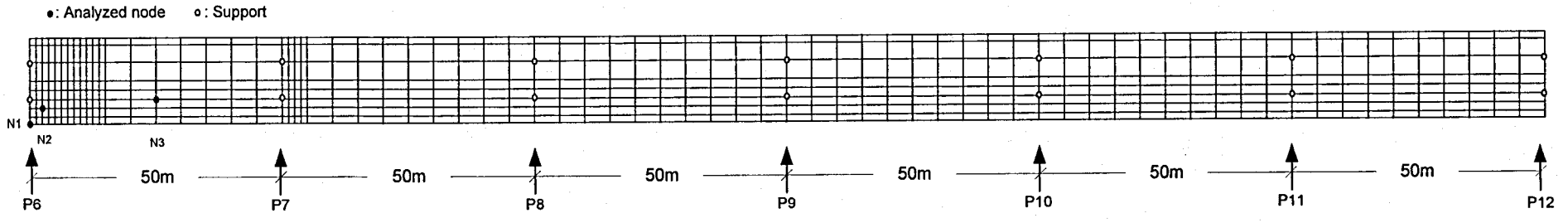

(a) Six-continuous span model

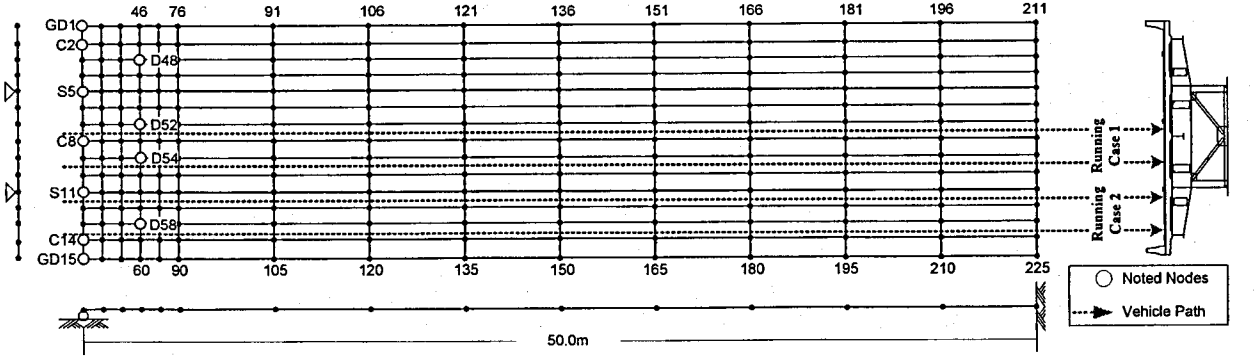

(b) Single span model

Fig. 6-14 FE model of two-girder bridge idealized

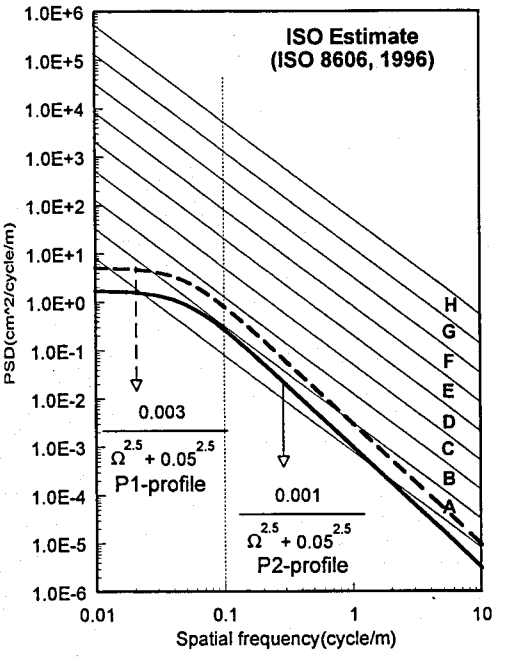

Fig. 6-15 PSD curves of roadway roughness

Vehicle model and roadway profile

A three-axle dump truck shown in the Table 4-2 of chapter 4 is adopted as a heavy vehicle running on the bridge.

Roadway surface profiles used in the dynamic response analysis are generated by Monte-Carlo simulation (MCS) method based on power spectral density (PSD) functions (Fig. 6-15) assumed as a stationary Gaussian random process with zero mean. In generating roadway profiles by using MCS method, the parameters in the PSD function are assumed as $\alpha=0.001$, $\beta=0.05$ and $n=2.5$ for the P1 profile based on the measured data at the Hanshin Expressway and $\alpha=0.003$, $\beta=0.05$ and $n=2.5$ for the P2 profile. The bump at the expansion joint is idealized as rectangular shape with 20mm height and 300mm width. In analysis, one sample profile of MCS of a given roadway condition is used just to compare the relative vibration reduction effect according to the reinforcement, although a statistical analysis is necessary.

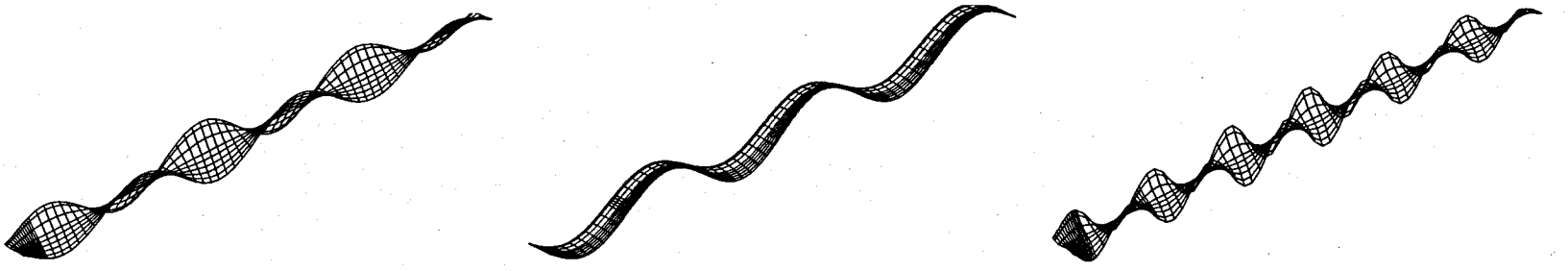

(1) 1st torsion: 1.744Hz (2) 1st bending: 2.045Hz (3) 2rd torsion: 5.636Hz

(a) Typical natural modes and frequencies of six-continuous span model

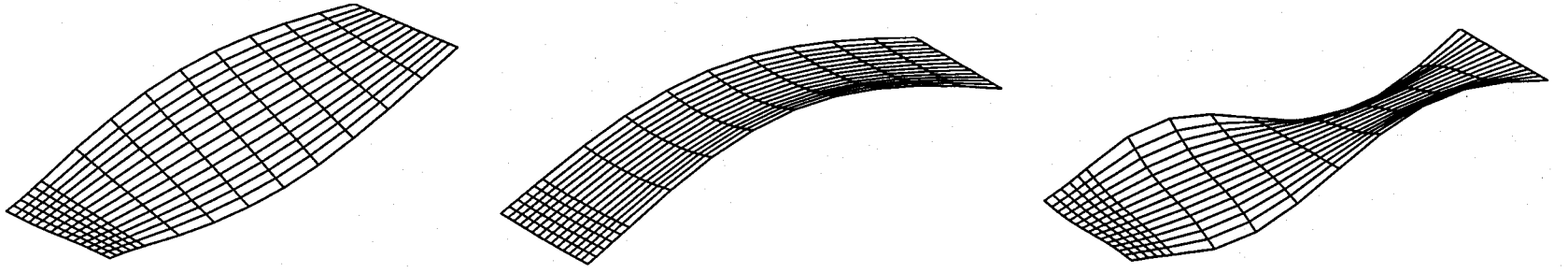

(1) 1st torsion: 1.750Hz (2) 1st bending: 2.066Hz (3) 2rd torsion: 5.483Hz

(b) Typical natural modes and frequencies of single span model

Fig. 6-16 Natural modes and frequencies of two-girder bridge with RC deck w.r.t modeling

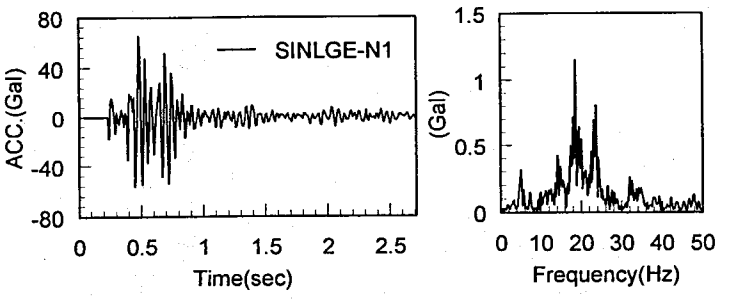

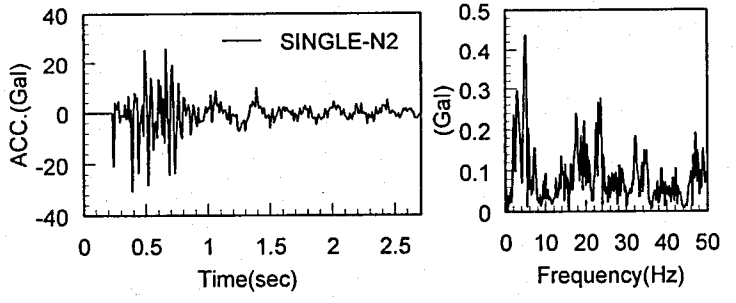

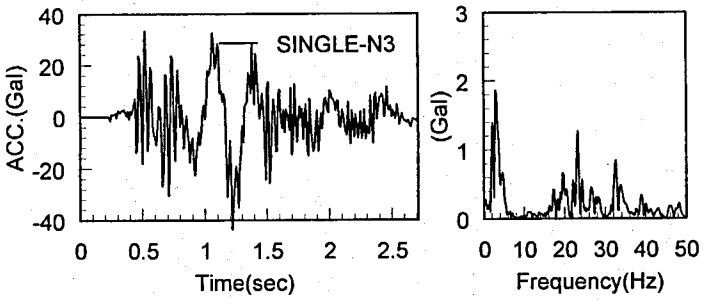

(a) Single span bridge model: v=80km/hr

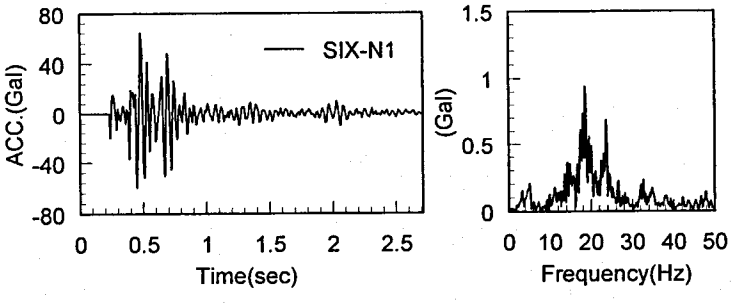

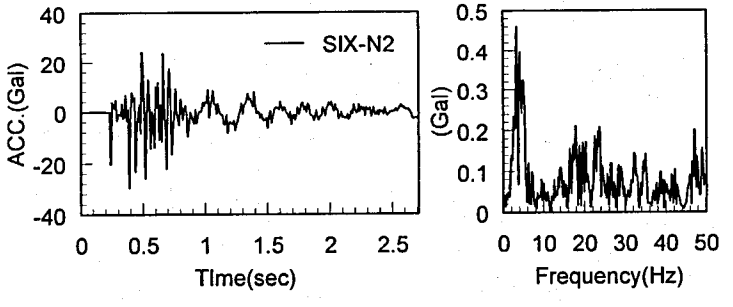

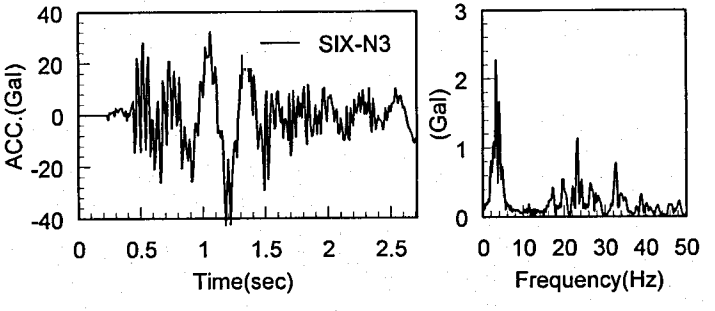

(b) Six-continuous span bridge model: v=80km/hr

Fig. 6-17 Acceleration responses and Fourier amplitudes of two-girder bridge: v=80km/hr

6.4.2 Analytical results

The natural frequency, natural mode, acceleration responses and Fourier spectra of the simplified single span model are compared with those responses of the six-continuous model, to verify the validity of the single span model. The vehicle speed is assumed to be 80km/hr, and the vehicle path follows the running case 2 in Fig. 6-14(b).

In Fig. 6-16, the first and second torsional modes and the first bending mode are appeared, and show the validity of the single span model for dynamic response analysis. Moreover the acceleration responses and their Fourier spectra between the two models show good agreement as shown in Fig. 6-17. Thus, the effect of the end-cross beam reinforcement is determined by using the single span model.

In the traffic-induced dynamic response analysis of the single span bridge model, vertical accelerations are estimated by superposing up to 100th modes (165.03 Hz for the model WO, 173 Hz for the model WG and 174 Hz for the model WB), since the dynamic responses at the deck slab and the end-cross beam are sufficiently converged within 100th mode from the preliminary analysis. During the analysis, vehicle speeds are adopted as 40km/hr and 60km/hr and assumed to be constant.

Vertical acceleration responses

Vertical accelerations at C14 and D58 nodes located on the bracket of the bridge according to the running case are shown in Figs. 6-18 and 6-19. It is noteworthy that the vertical scale of the Fig. 6-19 is 10 times larger than that of Fig. 6-18. The symbol B2 means that the bump height of 2 cm at the expansion joint is considered in the analysis. The letter P1 indicates the roadway surface profile P1 (see, Fig. 6-15), and V40 denotes the vehicle speed 40km/hr.

Figure 6-18 demonstrates that both reinforcing patterns WG and WB act on reducing the peak acceleration at the end-cross beam and decks near a bump due to the vehicle running on the central lane (Running case 1, see Fig. 6-14(b)). When the vehicle is running on the slow speed lane (Running case 2, see Fig. 6-14(b)), however, it is observed that the peak acceleration response of the nodes located on the bracket of the bridge is difficult to reduce by the reinforcing pattern WG, as shown in Fig. 6-19. On the other hand, the reinforcing pattern WB acts on reducing peak vertical accelerations of the nodes on the bracket, although the reducing effect is weaker than the case of vehicle running on the central lane.

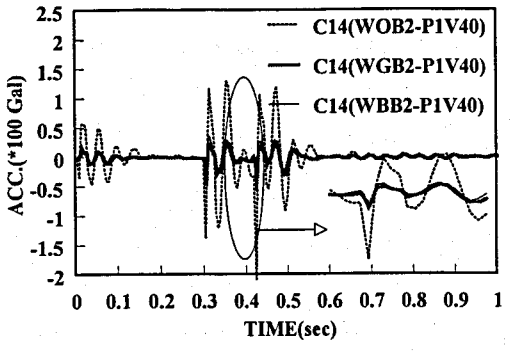

a) Node C14

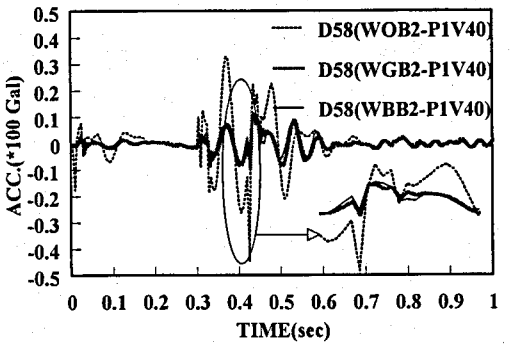

b) Node D58

Fig 6-18 Acceleration responses at C14 and D58 nodes: Running case 1; *v=40 km/hr*; $S(\Omega)=0.001/(\Omega^{2.5}+0.05^{2.5})$; bump=2cm

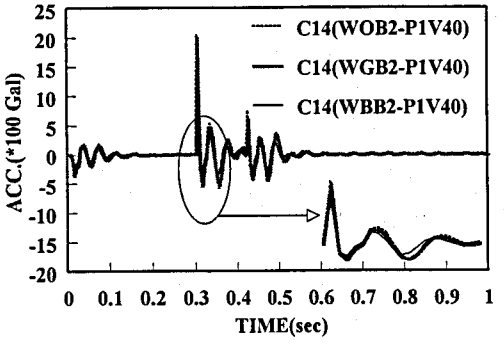

a) Node C14

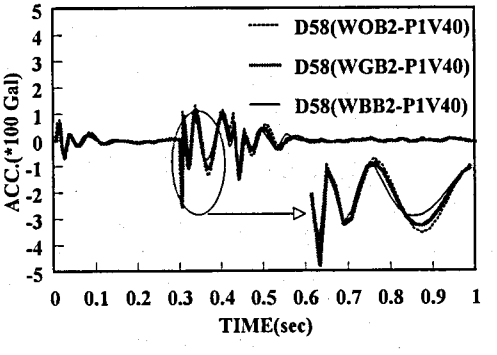

b) Node D58

Fig 6-19 Acceleration responses at C14 and D58 nodes: Running case 2; *v=40 km/hr*; $S(\Omega)=0.001/(\Omega^{2.5}+0.05^{2.5})$; bump=2cm

Dynamic characteristics

How bumps affect the dynamic characteristic of members located near the bump of an expansion joint is shown in Fig. 6-20. Natural modes of the bridge corresponding to the dominant frequencies appeared in Fig. 6-20 are shown in Fig. 6-21 with natural frequencies. It is observed that the power spectrum above 9Hz tends to increase due to the impulsive dynamic wheel load of vehicles generated during running on bumps, from the Fig. 6-20.

The dominant frequencies near 3.7Hz (Fig. 6-20(b)) and 18Hz (Fig. 6-20(a)), which cannot be found in natural frequencies of the bridge, are considered to depend on the effect of

vehicle's bouncing (3.0Hz) and axle-hop motion (17.9Hz), respectively. It demonstrates that the 8th (9.15Hz), 9th (10.45Hz), 18th (16.76Hz), 25th (25.27Hz) and 27th (32.41Hz) modes shown in Fig. 6-21, which are in relation with modes of cross beams and decks near the end-cross beam, are the modes corresponding to the dominant frequencies appeared in Fig. 6-20.

Power spectra of vertical acceleration responses at the C8, C14, D54 and D58 nodes with respect to reinforcing patterns under the condition of running case 2 are shown in Fig. 6-22. For the nodes C8 and D54 located between main girders, it is observed that power of the PSD curve at the frequency region higher than 7Hz is reduced by the reinforcing pattern WG as well as the pattern WB.

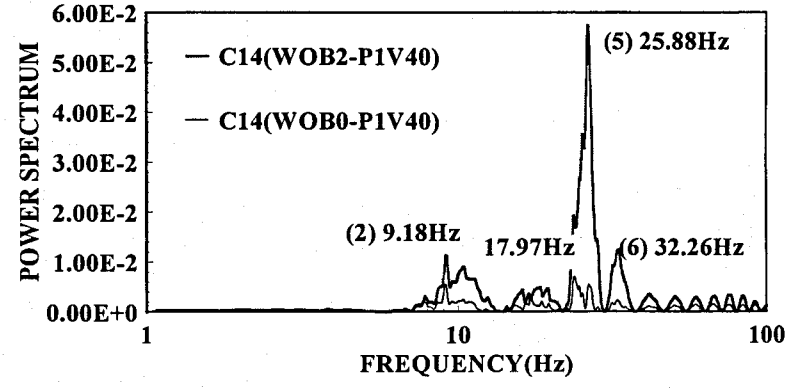

a) End-cross beam

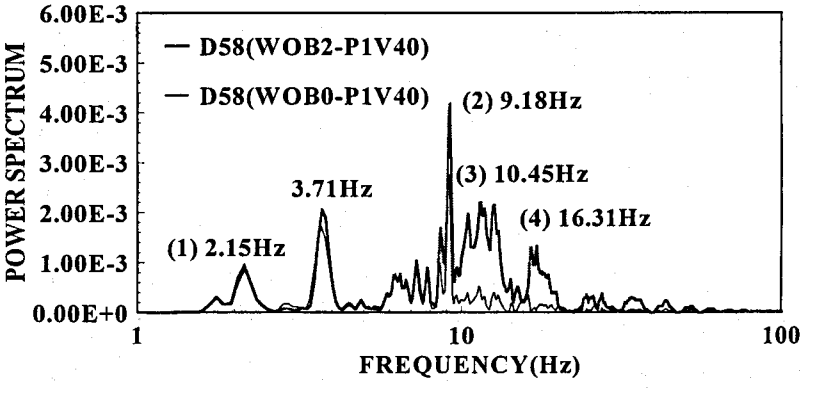

b) Deck slab

Fig. 6-20 PSD Curves of acceleration at C14 and D58 nodes: Running case 2; *v=40km/hr*; P1-profile

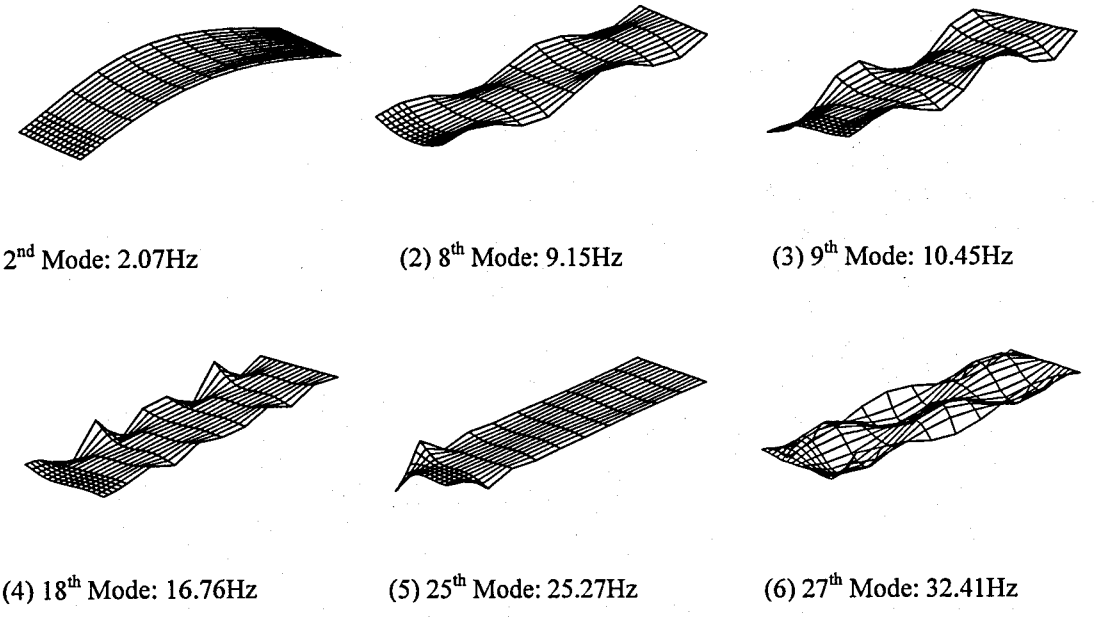

(1) 2nd Mode: 2.07Hz (2) 8th Mode: 9.15Hz (3) 9th Mode: 10.45Hz

(4) 18th Mode: 16.76Hz (5) 25th Mode: 25.27Hz (6) 27th Mode: 32.41Hz

Fig. 6-21 Mode shapes corresponding to dominant frequencies in Fig. 6-20

For the nodes C14 and D58 located on the bracket, the reinforcing pattern WB results more effective reduction than the reinforcing pattern WG does. It is also observed that the power due to the axle-hop motion (around 18Hz) is reduced by the end-cross beam reinforcement.

It is thus possible to conclude that dominant frequencies of the end-cross beam and decks near bumps have tendency to transfer to higher frequency regions due to the impulsive dynamic wheel load generated by a vehicle running over bumps, and the power spectrum at the higher frequency can be diminished by the reinforcement.

Vibration acceleration level (VAL)

The VAL taken from the 1/3 octave band spectral analysis at the noted nodes with respect to the reinforcing patterns are shown in Fig. 6-23 and Fig. 6-24. The vertical and horizontal scales in the figures indicate VAL (dB) and Frequency (Hz), respectively.

Figure 6-23 represents that both reinforcing patterns WG and WB give similar reduction effect under the condition of running case1 (running on central lane). The reducing effect can be expected covering most of the frequency range; 1Hz ~ 100Hz for the end-cross beam; 4Hz ~ 100Hz for the deck slab. On the other hand, when vehicle is running on the low speed lane (running case2), the vibration reduction cannot be observed by the reinforcing pattern WG but by the pattern WB as shown in Fig. 6-24.

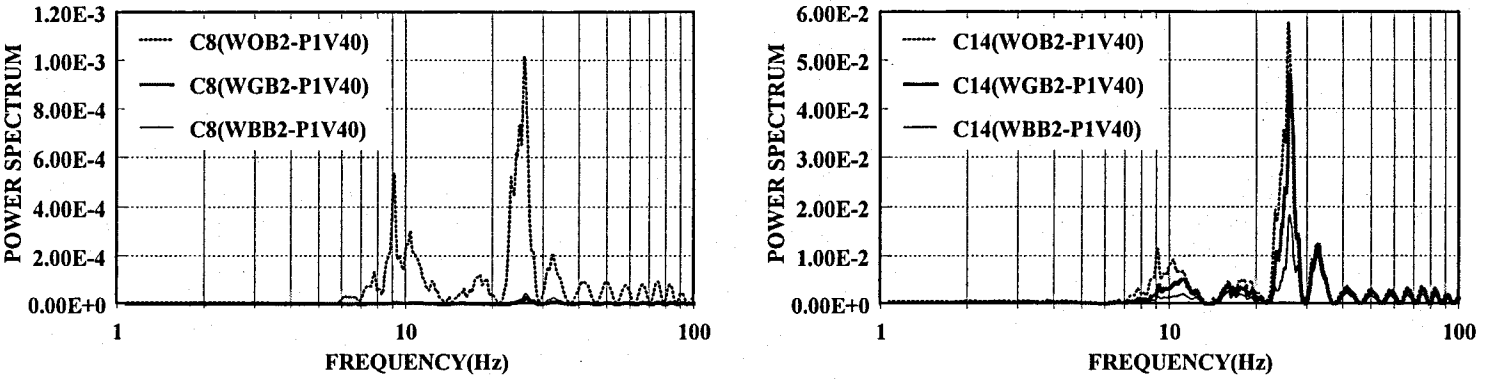

a) End-cross beam

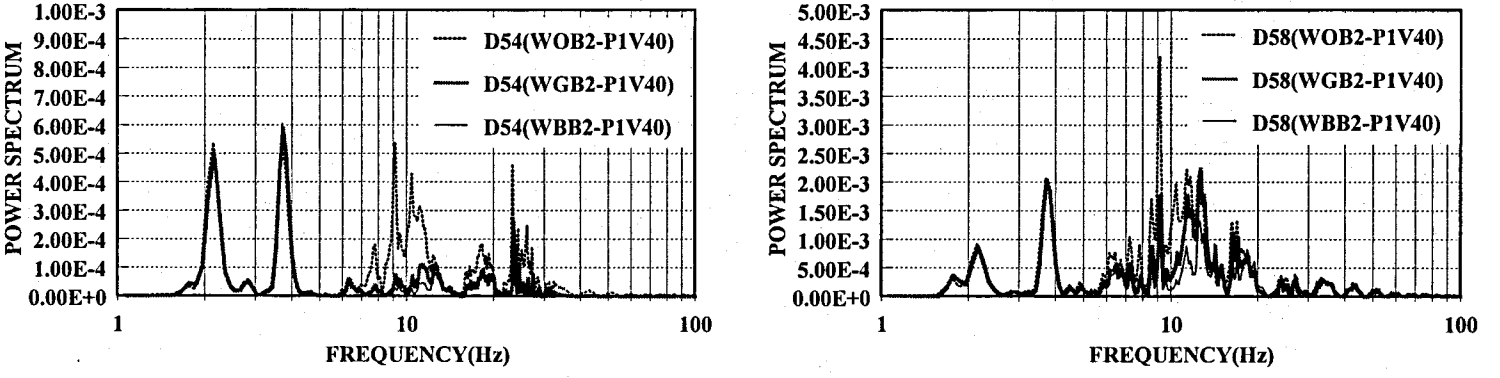

b) Deck slab

Fig. 6-22 PSD Curves of acceleration responses: Running case 2; *v=40 km/hr*; P1-profile; bump=2cm

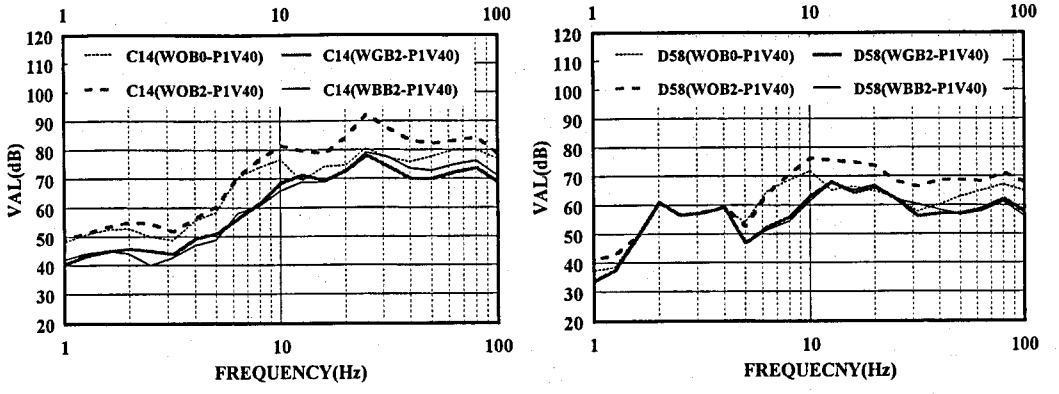

Fig.6-23 1/3 octave spectra of noted nodes at bracket due to running case1

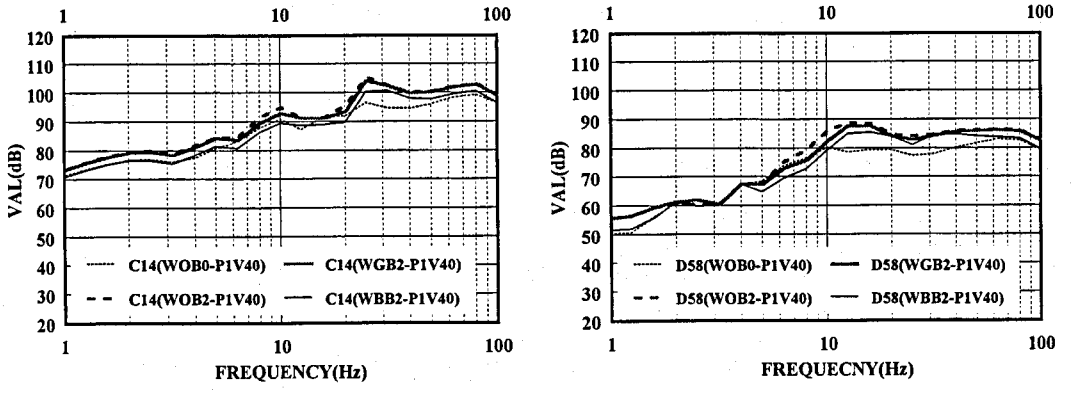

Fig. 6-24 1/3 octave spectra of noted nodes at bracket due to running case2

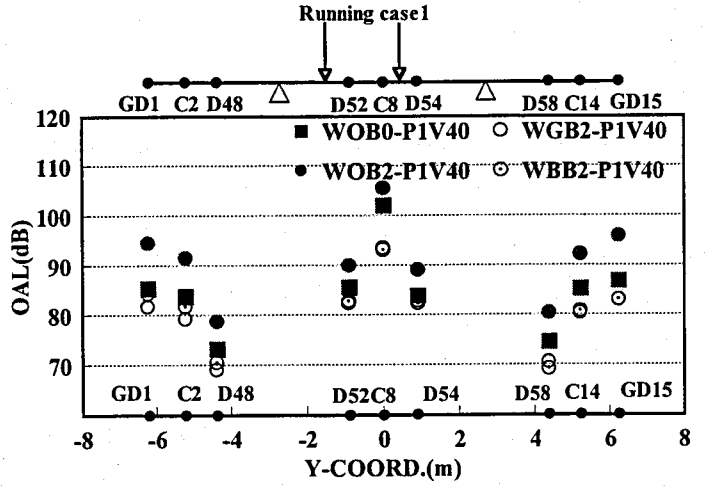

Fig. 6-25 Over all acceleration level at noted nodes due to running case1

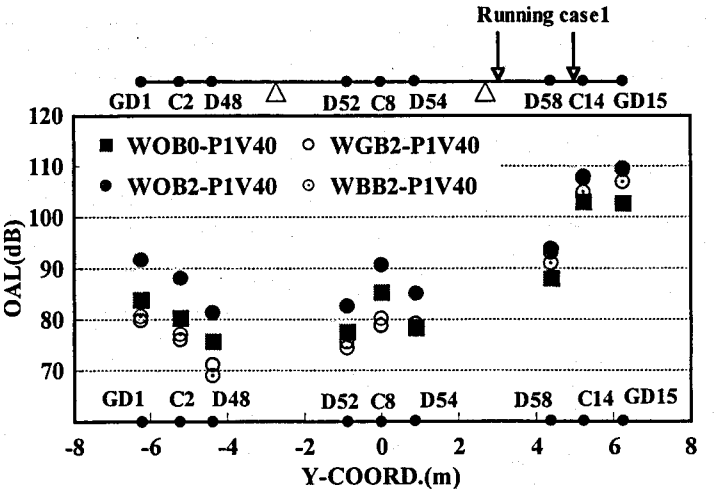

Fig. 6-26 Over all acceleration level at noted nodes due to running case2

From the 1/3 octave spectral analysis, it is also observed that the reinforcing the end-cross beam can suppress high-frequency vibrations.

To investigate the effect of vehicle path to bridge members, the over all acceleration level (OAL) is estimated at each noted node. The OAL with respect to each node is summarized in Figs. 6-25 and 6-26. The OAL due to vehicle running on roadway without any bump at each node are also illustrated to affirm the effect of bump on vibration serviceability. It is observed the member under vehicle path shows the most severe vibration level: node C8 under running case 1 and node GD15 under running case 2.

Assessment of reduction effects

To investigate the vibration reduction effect with respect to the end-cross beam reinforcing patterns quantitatively, a vibration reduction level (Eq. (6.3)) of the acceleration responses is defined.

$$VRL(dB) = -20\log_{10}\frac{A_{WR}}{A_{WO}} \tag{6.3}$$

where, A_{WR} is the root mean square (RMS) values of dynamic responses due to reinforcing end-cross beam; A_{WO}, the RMS values of dynamic responses due to without any reinforcement; VRL, the vibration reduction level in deci-Bel (dB).

Figure 6-27 shows the summarized results of the VRL under the condition of running case1 according to reinforcing patterns. For C8 node located under the vehicle path, the VRL reaches to about 12dB and 13dB according to reinforcing pattern WG and WB, respectively.

The summarized result for running case 2 is shown in Fig. 6-28, and it shows the VRL of nodes under the vehicle path reach to 3dB according to the reinforcing pattern WB, on the other hand, those vibration reduction effects are less than 1.5dB by the reinforcing pattern WG.

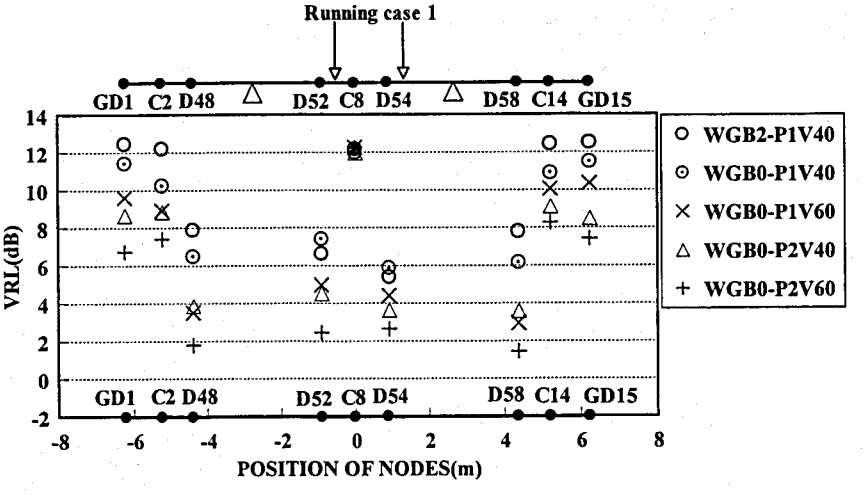

(a) Reinforcing pattern WG

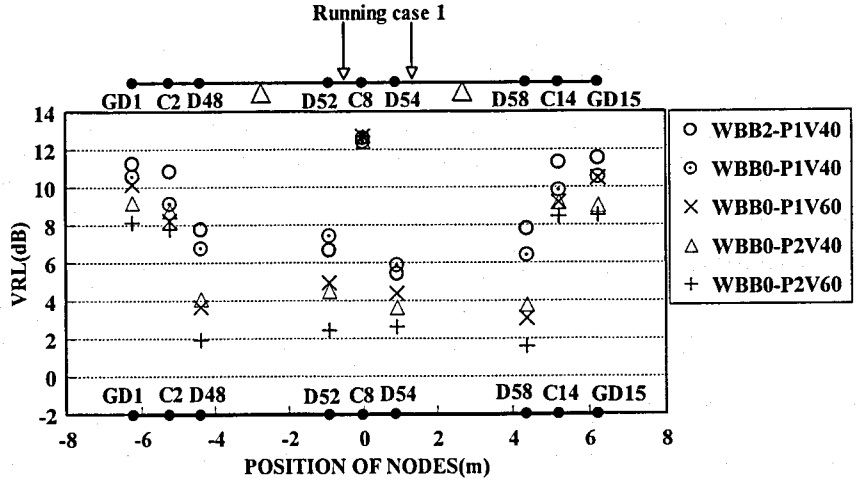

(b) Reinforcing pattern WB

Fig. 6-27 Vibration reduction level at noted nodes; Running case1

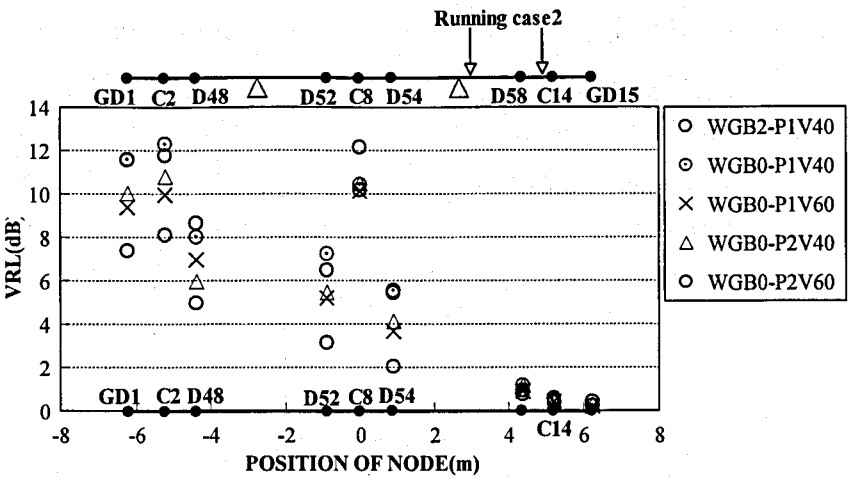

(a) Reinforcing pattern WG

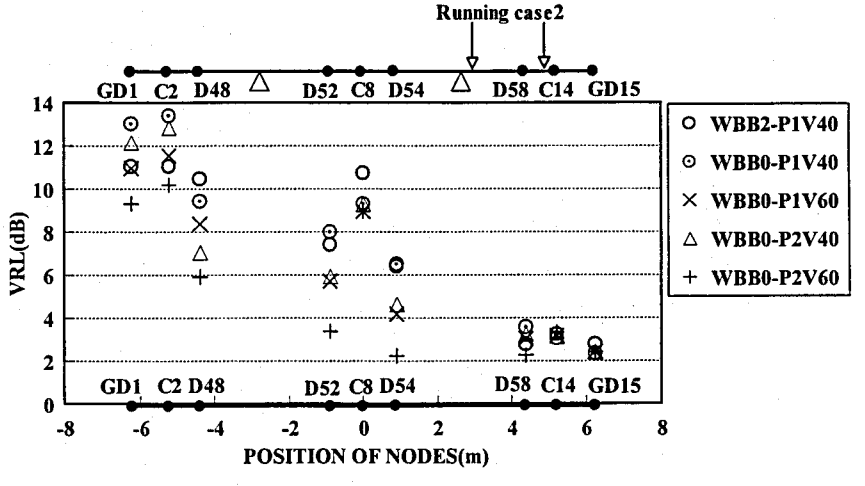

(b) Reinforcing pattern WB

Fig. 6-28 Vibration reduction level at noted nodes; Running case2

For nodes under the vehicle path, the vibration reduction effect at each running case keeps constant level regardless of the vehicle speed and the roadway roughness condition. The results thus represent, when a vehicle is running on the central lane (running case 1), both reinforcing patterns WG and WB give similar reduction effect for the nodes under the vehicle path. On the other hand, more reliable reduction effect can be expected by reinforcing pattern WB than by reinforcing pattern WG, when vehicle is running on the low speed lane. For the members experiencing peak vibration under vehicle paths, constant vibration reduction effects can be expected regardless of the parameters by the end-cross beam reinforcement.

6.5 Conclusions

To improving the vibration serviceability of a two-girder bridge, some countermeasures for reducing vibration are applied, and the effectiveness of the countermeasures are investigated by means of analytical approach in this chapter. The major conclusions are as follow:

1. It is observed that the deck of the steel two-girder bridge with PC deck is more severely affected than that of the conventional steel multi-girder bridge by the traffic-induced vibration. Moreover, the two-girder bridge with elastomeric bearings is relatively easily vibrated by moving vehicles in comparing with the bridge with steel pin bearings. However, the response of the main-girder of the three-girder bridge is more amplified by the moving vehicle than that of the two-girder bridge. It supports the need of the end-cross beam reinforcement for the steel two-girder bridge with wide girder spacing.
2. The end-cross beam reinforcement is effective to curtail the impulsive response in the case of the pin supported two-girder bridges. On the other hand, although the end-cross beam reinforcement is also effective to buffer the impulsive vibration for the two-girder bridge with elastomeric bearings, the end-cross beam reinforcement using in combination with the removing bumps is recommended.
3. For nodes located near the A1 joint of the bridge supported by elastomeric bearings, the VL of the bridge is dominated by the dynamic characteristic of high-frequency range (20Hz ~ 30Hz). The VLs at the frequencies over 3Hz are reduced by the reinforcement as well as removing bumps.
4. Although the VL of the deck at the span center of the first span is dominated at the frequency of near 3Hz, those VLs at the frequency of near 20Hz increases due to the elastomeric bearings. The VL at the frequency of near 20Hz is reduced only by the removing bump. It also supports the result that the bridge with elastomeric bearings is easily vibrated by the impulsive wheel load generated by a vehicle at the moment of passing the bump.
5. The dynamic reaction due to the inertia effect of the two-girder bridge with elastomeric bearings can be reduced both reinforcing method and removing the bump, and the most effective result is obtained by combining the two methods.
6. For steel two-girder bridges with wide decks and brackets, the reinforcing up to the bracket gives effective vibration reduction.
7. The end-cross beam reinforcement can give vibration reduction effects on deck slab near expansion joints as well as the end-cross beam. Especially, for continuous bridge like the bridge adopted in this study, the reinforcement including intermediate-cross beam will guarantee expanding the life span of RC and/or PC decks suffering negative moment as

well as vibration reduction.

8. The end-cross beam reinforcement and removal of bumps in combination of the vibration control can give an effective reduction against environmental vibrations.

References

[1] Kato, M. and Shimada, S.: Statistical analysis on the measured bridge vibration data, Proc. of JSCE, 311, 49-58, 1981. *(in Japanese)*

[2] Kappos, A.J. edited: Dynamic loadings and design of structures: Chapter 8 Traffic and moving loads on bridges (by David, C.), Spon Press, London, UK, 2002.

[3] Kim, C.W. and Kawatani, M.: A comparative study on dynamic wheel loads of multi-axle vehicle and bridge responses, Proc. of DETC'01, 2001 ASME Design Engineering Technical Conference & Computers and Information in Engineering Conference, DETC2001/VIB-21526, CD-ROM, 2001.

[4] Kawatani, M. and Kim, C.W.: Effects of gap at expansion joint on traffic-induced vibration of highway bridge, Proc. Int. Conference on Developments in Short and Medium Span Bridge Engineering '98, Calgary, Canada, CD-ROM, 1998.

[5] Fukada, S., Kajikawa, Y., Hayashi, H., Yoshikawa, M. and Sanuki, Y.: Vibration characteristics of highway bridge with isolators and jointless system under moving vehicles, Proc. Int. Conference on Developments in Short and Medium Span Bridge Engineering '98, Calgary, Canada, CD-ROM, 1998.

[6] Fukasawa, Y., Sugiyama, K., Nakahara, K. and Mizukami, H.: Fundamental characteristics of low frequency sound radiated from highway bridges under the passage of heavy vehicles, J. of Structural Eng., JSCE, 37A, 945-956, 1991. *(in Japanese)*

[7] Yamada, Y. and Kawatani, M.: Analytical study on reduction of traffic-induced vibration due to reinforcement procedure at girder end, J. of Structural Eng., JSCE, 43A, 737-746, 1997. *(in Japanese)*

[8] Chubb, M.S. and Kennedy Reid, I.L.: Crossbeam replacement, Bridge Modification, Thomas Telford, London, 241-254, 1995.

[9] Nanjo, A., Mori, Y., Sasaki, K., Sonoda, K. and Kiso, S.: Experimental study on RC end cross beams for the seismic resistance of a steel plate girder bridge, J. of Construction Steel, JSSC, 8, 179-186, 2000. (*in Japanese*)

[10]ISO: Evaluation of Human Exposure to Whole-Body Vibration-Part 1: General requirements, ISO2631/1, 1985.

[11]ISO: Evaluation of Human Exposure to Whole-Body Vibration -Part 2: Continuous and shock-induced vibration in buildings (1 to 80Hz), ISO2631/2, 1985.

Chapter 7

Concluding remarks

It is not possible to generalize the vehicle-bridge interaction problems because of its complicate dynamic interaction system. Nevertheless of its complicate dynamic relations between vehicle motions and bridge responses with roadway roughness, if some effects of influence factors are defined, it can be seen that the variation is not purely random but must follow a certain physical law. Therefore, throughout this study, to step up to a certain physical law of the vehicle-bridge interaction problem, computer simulations on dynamic responses of bridges and wheel loads of heavy vehicles is carried out.

The major goal of this dissertation is devoted to investigate two main subjects, development of the general three-dimensional traffic-induced dynamic analysis and its application to dynamics of steel girder bridges. To meet the needs, a numerical model for the traffic-induced vibration of bridges is presented. To express the actual behavior of elastomeric bearings, the double node connected by linear and rotational springs is adopted. Lagrange equation of motion is adopted to develop governing dynamic differential equations for the bridge-vehicle interaction system. Newmark's β method is applied to solve the derived system governing equations of motion as a numerical integration method.

Confirming the validity of the developed simulation method and the algorithm is another important objective of this study. Simulated dynamic wheel loads and bridge responses are therefore compared with experimental results, to verify the validity of the analytical model. The concept of dynamic increment factor (DIF) is used to investigate the correlation between analytical and experimental results of bridge responses. To verify the validity of the analytical dynamic wheel loads of the two-axle cargo truck model, the time history, the dynamic load coefficient (DLC) and the dominant frequency of wheel loads at each tire are compared with experimental ones. The analytical responses of a three-girder steel bridge and a two-girder steel bridge are compared with in-field test results to verify the validity of the analytical model and the procedure.

The RC deck is the member more easily damaged than other structural members in steel highway bridges due to wheel loads of vehicles. Thus, the rational criterion of performance level of RC decks provides useful assessment tool for decision making related to the inspection, repair, upgrading and replacement of existing steel plate girder bridges based on life-cycle cost. Thus, the probabilistic assessment of code specified impact factors for decks of highway bridges are carried out based on the Monte-Carlo simulation (MCS) method.

A pioneering research on dynamic responses of web plates of the two-girder steel bridge is carried out in this study to examine the effect of deck's deformation to those of web plates,

since the investigation on dynamic responses of the web plate can give useful information in solving fatigue and infrasound problems of bridges.

The first chapter contains the introduction of dynamic phenomena of bridges due to moving vehicles so called traffic-induced vibration of bridges and a brief historical review on the traffic-induced vibration of bridges.

Viaducts with flexible structural features can easily produce annoying vibration for people living and working in neighboring buildings to a distance a little far from the bridge. Vibration is therefore one of the more important consequences to be considered, when planning new viaducts and upgrading older ones. Situations for vibration related problems are matters connected with various transmission routes in a structural system. It must be considered before making some engineering decisions dealt with vibration problems. Thus, the need of full 3-D traffic-induced vibration analysis and of development of the countermeasure against the undesirable vibration is also stated in Chapter 1.

The numerical modeling of a vehicle-bridge interaction problem including surface roughness profiles is presented based on the Lagrange equation of motion from Hamilton's principle in Chapter 2. The developed governing dynamic differential equations for the bridge-vehicle interaction system are treated in the time domain. The numerical model for the traffic-induced vibration of bridges is presented by using the direct stiffness method and modal analysis. Theories behind Guyan reduction and QR method adopted to improve the calculation efficiency and eigen-value analysis in respect are mentioned. The outline of the traffic-induced vibration analysis of bridges is summarized as a form of flow-chart.

The Chapter 3 contributes the verification of analytical responses of a vehicle model by using the equations of motion derived in Chapter 2. Major conclusions are drawn from the comparative investigation between analysis and experiment.

The data from a field test indicate that the analytical method is accurate for predicting the dynamic wheel loads of heavy vehicles. It is observed that dominant frequencies of the dynamic wheel loads vary with speed. One of reasons for the variation of the dominant frequency according to speeds can be that the dominant space frequency of the roadway profile which can resonant with the vehicle system changes with respect to the vehicle speed. Dominant frequencies of dynamic wheel loads and bounce motions of vehicles are strongly related with each other. The axle-hop motion of the relatively high dominant frequency compared to that of the vehicle wheel load can also influence to the dynamic wheel load with increasing speed.

In Chapter 4, the relationship between the dynamic response of vehicles and bridges are investigated by means of the experimentally verified analytical method. A pioneering investigation on the probabilistic assessment of deck's impact factors is also carried out based on the Monte-Carlo simulation technique.

The dynamic feature of bridge responses is dominated by the natural frequency of the bridge itself if vehicles are running on very smooth roadway. On the other hand, if vehicles are running on rough roadway, the dynamic feature of bridge responses is dominated by dynamic properties of vehicles because of enough ability of the rough surface to stimulate the vehicles. Moreover, the frequency characteristics of the dynamic wheel load, the bounce motion of vehicles and the bridge response are strongly related with each other.

The deck is another important member experiencing the dynamic wheel load, since the RC decks, being directly subjected to wheel loads of vehicles, are more easily damaged than other structural members in steel highway bridges. Moreover, the wide spreading adoption of the steel two-girder bridge needs higher performance of deck slabs than those of conventional multi-girder bridges because of the adoption of wider girder spacing than conventional bridges. The rational criterion of the performance level of RC decks provides useful assessment tool for decision making related to the inspection, repair, upgrading and replacement of existing steel plate girder bridges based on life-cycle cost.

The probabilistic assessment of code specified impact factors for decks of highway bridges are carried out based on MCS method. The straight lines on the lognormal and extreme Type I distribution papers can approximately represent probabilistic properties of the impact factor for the RC deck slab. If the impact factor can be classified in the serviceability limit state then reliability index for the panel near bumps is lower than that of the target reliability index for the SLS, although what kind of limit state the impact factor is classified in has not been defined yet. On the other hand the reliability considering the condition of no bump at the expansion joint satisfies the SLS. It indicates that the bump is one of important factors for impact factor of decks, and the impact factor of the deck located near the expansion joint dominates the design impact factor under the conditions considered. Thus, if the impact factor of the deck slab near an expansion joint of approaching side of a bridge satisfies a given reliability due to a vehicle with tandem axle running on a bump, those reliabilities of other deck slabs are satisfied automatically.

The strong demand for safe and economical bridges induces the advent flexible bridges and it means that more attention must be given to the dynamic behavior. Moreover, the adoption of elastomeric bearings against the seismic load will produce the occurrence of additional vibration problems. It will be desirable to identify factors that affect the vibrations of the bridge before design is carried out. Thus, the Chapter 5 demonstrates the result of a

three-dimensional analysis of a two-span continuous steel two-girder bridge with PC decks and elastomeric bearings.

The effectiveness of the three-dimensional analysis with flat shell elements for decks, main girders, cross beams and guardrails, beam elements for stiffeners and double nodes including spring elements for elastomeric bearings is verified by comparing with experimental results. The acceleration response of decks at the moment of the following vehicle entering tends to be amplified by vertical deformations caused by the elastic deformation of elastomeric bearings as well as the bending of the deck at the end-cross beam. The 3-D plane model can be effectively used in the traffic-induced vibration of steel two-girder bridges, if the vertical response of girders and decks is mainly focused on.

At the moment of a vehicle entering the bridge the response of the main girder can be strongly affected by vertical deformations due to the bending of a deck and the elastic deformation of elastomeric bearings at the support. The amplitude of the acceleration response of the main girder as well as the Fourier amplitude is more easily affected by the vehicle running outside of the G1-girder because of the coupled effect between torsional modes and vehicle loadings. On the other hand, the out-of-plane dynamic response of web plates is more easily affected by deformations of deck slabs between girders than by deformations produced by vehicles running on the cantilevered part of decks.

The amplitude of the acceleration response of decks is more easily amplified by passage of vehicle series than by single vehicle running, since the impulsive wheel load of the following vehicle is amplified by the additional bump height generated by the elastic deformation of elastomeric bearings and decks under the load of the head vehicle. The acceleration responses of the nodes on the web plate that is connected with a cross beam is observed to have relatively small amplitudes compared with those of the nodes on the web plate that is apart from cross beams. The appearance of the dominant frequency near 3Hz of the web plate connected with a cross beam demonstrates that the dynamic property of the web plate connected with cross beams can be easily affected by dynamic characteristic of the bounce motion of heavy vehicles. On the other hand, the response of web plates apart from the cross beam can be dominated by dynamic sources with higher frequency features like the axle-hop motion of vehicles. Thus, if the main object of an analysis is the response of local members, the use of tire property well defined is necessary.

In Chapter 6, the end-cross beam reinforcement is applied to two-girder bridges, as a countermeasure against traffic-induced vibration. In addition, the method removing the bump is applied as another method to reduce the traffic-induced vibration.

It is observed that the deck of the steel two-girder bridge with PC deck is more severely affected than that of the conventional steel multi-girder bridge by the traffic-induced vibration.

Moreover, the two-girder bridge with elastomeric bearings is relatively easily vibrated by moving vehicles in comparing with the bridge with steel pin bearings. However, the response of the main-girder of the three-girder bridge is more amplified by the moving vehicle than that of the two-girder bridge. It supports the need of the end-cross beam reinforcement for the steel two-girder bridge with wide girder spacing. Elastomeric bearings are one of the sources to magnify the dynamic reaction due to the inertia effect of bridge itself. The dynamic reaction due to the inertia effect of the bridge can be reduced by the reinforcing method as well as the method of removing the bump. The most effective result is obtained by combining the two methods.

The end-cross beam reinforcement can give vibration reduction effects on the deck slab near the expansion joint as well as the end-cross beam. Especially, the reinforcement including intermediate-cross beam of continuous bridges will guarantee expanding the life span of RC and/or PC decks suffering negative moment as well as vibration reduction.

Although the VL of the deck at the span center of the first span is dominated at the frequency of near 3Hz, those VLs at the frequency of near 20Hz increases due to the elastomeric bearings. The VL at the frequency of near 20Hz is reduced only by the removing bump. It shows that the bridge with elastomeric bearings is easily vibrated by the impulsive wheel load generated by a vehicle at the moment of passing the bump.

The dynamic reaction due to the inertia effect of the two-girder bridge with elastomeric bearings can be reduced both reinforcing method and removing the bump, and the most effective result is obtained by combining the two methods.

For steel two-girder bridges with wide decks and brackets, the reinforcing up to the bracket gives effective vibration reduction. The end-cross beam reinforcement can give vibration reduction effects on deck slab near expansion joints as well as the end-cross beam. Especially, for continuous bridge like the bridge adopted in this study, the reinforcement including intermediate-cross beam will guarantee expanding the life span of RC and/or PC decks suffering negative moment as well as vibration reduction. Moreover, the end-cross beam reinforcement and removal of bumps in combination of the vibration control can give an effective reduction against environmental vibrations.